UNIVERSITY OF CALIFORNIA SAN DIEGO

Neuropilin-1/Heparan Sulfate Interactions and Angiogenesis-Dependent Tumor Growth

A dissertation submitted in partial satisfaction of the requirements for the degree Doctor of Philosophy

in

Biomedical Sciences

by

Chelsea Danielle Painter

Committee in charge:

Professor Jeffrey Esko, Chair
Professor Richard Gallo
Professor Tracy Handel
Professor Yishi Jin
Professor Karl Willert

2021

The Dissertation of Chelsea Danielle Painter is approved, and it is acceptable in quality and form for publication on microfilm and electronically.

University of California San Diego

2021

DEDICATION

To my life partner and love of my life, Afsheen

To my family, especially my parents, Daniel and Roberta,

and my siblings, Ashley and Zachary

To all of my students (past, current, and future)

EPIGRAPH

“Life is not easy for any of us. But what of that? We must have perseverance and above all confidence in ourselves. We must believe that we are gifted for something and that this thing must be attained.”

- Marie Curie, PhD

TABLE OF CONTENTS

Dissertation Approval Page iii

Dedication iv

Epigraph v

Table of Contents vi

List of Figures ix

List of Tables x

List of Supplemental Videos xi

Acknowledgements xii

Vita xvii

Abstract of the Dissertation xviii

Chapter 1: Neuropilin-1 Structure/Function Relationships in Angiogenesis 1

1.1 Introduction 2

1.2 Neuropilin Family: Expression and Structure 3

1.3 Introduction of the VEGF/HSPG/Nrp1/VEGFR2 Complex 9

1.4 The Role of Neuropilin-1 in the Complex 14

1.5 Interactions Between VEGF and Neuropilin-1 14

1.6 Neuropilin-1 Binds to Heparin/Heparan Sulfate 20

1.7 Heparin Binding Capabilities of VEGF and VEGFR 29

1.8 Investigations of the Entire VEGF/HSPG/Nrp1/VEGFR2 Complex 32

1.9 Summary of the VEGF/HSPG/Nrp1/VEGFR2 Complex 34

1.10 Neuropilin Structure/Function Relationship *in vivo* 37

1.11 Examination of the Role of Neuropilin-1 in Angiogenesis 37

1.12 Acknowledgements 47

Chapter 2: Alteration of Neuropilin-1 and Heparan Sulfate Interaction Impairs Angiogenesis-Dependent Tumor Growth....48

2.1 Abstract....49

2.2 Introduction....50

2.3 Materials and Methods....52

2.3.1 Computational Studies to Elucidate the GAG-Binding Site(s) of Neuropilin-1....52

2.3.2 Molecular Dynamics....53

2.3.3 Evolutionary Conservation....56

2.3.4 Expression and Purification of Neuropilin-1....56

2.3.5 SDS-PAGE/Western Blotting Methods....58

2.3.6 Immunoblotting of Purified Neuropilin-1....59

2.3.7 Gel Electrophoresis....59

2.3.8 Analytical Heparin-Sepharose Chromatography....60

2.3.9 Neuropilin-1 Binding to Immobilized Heparin-BSA....60

2.3.10 Size-Exclusion Chromatography and Multi-Angle Light Scattering (SEC-MALS)....61

2.3.11 Differential Scanning Fluorimetry....62

2.3.12 Cell Surface Binding....62

2.3.13 Generation and Genotyping of Mouse Lines....63

2.3.14 Tumor Experiments....66

2.4 Results....67

2.4.1 Molecular Modeling of Heparin Binding Site in Neuropilin-1....67

2.4.2 Recombinant Protein Production....70

2.4.3 Binding of Recombinant Nrp1 Mutants to Heparin....75

2.4.4 Heparin Stabilizes Neuropilin-1 Against Thermal Denaturation. 76

2.4.5 Heparin-Induced Dimerization of Neuropilin-1 81

2.4.6 Neuropilin-1 Binds Heparin Oligosaccharides in a 1:2 Heparin/Protein Complex 87

2.4.7 Interaction of Neuropilin-1 with Heparan Sulfate 90

2.4.8 Generation of Heparan Sulfate Binding Deficient Nrp1 Mouse Model 94

2.4.9 Pathological Angiogenesis in the Heparan Sulfate Binding Deficient Nrp1 Mouse Model 95

2.4.10 Summary 99

2.5 Discussion 99

2.6 Acknowledgements 106

Chapter 3: Concluding Remarks 108

3.1 Project Summary 109

3.2 Modeling Studies 109

3.3 Heparin Binding 111

3.4 Structural Requirements for Heparin Binding and Heparin-Induced Dimerization 112

3.5 Investigating Effects of Heparin Binding Deficient Neuropilin-1 116

3.6 Influence of Heparan Sulfate on Neuropilin-1 Function *in vivo* 117

3.7 Summary 120

References 121

Appendix 137

LIST OF FIGURES

Figure 1.1: Domain Structure of Neuropilin-1 8

Figure 1.2: Representations of the splice variants of human VEGF-A 11

Figure 1.3: Terminal Arginine Residues of VEGFA and Tuftsin Occupy Binding Recess in b1 Domain of Neuropilin-1 18

Figure 1.4: Heparin Binding Cleft in Human Neuropilin-1 22

Figure 1.5: Heparan Sulfate Biosynthesis 26

Figure 1.6: Updated Model of the VEGF165/HSPG/Nrp1/VEGFR2 Complex 36

Figure 1.7: Progression of Vascularization of the Hindbrain and Retina During Development 45

Figure 2.1: Molecular Modeling of Nrp1 with Combinatorial Virtual Library Screen (CVLS) and Amino Acid Selection 72

Figure 2.2: Supplement to Figure 2.1 74

Figure 2.3: Heparin Binding of Nrp1 Mutants 78

Figure 2.4: Supplement to Figure 2.3 79

Figure 2.5: Size-Dependent Heparin-Induced Dimerization of Nrp1 83

Figure 2.6: Supplement to Figure 2.5 84

Figure 2.7: Neuropilin-1 and Heparin Oligosaccharide Form a 2:1 Nrp1:Heparin Complex 88

Figure 2.8: Supplement to Figure 2.7 89

Figure 2.9: Neuropilin-1 Binding to Cell Surface Heparan Sulfate 92

Figure 2.10: Supplement to Figure 2.9 93

Figure 2.11: Alteration of Neuropilin-1 and Heparan Sulfate Binding Impairs Subcutaneous B16 Tumor Growth 97

Figure 2.12: Generation and Characterization of *Nrp1*$^{D/D}$ Mouse 98

LIST OF TABLES

Table 2.1: Salt Concentrations for Heparin Sepharose Elutions and K_d and B_{max} Values for BSA-Heparin ELISAs 80

Table 2.2: Determined Molar Masses for Heparin Oligosaccharides:Protein Complexes 85

Table 2.3: Determined Molar Masses for dp18/Nrp1 and dp20/Nrp1 Complexes 86

LIST OF SUPPLEMENTAL VIDEOS

Supplemental Video 1

ACKNOWLEDGEMENTS

I would like to thank my PhD thesis advisor, Jeffrey Esko, for his guidance and mentorship during my doctoral research. I actually came to UC San Diego to work specifically in a glycoscience-based research lab. During my rotation in Jeff's lab, I didn't end up doing much science, but we bonded over wrapping glassware and Jeff's stories of his dad's fish shop in Chicago while we were moving the lab. Thank you, Jeff, for taking a chance on me and seeing me through my entire doctoral process. Your guidance has been instrumental in the success of my project. I especially want to thank you for encouraging me to mentor students in the lab and teach at UC San Diego during the summer sessions.

I would also like to thank Thomas Mandel Clausen. I know you joined this marathon of a project towards the end, but I really appreciate your support that kept me going in the last mile or so. I appreciate your encouraging words and all of our conversations, especially about what it means to be a scientist.

Thank you to my undergraduate mentees, Jeeyoung Park and Gabriel Vasquez. I know our time in lab was cut short due to the pandemic, but I enjoyed introducing you to the world of glycosciences and biomedical research. I appreciate all of your hard work and support during my thesis project. I am so proud of you two and can't wait to see what you accomplish!

I would like to thank all of the members of the Esko and Gordts labs, especially Chrissa, Anne, Bryan, Patrick, Daniel, Phillip B., Philip G., Miguel, Jessica and Charlotte. I have really appreciated the social and collaborative nature

of our labs. The camaraderie we share was a major highlight of my graduate school experience. From a technical point of view, I want to thank everyone who has taken time to teach me a new technique, explain scientific analyses, or discuss my projects with me.

Thank you to my committee members, Richard Gallo, Tracy Handel, Yishi Jin, and Karl Willert. I appreciate your constructive, yet kind, ways of pushing me and my project to the best that we could be. Thank you for your words of wisdom and guidance along the way.

Thank you to the Programs of Excellence in Glycosciences (PEG) for funding support during my doctoral research. Thank you to Tracy, Jeniffer, Amanda, and Cassandra in the Glycobiology Research and Training Center office for all your support during this time. I would also like to thank Leanne, Pat, Nicolette, and Gina in the Biomedical Sciences Graduate Program office. I deeply appreciate our interactions and how helpful you all have been throughout the years.

I am extremely grateful to have had the support of my friends along the way. The trials and tribulations of graduate school cast strong bonds of friendship among those who travel its journey together. I have appreciated developing long-lasting friendships during graduate school. I could not have completed my studies without all of you: Terry, Hannah, Elaine, Vanessa, Yon, Alex M., Michael, Sarah, Alex W., Nick, Nate, David, Vanessa, Doug, and Nessa amongst many more. You

all have helped me celebrate my victories and encouraged me throughout challenges I've faced. I am very blessed that you all are in my life.

Thank you to my entire family: my father Daniel, my mother Roberta, my sister Ashley, my brother Zach, and my brother-in-law Ian. You all have been so loving, supportive and encouraging during this time. Thank you to my father for always demonstrating working hard to get to where you want to go and helping me develop a healthy work ethic. Thank you to my mother for instilling confidence in me and helping me push past own comfort zones. Thank you to my sister for encouraging me to be myself and pursue my passions no matter what challenges I face. Thank you to my brother for exemplifying passion and persistence in pursuit of his dreams. Thank you to my brother-in-law for always providing prospective.

Thank you to my Aunt Terri, Uncle Cory, Aunt Patti, and Nana for encouraging me to pursue science and supporting me while I did my undergraduate work in biochemistry at the University of Utah. Experiences during this time led to my fascination with glycoscience research.

To Afsheen's family, Farhad, Homa, Bahram, and Alexa, who have always treated me as one of your own. I appreciate all of the love and support you all have provided over the years. We especially appreciate Homa's care packages with healthy snacks to keep our brains and bodies fueled during our late nights in lab.

Lastly, to my partner in life and the love of my life, Afsheen. I am grateful that we have walked hand-in-hand with each other through this graduate school journey. I appreciate how loving and supportive we have been to each other while

understanding the demands and sacrifices of doctoral work. As the swing says in our engagement photo, "It's the worlds job to come at you in waves. It's your job to learn how to surf." Thank you for being my partner as we learn to surf life together. Thank you for always encouraging me to pursue interests in graduate school and beyond. Thank you for being the light of my life by bringing so much laughter and joy into my life to keep me from being serious all the time. I can't wait to finish up this chapter of our lives and move onto the next with you by my side.

Chapter 1, in full, is currently being prepared as a manuscript for submission for publication of the material. CD Painter and JD Esko. Neuropilin-1 Structure/Function Relationships in Angiogenesis. *In preparation*. The dissertation author is the primary investigator and author of this material.

Chapter 2, in full, is currently being prepared as a manuscript for submission for publication of the material. CD Painter, NV Sankaranarayanan, B Nagarajan, TM Clausen, AMV West, J Park, PL Bartels, RN Porell, DR Sandoval, GJ Vasquez, PLSM Gordts, CW Vander Kooi, KD Corbett, UR Desai, JD Esko. Alteration of Neuropilin-1 and Heparan Sulfate Interaction Impairs Angiogenesis-Dependent Tumor Growth. *In preparation*. The dissertation author is the primary investigator and author of this material.

Special thanks to all of the Jeffrey Esko and Philip Gordts lab members for their help and guidance along the way. Thank you to our collaborating labs (the Desai lab at Virginia Commonwealth University, the Corbett Lab at UC San Diego, and the Godula Lab at UC San Diego) for their intellectual and scientific

contributions. Thank you also to Craig Vander Kooi at the University of Kentucky for advice on the project.

Thank you to the UC San Diego Microscopy Core, especially Marcy Erb and Jennifer Santini for their assistance with various microscopy methods and immunofluorescence staining. Thank you to the La Jolla Institute of Immunology Microscopy and Histology Core, in particular Katarzyna Dobaczewska for histology. Thank you to the Sanford Burnham Prebys Medical Discovery Institute Protein Analysis Facility, especially Andrey Bobkov, for performing and analyzing isothermal calorimetry experiments. Thank you to the UC San Diego Transgenic Mouse Core, especially Jun Zhao and Ella Kothari for performing our CRISPR RNA injections for transgenic mouse generation. Thank you to the Steven Dowdy lab for the B16-F10 melanoma cells for the tumor experiments. Thank you to the E. Yvonne Jones lab for the *mNrp1* plasmids. Thank you to these funding sources: National Institutes of Health (NIH) grants P01 HL131474 and AR073031 to J.D.E.; NINDS P30 NS047101 to UC San Diego Microscopy; and NIH grants: P42 ES010377, P30 CA023100, and P30 DK063491 to UC San Diego Transgenic Mouse Core.

VITA

2012 Honors Bachelor of Science, Biological Chemistry, University of Utah
2021 Doctor of Philosophy, Biomedical Sciences, University of California San Diego

Field of Study

2011 – 2021 Glycobiology

Publications

DR Sandoval, A Gomez Toledo, CD Painter, EM Tota, M Osman Sheikh, AMV West, MM Frank, L Wells, D Xu, R Bicknell, KD Corbett, JD Esko. Proteomics-based Screening of the Endothelial Heparan Sulfate Interactome Reveals That C-type Lectin 14a (CLEC14A) is a Heparin-binding Protein. J Biol Chem. 2020 Feb 28;295(9):2804-2821.

TM Clausen, DR Sandoval, CB Spliid, J Pihl, HR Perett, CD Painter, A Narayanan, SA Majowicz, EM Kwong, RN McVicar, BE Thacker, CA Glass, Y Zhang, JL Torres, GJ Golden, PL Bartels, RN Porell, AF Garretson, L Laubach, J Feldman, X Yin, Y Pu, BM Hauser, TM Caradonna, BP Kellman, C Martino, PLSM Gordts, SK Chanda, AG Schmidt, K Godula, SL Leibel, J Jose, KD Corbett, AB Ward, AF Carlin, JD Esko. SARS-CoV-2 Infection Depends on Cellular Heparan Sulfate and ACE2. *Cell*, 2020. 183 (4), 1043 – 1057

Honors and Awards

2018 Perseverance Award, UCSD Biomedical Sciences Program Retreat
2018 Summer Graduate Teaching Scholar, UC San Diego
2016 Outstanding Poster Presentation Award, GRC on Proteoglycans
2014-2018 Programs of Excellence in Glycosciences (PEG) NIH Training Grant
2012 *Cum Laude*, Biological Chemistry, University of Utah
2012 Undergraduate Research Scholar Designation (URSD), University of Utah
2009-2012 Crocker Science House Scholar, College of Science, University of Utah

ABSTRACT OF THE DISSERTATION

Neuropilin-1/Heparan Sulfate Interactions and Angiogenesis-Dependent Tumor Growth

by

Chelsea Danielle Painter

Doctor of Philosophy in Biomedical Sciences

University of California San Diego, 2021

Professor Jeffrey Esko, Chair

Neuropilin-1 (Nrp1) acts as a coreceptor with Vascular Endothelial Growth Factor Receptor (VEGFR) to facilitate binding of its ligand, Vascular Endothelial Growth Factor (VEGF) and downstream signaling that leads to angiogenesis.

Heparan sulfate has been shown to be a cofactor facilitating the interaction of Nrp1 with VEGF/VEGFRs, but the functional significance of this interaction has not been established. Nrp1 mediates angiogenesis including branching and organization of vessels through its role in tip cell function and interactions with VEGFR/VEGFs. This dissertation focuses on how Nrp1 interaction with heparin/heparan sulfate influences its function as a part of the VEGF/HSPG/Nrp1/VEGFR2 complex and the resulting effects on tumor angiogenesis. Chapter 1 is a mini-review on the VEGF/HSPG/Nrp1/VEGFR2 complex, which serves as a model for understanding how binding of glycan ligands to proteins modulate their biological effects. Chapter 2 focuses on the molecular modeling and biochemical mapping of the heparin/heparan sulfate binding site in Nrp1 along with investigations into the biological significance of the interaction *in vivo*. In order to map the heparin/heparan sulfate binding site in Nrp1, we completed a combinatorial library screening using heparin oligosaccharides followed by molecular dynamic simulations of a best-fit tetradecasaccharide. We then created and expressed a series of recombinant Nrp1 mutants to identify the specific amino acids that interact with heparin and heparan sulfate. Specific mutations in the b1 and b2 domains of Nrp1 decreased binding to heparin and cell surface heparan sulfate. These mutants also prevent heparin-induced stabilization of the protein during thermal denaturation. Heparin-induced dimerization of Nrp1 was found to be length-dependent and dependent on key amino acid residues in the b1 and b2 domains, specifically arginine 513 and lysine 514. Heparin icosasaccharides induced a

1:2 heparin/Nrp1 complex as measured by isothermal calorimetry. Knock-in mice expressing Nrp1 deficient in heparan sulfate binding (*Nrp1^{D}*) were created using CRISPR/Cas9 gene targeting. Analysis of subcutaneous tumor formation revealed that *Nrp1^{D}* mice exhibit a reduction in angiogenesis-dependent tumor growth compared to wildtype controls. This finding suggests that the interaction of Nrp1 with heparan sulfate modulates its function in pathological angiogenesis. Chapter 3 is an extended discussion on these findings, their significance and future directions. The work completed in this dissertation confirms and further elucidates the heparin/heparan sulfate binding groove in mouse Nrp1, establishes a 1:2 heparin/protein complex, and demonstrates the biological significance for the heparan sulfate/Nrp1 interaction *in vivo*.

Chapter 1: Neuropilin-1 Structure/Function Relationships in Angiogenesis

1.1 Introduction

The circulatory system is one of the earliest systems to develop *in utero* [1]. This critical system brings nutrients and oxygen to the rapidly developing parts of the body as well as carry away waste products from metabolism. The primitive circulatory system is developed through vasculogenesis, where endothelial cells encapsulate blood cells to form the initial blood vessels [2]. As these initial vascular networks must expand to fulfill the needs of the developing tissue, the development of new blood vessels from the existing vasculature, known as angiogenesis, must occur [2]. Existing endothelial cells respond to angiogenic stimuli, such as Vascular Endothelial Growth Factor (VEGF) ligands, and begin the process of constructing a new blood vessel in the direction of the signal. This process allows for the intense expansion of the early circulatory system, on which, depends the rest of development [2, 3].

This programming of the endothelial cells to respond to angiogenic signals can also be manipulated by tumors [4]. As tumors grow, they become hypoxic and express HIF-1a, which induces pro-angiogenic ligands, including VEGF [5]. The resulting increase in blood vessels and therefore blood flow and nutrients to the tumor cells allows them to continue their rapid proliferation [6]. Indeed, in the absence of angiogenesis, tumors can only reach a small diameter, limited by access to nutrients and the disposal of waste products.

The signaling processes that support and guide angiogenesis are based on molecular interactions between a number of growth factors, receptors and

coreceptors, and a carbohydrate ligand called heparan sulfate. Understanding these interactions requires exploration of the structure and function of these macromolecular signaling complexes. This chapter discusses the interactions between ligands, receptor, and co-receptor in the VEGF/HSPG/Nrp1/VEGFR2 complex with an emphasis on how these interactions contribute to its overall function. Neuropilin-1 (Nrp1) is the foundational member of the complex due to its interactions with all other complex components. Examples are provided of methodologies to study interactions between VEGF, Vascular Endothelial Growth Factor Receptor-2 (VEGFR2), Nrp1, and heparan sulfate proteoglycans (HSPGs) as well as the complex in its entirety. Lastly, the application of these findings to the role of Nrp1 in cardiac development and angiogenesis *in vivo* are addressed.

1.2 Neuropilin Family: Expression and Structure

One functional complex that responds to the proangiogenic growth factor, VEGF, is composed of a signaling receptor, VEGFR2, a co-receptor Nrp1 and one or more heparan sulfate proteoglycans [7]. The structures of these three cell surface receptors promotes their interaction in order to form a complex that is responsive to VEGF. In addition, Nrp1 also plays a role in a complex composed of plexin, Nrp1, and one or more semaphorins (Sema), which provides guidance cues during axon guidance [8-12]. The location of Nrp1 as a plasma membrane protein allows its interaction with ligands and coreceptors whose signaling drives angiogenic responses in endothelial cells and axon guidance in the neurons. This

ability to bind a multitude of co-receptors and ligands is possible due to the structure of the extracellular domain of Nrp1 [13].

The first neuropilin glycoprotein was originally discovered as a cell adhesion molecule in the nervous system of *Xenopus Laevis* tadpoles in 1987 [14]. After the identification of its homologs in chicken and mice, Nrp1 was considered to be a heavily conserved protein amongst vertebrates [15-17]. Another member of the neuropilin family, neuropilin-2, was discovered in 1997 as a receptor for semaphorin ligands and in 1998, it was shown to be a co-receptor for VEGF ligands [18, 19]. These two conserved Nrp family members, Nrp1 and Nrp2, possess almost identical domain structure and share 44% identical amino acids [18, 20, 21]. The *Nrp* genes have alternative splice forms including a full-length transmembrane cell surface receptor as well as shorter, soluble forms consisting of the extracellular domains only that are secreted. The soluble forms of the Nrp1 proteins are unable to signal due to the lack of the transmembrane and intracellular domains so they are thought to act as extracellular decoys for Nrp1 ligands [22, 23].

During development, Nrp1 is primarily expressed in the nervous system and the cardiovascular system [13]. Specific types of neurons express *Nrp1* in the developing nervous system including some of the cranial nerves as well as the sensory and motor nerves in the spinal cord [13, 16]. In the developing cardiovascular system, *Nrp1* is expressed mainly by the endothelial cells as well as cardiac neural crest cells [19, 24-26]. As for the *Nrp1* splice variants, *in situ*

hybridization was used to look at their expression in human tissues [22]. The full length transmembrane *Nrp1* was found in the keratinocytes and blood vessels of skin, the epithelium and endothelium of breast tissue, the glomeruli capillaries of the kidney and the veins in the liver. Interestingly, soluble *Nrp1* was detected in the hepatocytes and the tubules of the liver and kidney, respectively, but was not detected in the blood vessels of either organ. mRNA for soluble *Nrp1* was also not present in the skin or breast tissue [22]. More recently, *Nrp*1 was also found to be expressed in a variety of immune cells, including dendritic cells and some T cells [27, 28].

Multiple tumor types express *Nrp1* where it promotes pathological angiogenesis [29]. Tumor progression of various tumor types is associated with increased expression of *Nrp1* [29]. *Nrp1* is the major isoform expressed in carcinomas while neuronal tumors and melanomas primarily express *Nrp2* [30]. Overexpression of *Nrp1* in a rat prostate carcinoma model led to considerable increase in tumor size likely due to increased vascularization as well as a reduction in tumor cell apoptosis [31]. The various roles of Nrp1 in tumor biology have been reviewed previously [29, 30]. The spatiotemporal expression of Nrp1 gives rise to its key roles in a variety of biological processes.

The Nrp1 protein is 923 amino acids long and consists of a signal peptide (21 amino acids), five extracellular domains (835 amino acids total), a transmembrane domain (23 amino acids) and a small catalytically inactive intracellular domain (44 amino acids) [23, 32]. The domain structure of Nrp1

includes two complement binding CUB (complement C1r/C1s, Uegf, Bmp1) domains (a1 and a2), two coagulation factor domains (b1 and b2), a MAM (meprin, A-5 protein, and receptor protein-tyrosine phosphatase mu) domain (c), a transmembrane domain and a short C-terminus cytoplasmic tail (Fig. 1.1) [33, 34]. The a1 and a2 domains are responsible for binding to the Sema domain of Sema3 ligands and also facilitate interaction with VEGF [35, 36]. The b1 and b2 domains bind the c-terminal domain of both VEGF and Sema3 ligands [36, 37]. The b1 and b2 domains interact to form an electropositive patch implicated as the heparin binding domain [36, 38]. The c domain has been demonstrated as necessary, but not sufficient, for oligomerization of the Nrp1 into either homo- or hetero-oligomer complexes [8, 39]. The transmembrane domain also contributes to the oligomerization of Nrp1 [40]. Lastly, the cytoplasmic intracellular domain of Nrp1 is composed of three amino acid residues, SEA (serine-glutamine-alanine), that are able to engage with PDZ-domain (post synaptic density protein (PSD95), Drosophila disc large tumor suppressor (Dlg1), and zonula occludens-1 protein (zo-1)) containing intracellular proteins [23]. Neuropilins have also been shown to be post-translationally modified with asparagine linked N-glycans and glycosaminoglycan chains. Both Nrp1 and Nrp2 have N-glycans present as demonstrated by altered molecular weight in immunoblots following tunicamycin treatment of COS7 cells to prevent N-glycosylation [32, 41]. Between its ligand binding domains and its oligomerization domain, Nrp1 has an attachment site for a covalently attached glycosaminoglycan (GAG) chain that can be either

chondroitin sulfate or heparan sulfate at conserved residue Ser612 [27, 42]. Typically, this GAG-modified Nrp1 is only a minor fraction of the total Nrp1 seen by immunoblotting [32]. In HUVECs, the GAG containing Nrp1 is decorated with comparable levels of chondroitin sulfate and heparan sulfate while vascular smooth muscle cells primarily express Nrp1 with chondroitin sulfate [42]. Chondroitin sulfate-modified Nrp1 has also been identified in a wide variety of human tumor cell lines including ACHN, MDA-MB-231, Skov-3, A549 and U87MG [43]. Neuropilin-2 has not been found to be modified by GAGs [32].

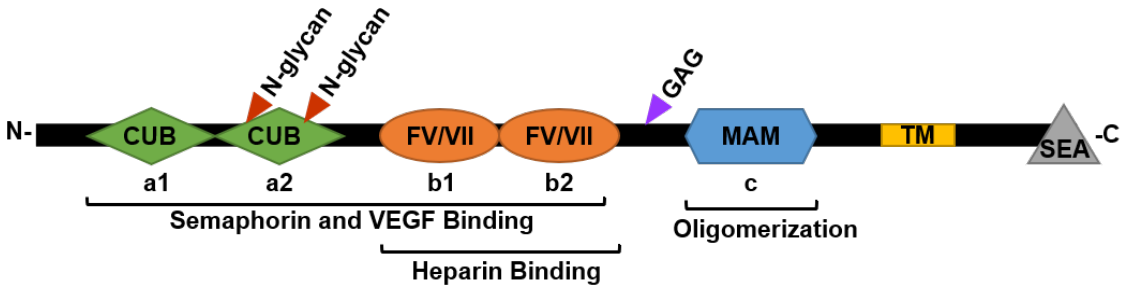

Figure 1.1: Domain Structure of Neuropilin-1

The domain structure of Nrp1 includes two complement binding CUB domains (a1 and a2; green diamonds), two coagulation factor domains (b1 and b2; orange ovals), a MAM domain (c; blue hexagon), a transmembrane domain (yellow rectangle) and a short C-terminus cytoplasmic tail (gray triangle) [33, 34]. The a1, a2, b1, and b2 domains have been implicated in mediating Nrp1 interaction with its ligands, semaphorins and VEGFs [35-37]. In addition, the b1 and b2 domains also contain the heparin binding domain of Nrp1 [36, 38]. The c domain is necessary for oligomerization, but has been determined to be insufficient to promote oligomerization by itself [8, 39]. The transmembrane domain also contributes to the oligomerization of Nrp1 [40]. Neuropilins have also been shown to be post-translationally modified with asparagine linked N-glycans (red triangles) [32]. Between its ligand binding domains and its oligomerization domain, Nrp1 has an attachment site for a covalently attached glycosaminoglycan (GAG) chain (purple triangle) that can be either chondroitin sulfate or heparan sulfate at conserved residue Ser612 [27, 42].

1.3 Introduction of the VEGF/HSPG/Nrp1/VEGFR2 Complex

The VEGFR/Nrp1/HSPG complex binds and transduces signaling of the VEGF ligand. VEGFA is a secreted glycoprotein that is dimeric in nature due to disulfide bonds [44]. The *vegfa* gene is eight exons long and produces three major alternative splice variants, although sixteen distinct isoforms have been identified (Fig. 1.2A) [45, 46]. Each isoform annotation refers to the number of amino acids it contains which differs between the human and mice isoforms by one amino acid. $VEGF_{189}$, $VEGF_{165}$, and $VEGF_{121}$ are the major isoforms in humans while $VEGF_{188}$, $VEGF_{164}$, and $VEGF_{120}$ are the major isoforms in mice [23]. This difference in amino acids is due to the number of domains presence in each isoform of the protein. Exon 6 and 7 are the most variable between the isoforms. $VEGF_{120}$ does not contain the domains produced from exons 6 and 7, $VEGF_{165}$ contains the domain produced from exon 7, and $VEGF_{189}$ contains both of the domains produced from exons 6 and 7 (Fig. 1.2A) [47]. Additional VEGF isoforms can be generated from proteolytic processing of these major splice variants [48].

The presence or absence of domains in each of the isoforms impacts each isoform's binding to its receptors and co-receptors. Domains encoded by exons 1 through 5 are present in all VEGFA isoforms and includes a cysteine knot motif [49]. These domains mediate VEGF binding to VEGFR2, one of the main receptor tyrosine kinases (RTKs) for VEGF, especially in endothelial cells [48, 50-54]. Since these domains are present in all VEGFA isoforms, they are considered to all have the same affinity for the VEGFR2 [55]. All of the major

isoforms share the same C-terminus encoded by exon 8. This terminal domain as well as the domains encoded by exons 6 and 7 have been found to be involved in VEGF binding to Nrp1 [7, 23]. The C-terminal end encoded by exon 8 has been shown to be critical for Nrp1 binding, but it has yet to be thoroughly demonstrated that it is sufficient for binding [7, 49]. Some studies have indicated that $VEGF_{121}$, which lacks exon 7, but contains exon 8, is still able to bind Nrp1 albeit with altered kinetics and affinity [49, 52]. Other studies, reviewed thoroughly by Sarabipour and Mac Gabhann, have not provided conclusive evidence that $VEGF_{121}$ is able to bind Nrp1 [7]. Critics point out that $VEGF_{121}$ contains exon 8, which has been shown to be necessary to bind Nrp1, while others conjecture that a form of cleaved $VEGF_{121}$ has been unintentionally used in other assays [52, 56]. Exons 6 and 7 encode a heparin binding domain that is present in $VEGF_{165}$ (exon 6) and $VEGF_{189}$ (exon 6 and 7), which allows them to bind to heparan sulfate proteoglycans (Fig. 1.2B) [7].

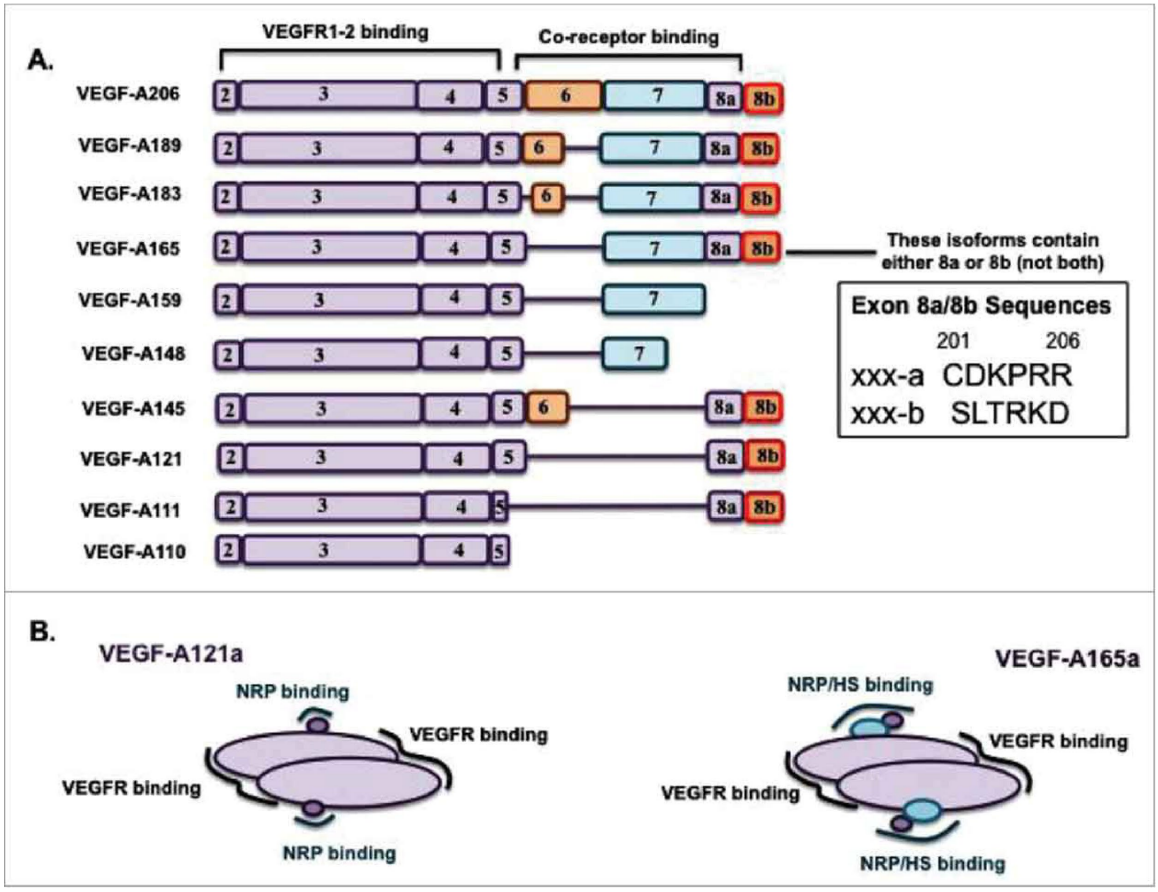

Figure 1.2: Representations of the splice variants of human VEGF-A

A, Alternative splicing of exons within the VEGF-A gene produces multiple splice isoforms. Isoforms are designated by the number of amino acids they contain in the mature protein. Exon 8 can be present as either its 8a or 8b sequence as shown in the insert. Not shown in this diagram is the signal peptide, which is cleaved in the mature protein, consisting of exon 1 and four amino acids at the beginning of exon 2. Exons 2-5 are used to bind to VEGFRs while exons 6-8a dictate VEGF interaction with co-receptors such as neuropilin-1 (NRP) and heparan sulfate (HS) proteoglycans. The presence or absence of these encoded domains within each isoform seems to determine the interaction and its affinity of VEGF with its co-receptors. **B**, VEGF is a secreted glycoprotein that is dimeric in nature due to disulfide bonds between cysteines [44]. As all isoforms contain exons 2-5, they are all able to engage VEGFRs. As $VEGF_{121}$ lacks exons 6 and 7 that compose the heparin binding domain (left), it is unable to engage HS. It may still interact with NRP through its exon 8 although studies have not yet provided conclusive evidence. $VEGF_{165}$ is able to engage with both NRP and HS since it contains exons 7 and 8. (Adapted from [7]. Permission granted from the publisher, Taylor and Francis.)

VEGF interaction with Nrp1 has been characterized, but Nrp1 may only serve as a co-receptor for the ligand due to its supposed lack of intrinsic catalytic activity [44]. The main cognate receptors for VEGFs are RTKs known as the Vascular Endothelial Growth Factor Receptors (VEGFRs), VEGFR1 and VEGFR2. The extracellular portion of these receptors is composed of seven Ig-like domains which are anchored to the membrane by a single-pass transmembrane region [57-59]. The intracellular section consists of a kinase insert domain within a split conserved tyrosine kinase domain [51, 52, 60]. VEGF binding is mediated by the second and third Ig-like domain of the VEGFR [61-63]. VEGFRs have been suggested to interact with Nrp1 in heterodimers through their transmembrane and intracellular domains [7]. In endothelial cells, VEGFR2 is the main receptor tyrosine kinase for VEGF-induced signal transduction leading to angiogenesis and vascular permeability [6, 48, 50, 52, 54]. Activation of VEGFR2 is induced by VEGF binding promoting homo- and hetero-dimerization of the receptor [52, 57-59]. The resulting phosphorylation of specific tyrosine residues within the intracellular portion of the receptor activates downstream signaling cascades through a multitude of recruited adaptor proteins [6, 55].

Since VEGF binds VEGFR2 and Nrp1 through different domains, it is thought to bridge the two cell surface receptors as part of a functional complex [7]. The dependence of the formation of the VEGFR2/Nrp1 co-complex on the presence of VEGF is disputed. Some studies have reported that co-complex formation requires induction by VEGF based on the demonstration that if

VEGF/Nrp1 binding is disrupted or if $VEGF_{165}$ is absent, VEGFR2 and Nrp1 do not coimmunoprecipitate [64, 65]. However, another study has observed Nrp1/VEGFR2 complex formation in the absence of the VEGF ligand [66].

This controversy has been examined through the use of quantitative FRET-based methods to look at complex formation on the cell surface [67]. When Nrp1 is allowed to self-associate on the cell surface, it appears to form an equilibrium between monomers and larger order oligomers. However, when $VEGF_{165}$ is present, Nrp1 tends towards the dimeric state. Interestingly, as the concentration of Nrp1 increases on the surface, the monomer accumulates, even in the presence of $VEGF_{165}$. This may be due to a shift from Nrp1 dimers bound to a VEGF dimer to a Nrp1 monomer engaging a VEGF dimer [67]. These findings suggest that VEGF binds to Nrp1 and shifts the equilibrium towards Nrp1 dimers. When VEGFR2 is allowed to self-associate on the cell surface, it also forms an equilibrium between monomers and dimers. When VEGFR2 and Nrp1 are both present on the cell surface, the amount of Nrp1 protein in the oligomeric state decreases, consistent with the idea that the two proteins interact and form stable complexes. When VEGF is added to cells expressing both VEGFR2 and Nrp1, Nrp1 homo-oligomers increase, as observed in the absence of VEGFR2, but in this case it is thought that a complex of VEGFR2/Nrp1/VEGF forms, most likely as a 2:2:2 complex [67]. However, when the FRET system is changed to measure energy transfer between VEGFR2 and Nrp1, no difference in FRET is observed whether $VEGF_{165}$ is present or absent suggesting that VEGFR2 and Nrp1 may

associate on the cell surface without induction by $VEGF_{165}$ [67]. Note that all of these studies were performed without regard to heparan sulfate.

1.4 The Role of Neuropilin-1 in the Complex

Nrp1 is generally accepted to be the co-receptor with VEGFR2 to engage the dimeric VEGF ligand through the promotion and stabilization of the resulting ternary complex [48]. In addition, its presence increases VEGF-induced VEGFR2 phosphorylation [65, 66, 68]. This effect is likely due to the ability of Nrp1 to enhance the affinity of $VEGF_{165}$ for the VEGFR2/Nrp1 complex over its affinity to each of the receptors alone as seen in both solution-based and computational experiments [69, 70]. Interestingly, Nrp1 may also regulate the expression of the VEGFR2 receptor as seen by a reduction of VEGFR2 expression by western blot of lung tissue from endothelial specific *Nrp1* knockout embryos [71].

1.5 Interactions Between VEGF and Neuropilin-1

Nrp1 was initially discovered as a receptor for the VEGF ligand in tumor cell lines and human umbilical cord endothelial cells (HUVECs) [72]. It was later determined to act as a co-receptor for VEGFR2 [19]. The domains in Nrp1 responsible for binding were initially identified by examination of binding by Nrp1 lacking different extracellular domains [35, 36]. In one study, Nrp1 protein expressed in COS-1 cells without the b1 domains showed a complete lack of binding to $VEGF_{165}$ whereas deletion of the b2 domain reduced binding by

50% [35]. These results suggest that the b1 domain of Nrp1 is required for $VEGF_{165}$ binding while the b2 domain partially contributes to the interaction. In another study, Nrp1 proteins with different combinations of the extracellular subdomains were expressed as secreted proteins and purified [36]. These recombinant proteins were then used in solution-based assays and cell surface competition assays to assess their binding to $VEGF_{165}$. In both assays, both of the b1 and b2 domains were needed to bind $VEGF_{165}$ [36]. In addition, a recombinant a1a2b1b2 Nrp1 protein demonstrated an increase in binding $VEGF_{165}$ compared to the b1b2 protein in both of the assays, suggesting that the a1 and a2 domains somehow augment the interaction between the b1b2 domains and $VEGF_{165}$ [36].

Further studies have characterized the molecular interactions between Nrp1 and $VEGF_{165}$ through the identification of amino acid residues critical for the interaction. The Nrp1 b1 domain contains a distinct binding pocket for C-terminal arginine residues, which have been found in all proteins and peptides that bind Nrp1 so far [38, 49, 73, 74]. Initial studies involved the co-crystallization of Nrp1 b1b2 domains with tuftsin, a short peptide (TKPR) that has a similar residue sequence to the terminal residues of exon 8 in VEGF including the C-terminal arginine [38]. The tetrapeptide was found to engage directly with residues Y297, W301, D320, S346, E348, T349, and Y353. Interestingly, upon tuftsin binding to Nrp1, residues D320, Y297, and Y353 all change the positioning of their side chains to engage the peptide compared to the unbound state [38]. These results were extrapolated to Nrp1 binding to $VEGF_{165}$ through the examination of a triple

alanine mutant in Nrp1 protein (b1b2 domains; S346A, E348A, T349A) for $VEGF_{165}$ binding. In a pull-down assay, this mutant protein was unable to pull down $VEGF_{165}$ unlike wildtype Nrp1 [38]. Individual alanine mutagenesis of the Y297, W301, D320, S346, T349, and Y353 residues were later found to completely abolish $VEGF_{165}$ binding to COS7 expressing these full-length mutant Nrp1 proteins [64].

The analysis of the $VEGF_{165}$ and Nrp1 co-crystal further supports that these Nrp1 residues contribute significantly to the interaction as well as characterizing the contributions of the residues in $VEGF_{165}$. Residues from both exon 7 and exon 8 were found to facilitate $VEGF_{164}$ interaction with Nrp1, but in different ways. Exon 7 residues contribute to the specificity of the interaction while exon 8 confer the high affinity [49]. More specifically, the C-terminal arginine, R164, in $VEGF_{164}$ was found to be the residue that contributes significantly to the interaction [49]. Mutagenesis of this residue to an alanine reduced VEGF binding to Nrp1 by 97% while a glutamic acid mutation abolished binding altogether [49]. The side chain of Arg164 in VEGF forms a salt bridge with Asp320 while its free carboxyl group engages with Tyr353, Ser346, and Thr349 in Nrp1 through hydrogen bonds (Fig. 1.3A) [49]. These same interactions are seen when Nrp1 binds tuftsin (Fig. 1.3B) [38]. Residues Lys146, Glu151, and Glu154 encoded by exon 7 in $VEGF_{164}$ were found to interact with Nrp1 with Glu154 being the major contributor [49]. Mutation of this residue decreased binding to Nrp1, but not nearly as efficiently as the R164 alanine or glutamic acid mutants. These residues were

shown to engage the L1 loop of Nrp1 which has a different sequence than the L1 loop of Nrp2 (Fig. 1.3C). When Nrp1 was mutated to mimic Nrp2 in this region, $VEGF_{164}$ binding was reduced by 75%. Therefore, these residues in exon 7 seem to confer specificity of $VEGF_{165}$ to Nrp1 over Nrp2. In addition, $VEGF_{120}$ which contains exon 8, but lacks exon 7, binds Nrp2 and Nrp1 with virtually the same affinity [49]. These results further elucidate how specific amino acids dictate binding between the different VEGF isoforms and the two Nrp co-receptors.

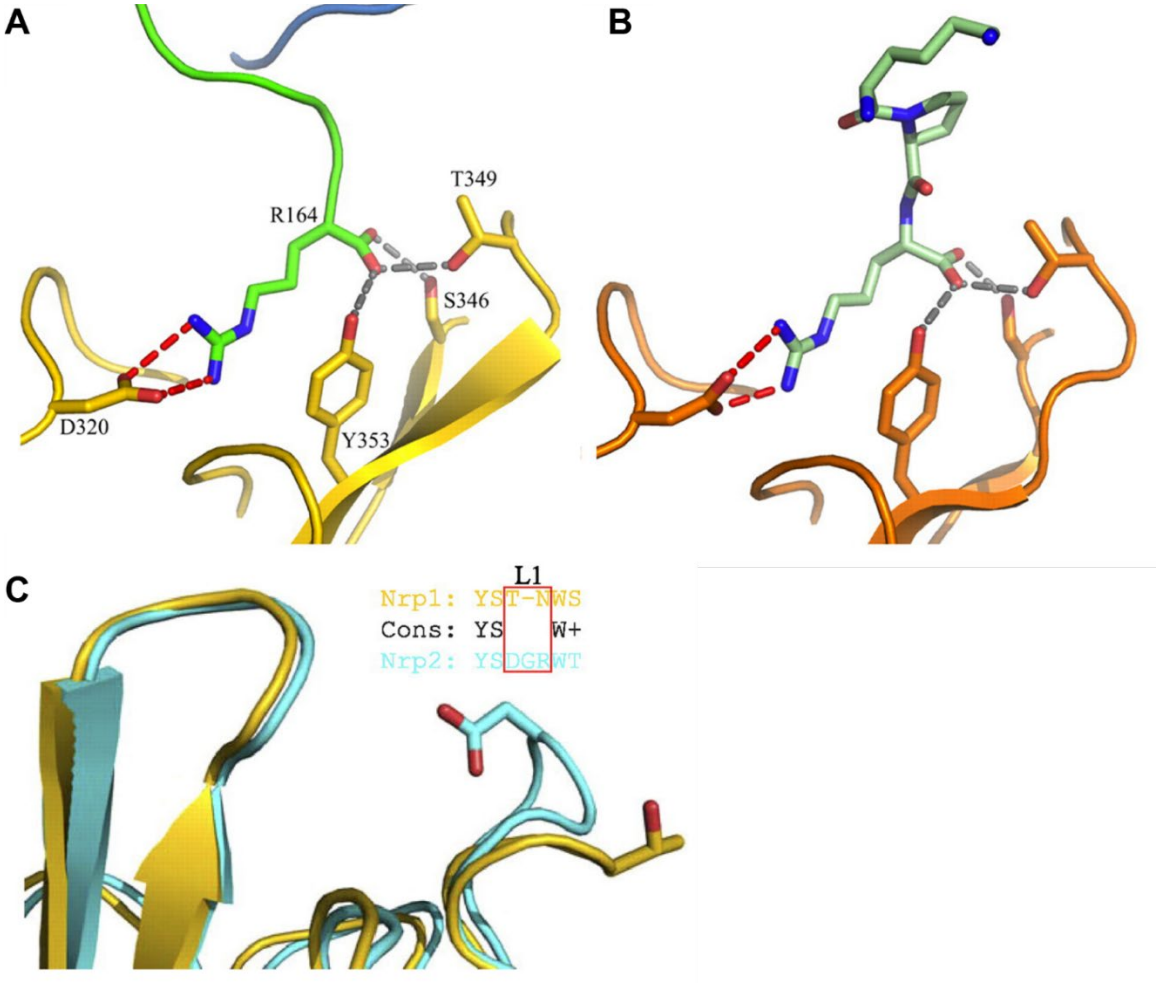

Figure 1.3: Terminal Arginine Residues of VEGFA and Tuftsin Occupy Binding Recess in b1 Domain of Neuropilin-1

A, The binding recess in the b1 domain of Nrp1 is accommodating to the terminal arginine residue in VEGFA. A salt bridge is formed between D320 residue of Nrp1 and the guanidinium group of the terminal arginine residue in VEGFA, R164. Three Nrp1 residues, S346, T349, and Y353 also form hydrogen bonds with the carboxyl terminal end of VEGFA. **B**, These same interactions are seen when this same binding recess engages tuftsin (PDB code: 2ORZ). **C**, When the b1 domains of Nrp1 and Nrp2 are superimposed, they share a similar positioning with a root mean square deviation of 0.7Å. The major difference is seen in the L1 loop of Nrp1 and Nrp2, which have a different sequence in this area as seen in the insert. Alignment shows the corresponding residues as T299 in Nrp1 and D301 in Nrp2, with an additional residue in the Nrp2 loop, G302. (Adapted from [49], which is an open access article.)

Another approach to identify critical amino acids in Nrp1 focused on mutations that eliminated VEGF binding, but maintain the protein's ability to bind Sema3a. Since both ligands bind the b1 domain of Nrp1 using their C-terminal arginine residues, mutations in this area may affect binding of both ligands [75]. Three residues in Nrp1 known to interact with tuftsin (S346, E348, T349) were mutated to alanine or lysine as single point mutations or in combination with each other. Mutation of these residues to opposing charges allows the hydrophilic patch to be conserved [71]. These mutants were successful in completely reducing $VEGF_{165}$ binding, but they also abolished Sema3a binding. One mutation, D320K, was identified that abrogates $VEGF_{165}$ binding, but retains its ability to bind Sema3a [71]. This residue was previously shown to lose $VEGF_{165}$ binding when mutated to an alanine as well, but Sema3a binding was not assessed [64]. The determination of mutants that differentiate Nrp1 binding between the two ligands may allow for the separation of ligand-induced biological effects.

The impact of the loss of VEGF binding in Nrp1 on biological effects such as angiogenesis has been addressed through *in vivo* cell culture methods. Mutant Nrp1 containing either a Y297A or D320A mutation renders the protein unable to bind VEGF [64]. In a VEGF-stimulated migration assay, HUVECs overexpressing Nrp1 with Y297A or D320A mutations demonstrated impaired responses compared to those overexpressing wildtype Nrp1. The ability to form extensive tubular networks in response to VEGF was also diminished in HUVECs overexpressing Nrp1 with Y297A or D320A mutations versus wildtype Nrp1 [64].

These results demonstrate the effect of impaired binding between $VEGF_{165}$ and Nrp1 and support the critical role of the $VEGF_{165}$-Nrp1 interaction in angiogenesis.

1.6 Neuropilin-1 Binds to Heparin/Heparan Sulfate

The interaction between Nrp1 and VEGF is enhanced by the presence of heparin, increasing the affinity by roughly 20 to 100-fold [36, 38, 60]. The b1b2 domains of Nrp1 contain the binding site for heparin as well as for VEGF [35, 36]. Previous work by Vander Kooi and colleagues sought to further elucidate the heparin binding site in Nrp1 [38]. They expressed b1b2 domains of hNrp1 in *E. coli* and the heparin binding ability of the recombinant protein was confirmed through binding to heparin sepharose columns. They then further defined the heparin binding site on Nrp1 by starting with a region involved in Nrp1-mediated cell adhesion. They mutated three basic residues within an alleged consensus heparin binding sequence in the b2 domain [38]. A decrease in heparin binding was shown when R513, K514 and K516 were mutated to glutamate residues. A smaller decrease of heparin binding was seen when a neighboring lysine residue, K509, was mutated to glutamate, which indicated that the heparin binding site is extended. A similar domain in b1 was identified and the mutagenesis of two conserved residues near this region, R359 and K373, negatively affected heparin binding [38]. A combination of the b1 and b2 mutation sets completely abolished heparin binding [38]. Finally, an electrostatic potential map was constructed for these residues which demonstrated an electropositive groove appropriate for

heparin binding (Fig. 1.4B). This groove defined by their mutants is approximately 40 angstroms in length which equates to the length of a heparin dodecasaccharide [38]. These results have yet to be recapitulated by the mapping of the heparin binding site in non-human Nrp1 protein, although the conservation of these residues would make them candidates for future mutagenesis studies.

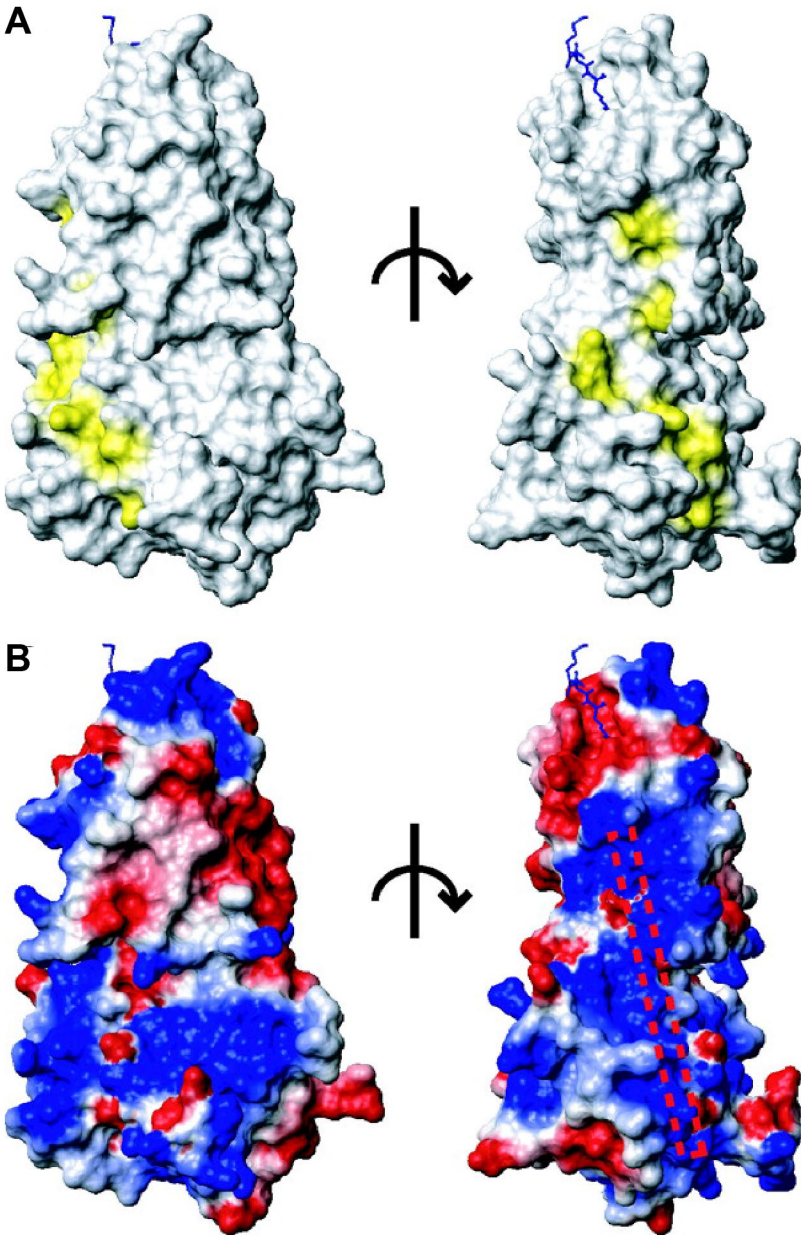

Figure 1.4: Heparin Binding Cleft in Human Neuropilin-1

A, Positioning along the hNrp1 surface of residues in the b1 and b2 domains that contribute to the interaction of hNrp1 and heparin. **B**, Electrostatic potential surface of hNrp1, where blue areas represent electropositive surfaces and red areas represent electronegative surfaces. The box (red dotted line) represents the heparin binding site as mapped by mutagenesis along the electropositive cleft. For both graphics, the blue stick representation is the peptide tuftsin in its binding pocket and the right-side images represent a 90° rotation around the vertical axis from the left-side images. (Adapted from [38], Copyright 2007 National Academy of Sciences.)

The size requirement of heparin bound by Nrp1 b1b2 was also explored through the use of native heparin and heparin oligosaccharides in a separate study. A minimum of eight saccharides was necessary to compete with the binding of native heparin to Nrp1 b1b2 while an icosasaccharide, an oligosaccharide with degree of polymerization of 20 (dp20), was able to completely inhibit [36]. However, work by Uniewicz and colleagues suggests that the heparin binding domain of Nrp1 may be more extensive [76]. Their analysis of the Nrp1 binding site involved the use a “protect and label” approach to identify lysine residues in Nrp1-Fc-dimer that interacted with heparin. The identified lysines were mapped to the a1, b1, c and L2 regions of the protein. They also explored the structural aspects of the heparin required for Nrp1 binding through analysis of the length and sulfation pattern of heparin oligosaccharides. Their results suggest a preference of a longer heparin chain over shorter oligosaccharides up to dp26. They rationalize their data by proposing that the binding site of Nrp1 in a dimeric state is longer or that its preference is for more sulfated forms of polysaccharides [76]. Although, in a separate study, the use of a Fc-chimera of the entire extracellular portion (a1a2b1b2c) of rat Nrp1 dimer demonstrated that at least a dp14 heparin oligosaccharide was needed to compete away bound heparin, but oligosaccharides longer than dp14 were not analyzed [77]. However, the use of an Fc construct of Nrp1, which occurs as a dimer, removes the effect of heparin on oligomerization and the use of heparin derivatives may not mimic heparan sulfate, which is less sulfated.

Vander Kooi and coworkers also showed by gel filtration that the addition of heparin or a heparin tetradecasaccharide was able to induce oligomerization of the Nrp1 protein [38]. Addition of a heparin hexamer was unable to induce oligomerization illustrating a minimum size requirement. Attempts to demonstrate the stoichiometry of the Nrp1b1b2 complex with heparin suggested a 2:2 ratio of Nrp1 and heparin, but efforts to accurately determine stoichiometry by isothermal calorimetry have been unproductive. In addition, it is still unknown whether the interaction between Nrp1 and heparin is biologically and functionally relevant, given that cells express heparan sulfate, which is less sulfated than heparin.

Previous experiments have used heparin to investigate Nrp1 binding because it is commercially available and various modified forms of the polysaccharide have been generated by selective desulfation. Heparin is often used as a mimetic of heparan sulfate, but heparin is more highly sulfated than heparan sulfate and is produced by mast cells [78]. However, Nrp1 is more likely to be interacting with heparan sulfate in the context of endothelial cells. Heparan sulfate is a sulfated glycosaminoglycan found as a component of extracellular matrix and plasma membrane proteoglycans. The linear polysaccharide is comprised of alternating glucosamine and uronic acid units [79]. Many types of sulfotransferases add sulfate groups at various locations on the polymerizing heparan sulfate chain (Fig. 1.5). Sulfate groups are added at the C2 of uronic acid and the N-, C6, and C3 positions of the glucosamine residues [80]. This sulfation process occurs substoichiometrically and in different sections of the chain resulting

in a variety of sulfation patterns. This produces defined domains within the chain that differ in the number of sulfated residues. N-sulfated (NS) domains contains sulfated residues while N-acetylated (NA) domains contain monosaccharides free from these sulfation and epimerization modifications [78]. The modification of the glucosamine units with a sulfate group is of interest due to its rarity, with most chains lacking the modification, and its position as the one of the last modifications in the biosynthetic pathway [81-83]. Therefore, by the time the 3-*O*-sulfotransferases (Hs3sts) act on the growing chain, the polysaccharide has already been sulfated by the N-, 2-*O*- and 6-*O*-sulfotransferases and the C5 epimerase [84, 85]. Therefore, the expression of the sulfotransferases affects the overall amount and pattern of sulfation on the resulting heparan sulfate chains [78].

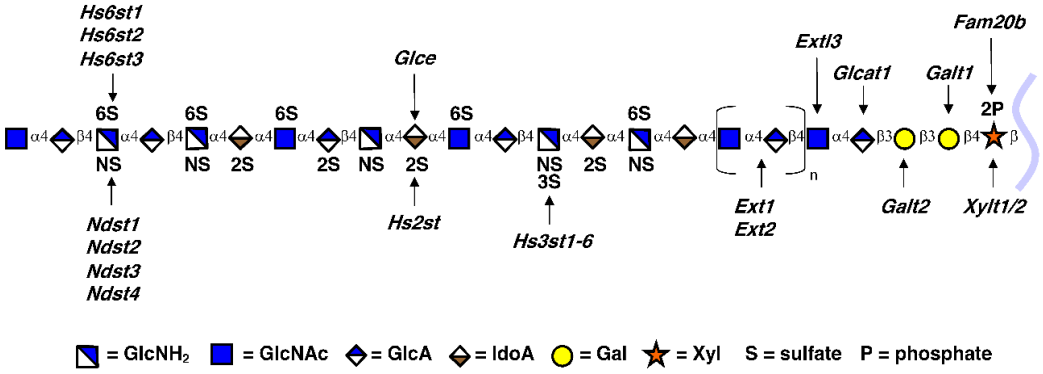

Figure 1.5: Heparan Sulfate Biosynthesis

Biosynthesis begins with the addition of a xylose to a serine residue of the protein core followed by the additional of three additional monosaccharides (glucuronic acid-galactose-galactose- xylose; GlcA-Gal-Gal-Xyl) to generate a tetrasaccharide linker. The initial *N*-acetyl-D-glucosamine (GlcNAc) sugar is added by the Extl3 enzyme which is then followed by the enzymes Ext1 and Ext2 to extend repeating units of *N*-Acetyl-D-glucosamine (GlcNAc) and glucuronic acid (GlcA). Meanwhile another family of enzymes, Ndsts removes the acetyl group from the GlcNAc residues and then decorates the resulting free amino groups with sulfate. Epimerization of some D-glucuronic acid residues is mediated by the C5 epimerase (HsGlce). Various sulfotransferases then add sulfate groups to specific positions of the monosaccharides. At the C2 position of iduronic and some glucuronic acids, sulfate is added by the uronyl 2-*O*-sulfotransferase (Hs2st). At the C6 position of the *N*-sulfoglucosamine and some *N*-acetylglucosamine residues, sulfate is added by the 6-*O*-sulfotransferases (Hs6st1-3). At the C3 position of the either *N*-sulfoglucosamine or *N*-glucosamine, sulfate is added by the 3-*O*-sulfotransferases (*Hs3st1, 2, 3a, 3b, 4, 5, 6*). The sulfation of the chain occurs substoichiometrically and in different sections of the chain resulting in a variety of sulfation patterns. This produces defined domains within the chain that differ in the number of sulfated residues. N-sulfate (NS) domains contains sulfated residues while N-acetylated (NA) domains contain monosaccharides free from these sulfation and epimerization modifications.

Nrp1 was picked up in a general screen that was focused on the identification of proteins that preferentially bound heparan sulfate containing 3-*O*-sulfation [86]. In this screen, a heparan sulfate affinity chromatography approach was used to screen various biological samples. Heparan sulfate was isolated from conditioned medium from CHO-S cells, which express heparan sulfate lacking 3-*O*-sulfation. The affinity matrices were composed of heparan sulfate modified by recombinant heparan sulfate 3-*O*-sulfotransferases and coupled to cyanogen bromide-activated Sepharose chromatography resin. Three affinity matrices were developed consisting of non-modified heparan sulfate, Hs3st1-modified heparan sulfate, and Hs3st2-modified heparan sulfate [86]. These matrices were then used to screen proteins from human, bovine and mouse sera, which is known to contain many proteins that can bind to heparin or heparan sulfate [87].

In this screen, Nrp1 demonstrated preferential binding to 3-*O*-sulfated affinity matrices, which was confirmed by western blots [86]. Recombinant human Nrp1 b1b2 domains were applied to the affinity matrices and showed very little binding to unmodified heparan sulfate, but bound significantly to the Hs3st-modified heparan sulfate. Cell surface binding assays utilizing CHO-K1, Hs3st1-transduced CHO-K1 and Hs3st2-transduced CHO-K1 demonstrated hNrp1 preference for 3-*O*-sulfated heparan sulfate over unmodified heparan sulfate on the cell surface [86]. Differential scanning fluorimetry experiments were performed utilizing structurally defined dodecasaccharides that differed only in

their modifications by Hs3sts. The dodecasaccharide with 3-*O*-sulfation provided additional stabilization to Nrp1 as reflected by a higher difference in melting temperature (ΔTm = 1.5 °C) compared to the difference in melting temperature in the presence of the non-3-*O*-sulfated dodecasaccharide (ΔTm = 0.7 °C) [86].

Since Nrp1 facilitates growth cone collapse in response to semaphorin3a (Sema3a) in neurons, studies by Thacker et al. explored how heparan sulfate 3-*O*-sulfation would affect growth cone collapse [9, 11, 86]. Growth cone collapse occurs in responsive to chemorepulsive factor, such as Sema3a, during axon guidance to help the neuron navigate to its target [10, 88]. Dorsal root ganglia (DRG) explants isolated from E13.5 C57Bl/6 mouse embryos were stimulated overnight with nerve growth factor, which promotes axonal growth from the explants. Subsequent Sema3a treatment causes growth cone collapse. 3-*O*-sulfated dodecasaccharides were potent inhibitors of collapse with an IC50 more than ten-fold reduced compared to the dodecasaccharide devoid of 3-*O*-sulfation (0.6 μg/ml versus 7.9 μg/ml) [86]. Genetic reduction of Hs3sts also influenced growth cone collapse. At low concentrations of Sema3a, DRGs from Hs3st2$^{-/-}$ embryos showed a decrease in growth cone collapse of >60% when compared to wild-type [86]. Interestingly, loss of Hs3st1 expression did not affect growth cone collapse, suggesting different functional roles for these two genes. 3-*O*-sulfation appears to affect growth cone collapse, but the Hs3sts may have different contributions to the 3-*O*-sulfation of the heparan sulfate. These *ex vivo*

experiments provide insights into how Nrp1 engagement with heparan sulfate may affect biological processes such as axon guidance.

In summary, Nrp1 contains a heparin binding site primarily in domains b1 and b2 with some support from domains a1 and a2. This site has been shown to also facilitate Nrp1 binding to heparan sulfate and cell surface heparan sulfate proteoglycans. Heparin binding induces dimerization of the extracellular domains of Nrp1, which suggests a possible role for heparan sulfate proteoglycans to promote Nrp1 dimerization on the cell surface. Nrp1 also demonstrated preferential binding to 3-*O*-sulfated heparan sulfate. The expression of the enzymes that add this rare modification to the chain is controlled in a spatiotemporal way during development [89-92]. Therefore, 3-*O*-sulfation may influence Nrp1 function *in vivo* depending on the context of their co-expression. However, how the Nrp1/heparan sulfate proteoglycan interaction affects Nrp1 roles in angiogenesis has not been explored.

1.7 Heparin Binding Capabilities of VEGF and VEGFR

In addition to Nrp1 binding heparin, other components in this complex have been found to engage with heparin. VEGF was originally found to be a heparin-binding protein as part of its purification from pituitary follicular cells [45, 93]. The structural requirements for heparin binding to VEGF and in complex with its receptors, VEGFR2 and Nrp1, has been assessed [36, 94, 95]. An octasaccharide was found to be sufficient for binding to VEGF alone which fits later modeling

studies that VEGF binding would likely require at least a hexasaccharide to fill the binding groove [95, 96]. Longer oligosaccharides (dp16-22) have been shown to be necessary to facilitate binding between VEGF and its receptors [36, 94]. VEGF has been shown to prefer more highly sulfated species, as desulfated varieties of heparin attenuate the interaction [94, 97, 98]. Despite its preference towards higher sulfated species, VEGF does not require the presence of the 3-*O*-sulfation group [95]. The length and sulfation pattern for engagement with heparan sulfate showed similar trends. A dp10 heparan sulfate oligosaccharide was the minimal length required to bind $VEGF_{165}$. Robinson and coworkers suggested that it is likely that $VEGF_{165}$ only engages seven to eight of the internal sulfated monosaccharides [99]. Longer oligosaccharides (dp22 or greater) were generated by digesting heparan sulfate with K5 lyase to release fragments containing the sulfated domains [99]. These fragments bind $VEGF_{165}$ homodimers more avidly. In competition assays, longer and more sulfated heparan sulfate chains were better competitors for full length heparan sulfate chains for $VEGF_{165}$ binding [100]. A continuous heparin/heparan sulfate binding patch formed by the interaction of Nrp1 and VEGF has been proposed as longer heparin/heparan sulfate oligosaccharides are needed to engage both ligand and receptor [38].

As mentioned above, heparin and heparan sulfate seem to strengthen the interaction between VEGF and its receptors, VEGFR2 and Nrp1 [48, 101-104]. Heparin enhanced the ability of Nrp1 b1b2 protein to pull down $VEGF_{165}$ in solution-based assays [36]. SPR studies demonstrated increased affinities of

$VEGF_{165}$ to Nrp1 when heparin was present [60]. $VEGF_{165}$ binding to cells expressing Nrp1 with mutations that abolish VEGF binding, Y297A, W301A, D320A, and Y353A, was not enhanced by the presence of heparin. However, heparin was able to partially rescue $VEGF_{165}$ binding in cells expressing Nrp1 with T316A, T349A, K351A, and W411A mutations [64]. On cells, heparan sulfate proteoglycans enhance VEGF binding to its receptors based on the observation that VEGF binding is abolished when cells were pretreated with heparin lyases [105-109]. Exogenous heparin was able to rescue this effect, suggesting that heparin and possibly heparan sulfate can act in trans to facilitate VEGF signaling [106, 107]. Similar results were found in studies using various lengths of heparin oligosaccharides to potentiate the interaction [94].

Glypican-1 was identified as a vascular specific heparan sulfate proteoglycan able to bind and augment the interaction between $VEGF_{165}$ and its cell surface receptors [109]. When VEGFR2 is expressed in CHO745 cells lacking heparan sulfate due to a deficiency in the xylosyltransferase 1 biosynthetic enzyme, VEGF binding did not occur unless exogenous heparin was added [110]. $VEGF_{164}$ demonstrated reduced binding to endothelial cells lacking N-acetylglucosamine N-deacetylase/N-sulfotransferase 1 (Ndst1) resulting in cellular heparan sulfate with lower amounts of sulfate [111]. Altered heparin oligosaccharides were unable to enhance VEGF-stimulated mitogenic activity and tube formation in HUVECs [108]. These results support the idea that VEGF binding

is potentiated by heparin and heparan sulfate and that more highly sulfated species are more potent.

Although VEGF binding to heparin/heparan sulfate has been thoroughly established, the interaction between VEGFR2 and heparin has been less well characterized. A heparin binding patch was identified in VEGFR2 and a peptide consisting of residues 647-652 (RKTKKR) was able to bind heparin [110]. In addition, VEGFR2/heparan sulfate proteoglycan complexes were identified in isolated mouse brain microvascular endothelial cells (mBMECs) by proximity ligation assays, even in the absence of added VEGF [112]. Addition of exogenous VEGF increased the number of complexes measured. Heparan sulfate proteoglycans have also been shown to affect the response of VEGFR2 to one of its agonists, gremlin [113].

1.8 Investigations of the Entire VEGF/HSPG/Nrp1/VEGFR2 Complex

Attempts to study the VEGF/HSPG/Nrp1/VEGFR2 complex in its entirety have been limited. SPR studies utilizing immobilized heparin begin to shed light on some of the intricacies of the interactions between complex members [77]. Initial heparin binding characterization of the recombinant proteins showed that VEGFR2-Fc-dimer and soluble monomeric Nrp1 does not bind heparin, but a Nrp1-Fc-dimer is competent. $VEGF_{165}$ was able to augment the interaction between VEGFR2-Fc-dimer and heparin, but no discernible difference was seen for the Nrp1-Fc-dimer. In a solid phase assay, heparin increased binding of

$VEGF_{165}$ to VEGFR2-Fc-dimer as well as Nrp1-Fc-dimer [77]. Interestingly, $VEGF_{165}$ was unable to bind the Nrp1-Fc-dimer in this method without heparin present.

The specific structural requirements to induce these interactions was also addressed with variably sulfated and sized heparin oligosaccharides in the plate binding assay [77]. None of the oligosaccharides (dp4-dp14) were able to assist $VEGF_{165}$ binding to the VEGFR2-Fc-dimer, whereas dp14 oligosaccharides were able to partially enhance the interaction between $VEGF_{165}$ and Nrp1. Overall loss of sulfation on heparin oligosaccharides impacted $VEGF_{165}$ binding to the VEGFR2-Fc-dimer while specific positional loss of sulfation along the chain affected $VEGF_{165}$ binding to the Nrp1-Fc-dimer. This study also examined how all four members of the complex engage together. Combinations of any of the members of the complex together increased binding to heparin and slowed dissociation. There was a striking synergistic increase in affinity when all three proteins (sNrp1, VEGFR2-Fc-dimer, and $VEGF_{165}$) were added to the immobilized heparin [77]. Interestingly, out of all of the combinations, the sNrp1 and VEGFR2-Fc-dimer complex demonstrated the slowest dissociation, suggesting that they may form a stable complex just between themselves. The stable interaction between VEGFR2-Fc-dimer, Nrp1 and immobilized heparin suggests that heparan sulfate proteoglycans on the cell surface may contribute to the formation and stabilization of the VEGFR2 and Nrp1 receptors on the cell surface.

1.9 Summary of the VEGF/HSPG/Nrp1/VEGFR2 Complex

In conclusion, the VEGF/HSPG/Nrp1/VEGFR2 complex is an interesting model of how heparin and heparan sulfate proteoglycans can modulate ligand/receptor/co-receptor interactions and cellular responses. Nrp1 seems to be the foundational unit of the complex as it engages every other member in the complex. The VEGF/heparin/Nrp1 complex has been suggested to have a stoichiometry of 2:2:2 while a similar ratio 2:2:2:2 for the VEGF/HSPG/Nrp1/VEGFR2 complex was recently proposed (Fig 1.6) [7, 38]. In this model, one heparan sulfate chain on the heparan sulfate proteoglycan is suggested to mediate the interaction of the $VEGF_{165}$ with the b1b2 domains in Nrp1 while a second chain may bind to the heparin binding patch on VEGFR2 between its 6th and 7th Ig-like domains. Based on the heparin binding site identification of Nrp1 [76], this second heparan sulfate chain may also engage the c domains in Nrp1 that contribute to its dimerization.

In addition, the heparan sulfate proteoglycans have been suggested to possibly interact with Nrp1 and VEGFR2 on the cell surface, even in the absence of the $VEGF_{165}$ ligand. Heparan sulfate proteoglycans may also act as through a templating mechanism in order to bring all of the components of the complex together [36, 78]. The structural requirements of $VEGF_{165}$, Nrp1 and VEGFR2 for binding heparin/heparan sulfate are inherently different, suggesting that the variably sulfated domain structure of heparan sulfate may provide a template for the formation of this complex. The preference of Nrp1 for 3-*O*-sulfation amongst

its requirements for other types of sulfation suggest that the functional form of heparan sulfate may be somewhat rare. While individual components of this quaternary complex have been examined for their ability to bind other members of the complex, the overall picture of the functional complex and its underlying molecular interactions has yet to be fully investigated. Other imaging methods are needed to understand the structure of this macromolecular complex, and new advances in cryogenic electron microscopy and chemoenzymatic methods for generating defined heparin oligosaccharides might provide the tools needed to solve this interesting structure [114].

My thesis work in chapter two addresses some of these unresolved questions about the interaction between Nrp1 and heparin/heparan sulfate. We demonstrated that longer heparin oligosaccharides (dp14-dp20) are able to induce dimerization of Nrp1 in a 1:2 heparin/Nrp1 stoichiometry. We showed that heparin binding stabilizes the protein against thermal denaturation and that Nrp1 binds heparan sulfate in the form of cell surface proteoglycans. We also mapped the heparin/heparan sulfate binding site in mouse Nrp1 which extended into in vivo mouse studies to assess the interaction between Nrp1 and heparan sulfate in pathological angiogenesis. We observed that a reduction in Nrp1 binding to heparan sulfate affects subcutaneous tumor growth.

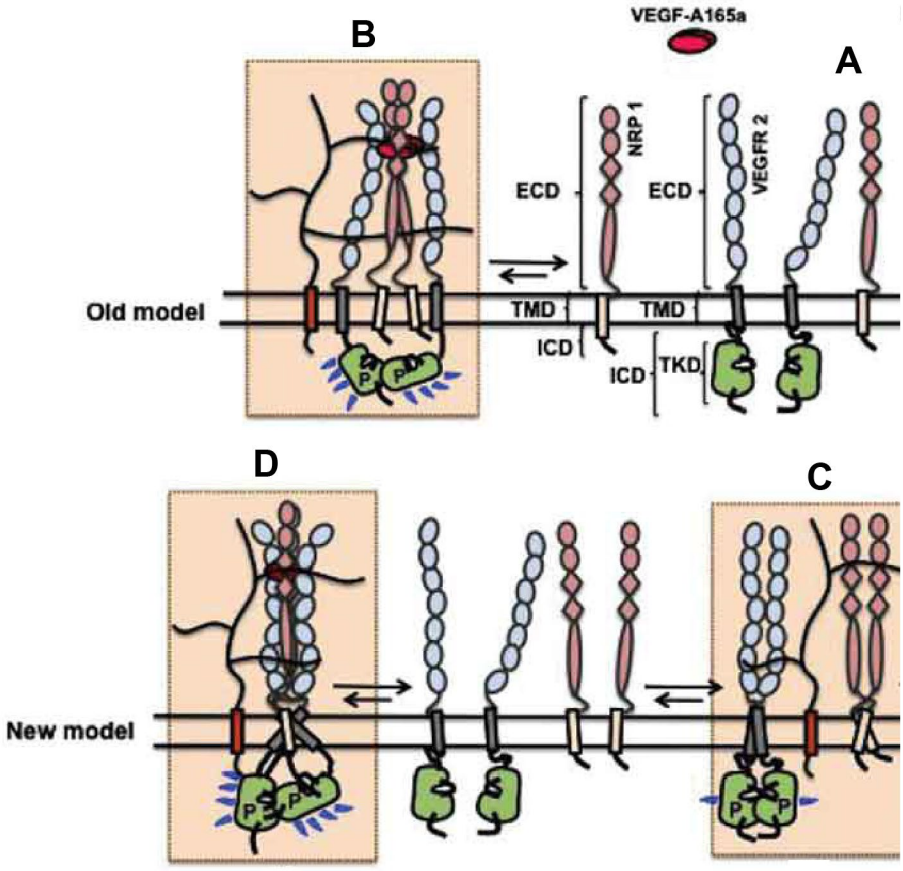

Figure 1.6: Updated Model of the VEGF165/HSPG/Nrp1/VEGFR2 Complex

Previous models of the VEGF165/HSPG/Nrp1/VEGFR2 complex implied that receptors/coreceptors in the plasma membrane are not dimerized until induced by the ligand (**A**) and that VEGF165 stimulation induces the dimerization and complexation of two VEGFR2 monomers and two Nrp1 monomers, resulting in the formation of the signaling complex (**B**). The newly proposed model [7] takes into account that HSPGs on the cell surface along with transmembrane and intracellular interactions may promote the formation of VEGFR2 homodimers, Nrp1 homodimers and VEGFR2/Nrp1 heterodimers on the cell surface independent of ligand (**C**). These dimers are then pre-posed to form the complete signaling complex when induced by the VEGF165 ligand. The binding of the heparan sulfate chains of the HSPG to the ectodomains of Nrp1 and VEGFR2 as well as VEGF165 promotes stabilization of the complex (**D**). (Adapted from [7]. Permission granted from the publisher Taylor and Francis.)

1.10 Neuropilin Structure/Function Relationship *in vivo*

Neuropilins play a role in cardiovascular development. Neuropilin expression appears to be spatiotemporally regulated in cardiovascular tissues during embryonic development, which may influence the separation of arterial and venous cells [32]. Nrp1 has been suggested to influence the trajectory of migrating cells such as endothelial tip cells at the forefront of new vessels, which parallels its influence on the trajectories of axons during neuronal development [32]. In addition, VEGF/Nrp1 signaling has been shown to be essential for cardiovascular development and Nrp1 is required in endothelial cells to support angiogenesis [26]. Nrp1 is suggested to enhance VEGF-stimulated VEGFR signaling through its complex formation with VEGFR [32]. Therefore, a change in Nrp1 structure that affects its function has the potential to affect angiogenesis, either developmental or pathological.

1.11 Examination of the Role of Neuropilin-1 in Angiogenesis

Multiple modes of altering Nrp1 structure/function relationship have been utilized in mouse models to study the structure/function relationship in the context of angiogenesis *in vivo*. Systemic overexpression models increase the expression of *Nrp1* throughout the animal, whereas systemic knockout (null) models allow studies of *Nrp1* in developmental vasculogenesis and angiogenesis. There are also conditional knockout models that use the Cre/lox system to abrogate *Nrp1* expression either temporally and/or spatially during development. In order to

examine the role of *Nrp1* in endothelial cells during angiogenesis, *Tie2-Cre+* animals, which express Cre recombinase in endothelial cells (and myeloid cells) were used to generate endothelial cell *Nrp1* null animals [115]. Lastly, there are knock-in models where some portion of the Nrp1 structure has been altered by incorporating point mutations that affect the interaction of Nrp1 with its binding partners. Two mouse models expressing Nrp1 that no longer binds to VEGF have been generated. One model contains a Y297A substitution in Nrp1 that also leads to a significant decrease in *Nrp1* expression and a hypomorphic state [116]. The other contains a D320K mutation that expresses normal levels of Nrp1 protein with altered function [71]. The study of these mutants allows a direct way to assess the impact of Nrp1 and on angiogenesis *in vivo*.

Transgenic overexpression of *Nrp1* in mice leads to embryonic lethality at 12.5-15.5 dpc [13]. Observation of the red-tinted embryos revealed various types of abnormalities in their vasculature including excessive number, dilation, and hemorrhaging of the blood vessels. Embryonic hearts were also maldeveloped with larger atria with thinner walls. Systemic *Nrp1* null mice die in utero (E10-13.5) due to cardiovascular and neuronal abnormalities [17, 117]. The embryos (*Nrp1*$^{-/-}$) present with vascularization deficits in neural tissues as well as in the yolk sac [117]. Heterozygous animals did not present the same vascular defects as the null animals in the neural tissues. *Nrp1*$^{-/-}$;*Nrp2*$^{-/-}$ mice showed earlier embryonic lethality (E8.5) as well as grievous vascular abnormalities that phenocopied *Vegf* and *Vegfr2* knockout animals [118-120]. Unlike the *Nrp1*$^{-/-}$ embryos, yolk sacs from

Nrp1$^{-/-}$;*Nrp2*$^{-/-}$ animals were completely devoid of organized vascularization [118]. The severe phenotypes due to the lack of *Nrp1* expression support a critical role for Nrp1 in developmental angiogenesis and suggests that normal cardiovascular development depends on the proper spatiotemporal expression of Nrp1 [13].

To isolate the effects of Nrp1 depletion to endothelial cells, conditionally null animals have been generated using *Nrp1*$^{flox/flox}$ animals crossed to *Tie2-Cre+* expressing mice. The *Nrp1*$^{flox/flox}$ (*Nrp1*$^{fl/fl}$) mouse does not show any gross physical or behavioral phenotypes and lives to adulthood [26]. However, *Nrp1*$^{fl/fl}$*;Tie2-Cre+* mice die in utero mid-to-late gestation [26]. To overcome the embryonic lethality in the systemic and conditionally null animals, knock-in mice containing point mutations in the *Nrp1* gene have been generated. *Nrp1*$^{Y297A/Y297A}$ mice survive through embryonic development, but they do exhibit postnatal lethality and reduced body mass [116]. In contrast, the *Nrp1*$^{D320K/D320K}$ mice survive embryonic and postnatal development into adulthood, providing a more robust model to study angiogenesis and cardiovascular development [71].

The formation of the cardiac outflow tract and embryonic hindbrain angiogenesis were severely impacted in the *Nrp1*$^{-/-}$ model. The aorta and pulmonary artery are the two main arteries that come out of the heart. The ascending aorta and pulmonary trunk come from the division of the truncus arteriosus, the original outflow tract from the developing heart. The dividing structure, known as the aorticopulmonary septum, is formed from the spiraling of connecting ridges within the truncus arteriosus and invasion of myocardial and

smooth muscle cells [121]. Utilizing Indian ink to fill the hearts, the heart outflow tracts were observed to be malformed in *Nrp1*$^{-/-}$ embryos displaying signs of persistent truncus arteriosus where the separation of the truncus arteriosus was insufficient [117]. Some embryos did not exhibit any separation of the truncus arteriosus resulting in a single outflow tract from the heart. Other groups sought to explore the cardiac output tract defects using immunolabeling on serial sections of the outflow tract. Staining for PECAM, a vascular endothelial cell marker, and smooth muscle actin (SMA) differentiated the stages of outflow tract septation that were disrupted in the *Nrp1*$^{-/-}$ animals [122]. This approach demonstrated that the entire outflow tract of *Nrp1*$^{-/-}$ embryos was affected. The outflow tract rotation was defective and there was a lack of myocardial and smooth muscle cells migrating to form the aorticopulmonary septum [122].

Analysis of *Nrp1*$^{fl/fl}$*;Tie2-Cre+* mice were found to display atypical cardiac development that likely causes their mid-to-late gestation lethality. Specifically, the mice had cardiac outflow tract defects that led to persistent truncus arteriosus [26]. These results were recapitulated in the same mouse model (*Nrp1*$^{fl/-}$*;Tie2-Cre+)* using PECAM and SMA immunolabeling on serial sections of the developing outflow tracts [122]. However, when the *Nrp1*$^{Y297A/Y297A}$ embryos were used to study only VEGF/Nrp1 interaction in this process, immunolabeling showed that these mutants displayed no signs of altered cardiac outflow tracts [122]. No cardiac defects were present in the *Nrp1*$^{D320K/D320K}$ model as well [71]. Endothelial Nrp1 is indispensable for proper outflow tract development, but both VEGF binding Nrp1

appears to be dispensable. The combination of these results suggests that cardiac outflow tract development likely occurs through a VEGF-independent, Nrp1-dependent process, possibly through semaphorins or extracellular matrix components [23, 122].

In the original *Nrp1*$^{-/-}$ mice, a limited extent of vascularization was seen in some parts of the developing brain such as the neocortex and midbrain, while other areas such as the hindbrain showed more extensive vascularization, but with branching defects. *Nrp1*$^{fl/-}$;*Tie2-Cre*+ mice also exhibited atypical vasculature in the brain [26]. Vessel branching was studied extensively in the subventricular zone of the hindbrain. The hindbrain is a useful model to study early embryonic vascular development due to the specific and well-timed manner in which the vascular patterning occurs (Fig. 1.7) [123]. At E12.5, typical vascularization of the hindbrain involves formation of a subventricular plexus from vessels that have reached just below the subventricular zone as they branch out sideways from the point of entry of the vessels [123, 124]. Hindbrains of *Nrp1*$^{-/-}$ mice show a distinct decrease of vessels reaching the subventricular zone (SVZ) and those that do, fail to branch correctly. This is thought to be due to an absence of filopodia that are able to extend and move perpendicularly from the tip cell at the end of the original vessel to form the new vascular plexus [123]. *Nrp*$^{+/-}$*;Tie2-Cre*+ animals were crossed with *Nrp1*$^{fl/fl}$ to generate *Nrp1*$^{fl/+}$*;Cre*-, *Nrp1*$^{fl/-}$*;Cre*-, and *Nrp1*$^{fl/-}$*;Tie2-Cre*+ littermates. At the macroscopic level, Nrp1 heterozygous animals did not exhibit any vascular defects in the developing brain [117]. However, *Nrp1*$^{fl/-}$*;Cre*- and *Nrp1*$^{fl/+}$*;Tie2-Cre*+

mice were found to have a subtle decrease in vessel branching in the hindbrain model. *Nrp1$^{fl/-}$;Tie2-Cre+* animals exhibited a much more distinct lack of vessel branching, indicating a gene dosage effect. Some vessels in the *Nrp1$^{fl/-}$;Tie2-Cre+* hindbrains have the same tuft-like appearance as in the *Nrp1$^{-/-}$* hindbrains likely due to a lack of filopodia able to respond to the guidance cues [123, 125]. To examine further the role of the VEGF/Nrp1 interaction, hindbrains from *Nrp1$^{Y297A/Y297A}$* mice were analyzed for vessel branching within the subventricular plexus. A reduction in vessel branching was also seen in these animals, but the effect was not as profound as in the *Nrp1$^{-/-}$* or endothelial cell specific knockout hindbrains. No direct comparison to *Nrp1$^{+/-}$* or *Nrp1$^{fl/+}$;Tie2-Cre* animals was performed, but the lowered expression of Nrp1 protein in the *Nrp1$^{Y297A/Y297A}$* could be responsible for the decrease in vessel branching [116]. Although this specific hindbrain model was not assessed for the *Nrp1$^{D320K/D320K}$* animals, embryonic and neonatal brain sections stained with isolectin revealed no vascular defects in these animals. These results were interpreted to suggest that VEGF/Nrp1 interaction does not seem to be necessary for embryonic angiogenesis in the hindbrain. However, the phenotypes Nrp1 clearly plays a role in embryonic angiogenesis, perhaps by affecting filopodia response to signaling cues.

Another model to study developmental angiogenesis is in the formation of the retinal vasculature. During the first week of postnatal development (P1-P7), the superficial vascular plexus begins to take shape as the new vessels grow radially out from existing vessels in the optic nerve (Fig. 1.7). Around P7, the superficial

vascular plexus reaches the edges of the retina and begins to sprout to form the deep and intermediate vascular plexuses. At 21 days postnatal (P21), the outgrowth of all three layers of the retinal vasculature is complete [23, 124, 126]. As this model is performed during the postnatal development period, transgenic mouse models that exhibit embryonic lethality are unable to be analyzed by this method, obviating the study of systemic *Nrp1* null animals and endothelial-specific knockout animals. However, since the knock-in mice expressing Nrp1 deficient in VEGF binding survive postnatally, this model can be used to examine how the VEGF/Nrp1 interaction affects postnatal angiogenesis.

Studies of P7 retinas of the hypomorphic $Nrp1^{Y297A/Y297A}$ showed sufficient vascular density and branching, but incomplete outgrowth of the superficial vascular plexus. Vessel outgrowth in P21 retinas of the mutant mice looked much similar to the wildtype retinas although an overall decrease in vessel density was attributed to delayed deep and intermediate plexuses formation [116]. These results were reproduced in the $Nrp1^{D320K/D320K}$ mouse model [71]. The results from the Nrp1 hypomorph alone are difficult are interpret as to whether the defect is due to the decrease in Nrp1 expression or its lack of binding to VEGF. However, in combination with the results from the $Nrp1^{D320K/D320K}$ animals that expresses proper levels of Nrp1, the VEGF/Nrp1 interaction is likely a significant contributor to retinal angiogenesis in the developing mouse [23].

In summary, the various *Nrp1* genetic mouse models shed light on how Nrp1 and its interaction with VEGF affect these vascular processes. In each of the

endothelial specific *Nrp1* null models, the vascular phenotypes mimic those found in systemic Nrp1 null animals. These results illustrate the critical role of Nrp1 in endothelial cells during embryonic angiogenesis. However, the knock-in mouse models suggest the role of Nrp1 is not simply involved in VEGF signaling. Based on these results, VEGF/Nrp1 interaction appears dispensable for embryonic angiogenesis, but is needed for postnatal angiogenesis. Therefore, the role of Nrp1 in angiogenesis likely is both VEGF-dependent and VEGF-independent depending on the context and the process.

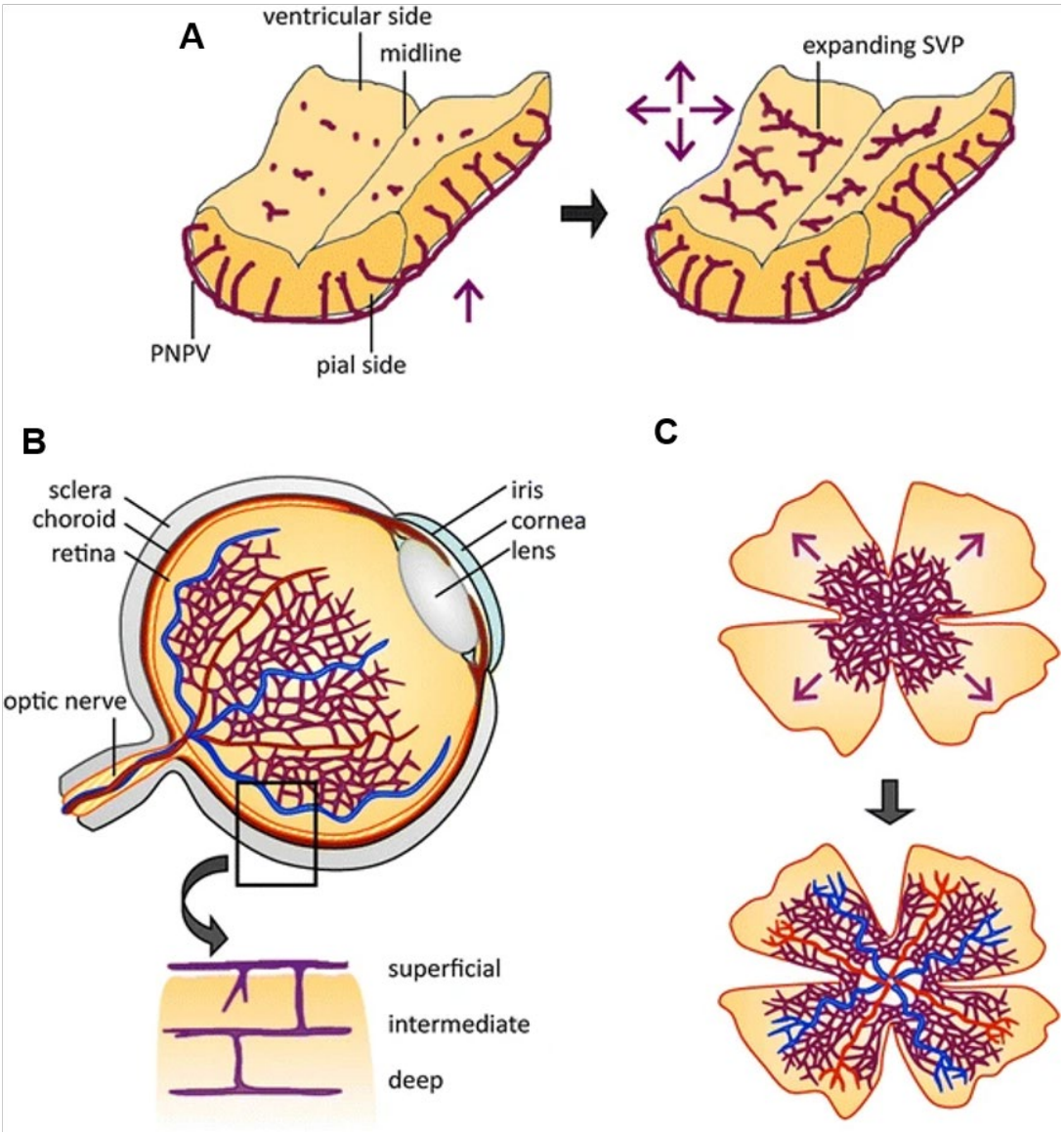

Figure 1.7: Progression of Vascularization of the Hindbrain and Retina During Development

A, Vessels extend from the perineural vascular plexus (PNPV) towards the subventricular zone (SVZ). Just below the surface of the SVZ, the vessels are guided to branch out perpendicular to their initial path to form a subventricular vascular plexus (SVP) by E12.5 [123]. **B**, Sagittal section of the human eye demonstrates the relative position of the retinal vasculature to other major structures in the eye. The zoomed view shows that the intermediate and deep plexuses come from the sprouting of the intermediate plexus. The outgrowth of all three layers of the retinal vasculature is completed by postnatal day 21 in mice [23, 126]. **C**, Vessels begin from the center of the eye near the optic nerve and extend radially to the periphery of the retina. This extension is followed by the remodeling of the vasculature to form the developed superficial plexus. (Adapted from [124], which is an open access article.)

Semaphorin signaling through neuropilins has been shown to be partially responsible for some of these developmental cardiac defects. Studies using a mouse model expressing Nrp1 deficient in semaphorin binding (*Nrp1*$^{Sema-}$) showed no signs of persistent truncus arteriosus [26]. However, in *Nrp1*$^{Sema-}$*;Nrp2*$^{-/-}$ animals, a persistent truncus arteriosus phenotype was seen in two-thirds of the embryos. These results suggest that Nrp1 also mediates signals from semaphorins during cardiac development and this signaling may occur through Nrp2 if Nrp1 is not available [122]. However, the *Nrp1*$^{Sema-}$ mouse also does not show the developmental vascularization defects characteristic of the *Nrp1*$^{-/-}$ mice [26]. Therefore, Nrp1 may also interact with other growth factor/receptor systems *in vivo* to promote developmental angiogenesis. Recent work has implicated that Nrp1 may also mediate interactions between integrins and their ligands which has been investigated through use of inhibitors blocking downstream signaling [23, 125, 127].

Through these genetic mouse models, the effects of Nrp1 interaction with its Sema and VEGF ligands have been explored. With the recent identification of heparan sulfate proteoglycans as Nrp1 ligands [86], genetic mouse models should be developed to explore how the interaction between heparan sulfate proteoglycans and Nrp1 affects Nrp1's roles in developmental and pathological angiogenesis.

1.12 Acknowledgements

Chapter 1, in full, is currently being prepared as a manuscript for submission for publication of the material. CD Painter and JD Esko. Neuropilin-1 Structure/Function Relationships in Angiogenesis. *In preparation*. The dissertation author is the primary investigator and author of this material.

Chapter 2: Alteration of Neuropilin-1 and Heparan Sulfate Interaction Impairs Angiogenesis-Dependent Tumor Growth

2.1 Abstract

Neuropilin-1 (Nrp1) acts as a coreceptor with vascular endothelial growth factor receptor to facilitate binding of its ligand, vascular endothelial growth factor. Neuropilin-1 also binds to heparan sulfate, but the functional significance of this interaction in angiogenesis has not been established. We performed a combinatorial library screening using heparin oligosaccharides followed by molecular dynamic simulations of a heparin tetradecasaccharide, which suggested a highly conserved binding site composed of amino acid residues extending across the b1 and b2 domains of murine neuropilin-1. Mutagenesis studies established the importance of arginine513 and lysine514 for binding of heparin to recombinant a1a2b1b2 subdomain. Recombinant protein bearing R513A,K514A showed significant loss of heparin-binding, heparin-induced dimerization, and thermal stabilization of recombinant protein. Isothermal calorimetry experiments suggested a 1:2 complex of dp14 heparin oligosaccharide:a1a2b1b2. To study the impact of altered heparin binding in vivo, a mutant allele of Nrp1 bearing the R513A,K514A alteration was created (*Nrp1*^{D}) and crossbred to *Nrp1*$^{+/-}$ mice to create a sensitized genetic background to examine the impact of altered heparan sulfate binding. Analysis of tumor formation showed variable effects on tumor growth in *Nrp1*$^{D/D}$ mice with a frank reduction in tumor growth in *Nrp1*$^{D/-}$ mice. Expression of the double mutant Nrp1 protein was normal in tissues, suggesting that the reduction in tumor growth was due to altered binding of heparin/heparan sulfate to Nrp1. This

finding suggests that the interaction of Nrp1 with heparan sulfate modulates its function in tumor formation most likely through altered pathological angiogenesis.

2.2 Introduction

Members of the Neuropilin (Nrp) family, neuropilin-1 (Nrp1) and neuropilin-2 (Nrp2) are plasma membrane surface receptors that have an important role in angiogenesis and axon guidance [18-20, 88, 117]. In angiogenesis, Nrp1 is a co-receptor for vascular endothelial growth factor receptor-2 (VEGFR2) and facilitates VEGF binding [19, 29]. In the central nervous system, Nrp1 forms a co-receptor with members of the plexin family to facilitate semaphorin binding and axon guidance [8, 9, 12]. Recently, Nrp1 was identified as a potential receptor for SARS-CoV-2 [128, 129]. Thus, there is great interest in understanding the structure and function of the Nrp proteins in angiogenesis, axon guidance, and infectious disease.

Nrp1 and Nrp2 are evolutionarily conserved, possessing almost identical domain structure and 44% amino acid identity [18, 20]. The domain structure of Nrp1 includes two complement binding CUB domains (a1 and a2), two coagulation factor domains (b1 and b2), a MAM domain (c), a transmembrane domain and a short C-terminal cytoplasmic tail [33, 34]. The a1 and a2 domains are responsible for binding to the Sema domain of Sema3 ligands and facilitate interaction with VEGF [35, 36]. The b1 and b2 domains bind the C-terminal domains of both VEGF and Sema3 ligands [36, 37]. The b1 and b2 domains also form an electropositive

patch implicated as a ligand binding domain for heparin [36, 38]. The c domain has been demonstrated as necessary, but not sufficient, for oligomerization of the Nrp1 into either homo- or heterooligomer complexes [18, 37, 130]. Evolutionary conservation of Nrp structure emphasizes its importance as a cell surface receptor and likely participation in angiogenesis and axon guidance across species.

Mamluk and colleagues reported that the b1b2 domain contains the binding site for heparin [36]. A minimum of eight saccharides was necessary to compete with the binding of native heparin to Nrp1 and a 20-mer was able to completely inhibit binding [36]. Heparin has also been shown to induce oligomerization of Nrp1, and the effect is size dependent [38].

Heparin is a form of heparan sulfate generated by connective tissue mast cells, and is derived from porcine or bovine intestinal mucosa [78]. The high charge density imparted to heparin by extensive sulfation of the chains makes it one of most electronegative polymers found in nature. In contrast, heparan sulfate is made by all animal cells and varies significantly in sulfation and overall structure. Recently, we showed that glucosamine 3-*O*-sulfation enhanced the binding of Nrp1 to heparan sulfate immobilized on plastic plates and to heparan sulfate present on cultured cells [86]. Chemoenzymatically synthesized 3-*O*-sulfated heparan sulfate dodecamers protected Nrp1 from thermal denaturation and inhibited Nrp1-dependent, sema-3a-induced growth cone collapse of neurons derived from murine dorsal root ganglia [86]. 3-*O*-sulfated heparan sulfate also enhanced the inhibition of endothelial cell sprouting by exogenous heparan sulfate [86].

Here, we have extended these studies to examine in greater detail the structure of the heparin/heparan sulfate binding site in Nrp1 using molecular modeling and biochemical binding assays. To explore heparin/heparan sulfate binding in Nrp1 function, key amino acid residues required for binding were identified and mutated. Inactivation of the capacity of Nrp1 to bind heparin/heparan sulfate resulted in destabilization of the protein to thermal inactivation, reduced dimerization of the protein, and reduced tumor formation *in vivo*.

2.3 Materials and Methods

2.3.1 Computational Studies to Elucidate the GAG-Binding Site(s) of Neuropilin-1

The coordinates of mouse Nrp1 were extracted from the Protein Data bank (ID 4GZ9) [12]. Protein preparation for modeling was carried out in a sequential manner by first removing water molecules from the crystal structure, adjusting the protonation states of amino acids to pH 7.2, and finally adding hydrogen atoms. The structure was then minimized with fixed heavy-atom coordinates using the Tripos force field for a maximum of 10,000 iterations subject to a termination gradient of 0.05 kcal/(mol-Å), followed by calculation of the electrostatic surface potential (ESP) of the protein (a1a2b1b2 subdomains, see Fig. 2.1A) using APBS tool in PyMOL. Based on the ESP, we divided the Nrp1 surface into 13 different plausible GAG-binding sites for implementation of the CVLS algorithm (see Fig. 2.2A). The radii of the binding sites for CVLS studies were assigned as

12 and 18 Å for di- and hexa- saccharides, respectively. The coordinates of structures in the heparin/heparan sulfate libraries were obtained from our in-house database, which was constructed earlier [131-133]. For this study, we utilized 72 disaccharides and 288 hexasaccharide sequences. CVLS screening of 72 disaccharides was performed on each of the 13 sites using the GOLD version 5.6, which uses a genetic algorithm (GA) to optimize the docking of ligands into the binding site [134]. Each sequence was docked using 100 GA runs, each consisting of 100,000 iterations. The GA runs were allowed to terminate early if the top three solutions displayed an RMSD of 2.5 Å or lower. The two best poses from each GA run were stored and analyzed at the end of the docking experiment. Experiments were carried out in triplicate, which would yield at least six solutions for each sequence. GOLDScore and RMSD were used to assess the fitness of the docked poses, as described earlier [135].

2.3.2 Molecular Dynamics

The initial structures for Molecular Dynamics (MD) runs were taken from the CVLS output files, which provided the docked complexes for the best sequence(s) in preferred sites of binding. The residue and atom labeling of the bound hexasaccharide (HS06) were altered to match the GLYCAM library (see http://glycam.org/docs/forcefield/glycam-naming-2/).

Both, protein (PDB ID: 4GZ9) and ligand (HS06), were loaded in XLEAP of AMBER18 suite and glycosidic linkages and the formal charge of HS06 were re-

checked to ensure their appropriateness [136]. Residues 1 to 143 of the protein were deleted for MD simulations because they do not play any role in GAG binding. The overall charge of the protein – ligand system was neutralized by adding appropriate number of counter ions (Na^+). Amber-ff14SB force field and GLYCAM06 force field parameters were used for protein and ligand preparation, respectively [137, 138]. This charge-neutralized complex was solvated using a three-point water (TIP3P) molecule box with a minimum distance of 12 Å between the walls to any atom of the complex. Finally, the initial parameters and the coordinate files were saved for each protein – GAG complex, respectively. Each solvated protein – GAG complex was minimized in two steps with 10 Å non-bonded cutoff. In the first step, the solute atoms were restrained with a force constant of 100 kcal/(mol. $Å^2$), while the water molecules were relaxed using 500 cycles of steepest descent and 2000 cycles of conjugate gradient method. In the second step, the whole system was relaxed using conjugate gradient minimization of 2500 cycles without any restraints.

Each solvated GAG-protein complex was equilibrated in three phases to achieve desired temperature and pressure with the integration step of 2 fs. In the first phase, the temperature was brought to 300 K using the temperature coupling with time constant 2 ps. In the second phase, the system was brought to a constant pressure using the isotropic position scaling. Equilibration was carried out for 1 ns with initial strong restrains on solute, which were systematically reduced. The production run was performed in NPT ensemble with the integration time step of

2 fs. Bonds involving hydrogen atoms were constrained using the SHAKE algorithm. Maxwell distribution was used to assign the initial velocities. Each MD trajectory was computed for one microsecond. Equilibration and simulation processes were validated by monitoring physical observables of the system including the energy (total, potential and kinetic), temperature and pressure as the function of the simulation time, which confirmed NPT ensemble settings (not shown). During the entire process, the ring puckers of IdoA/IdoA2S were maintained in their respective $^{1}C_{4}$ or $^{2}S_{O}$ using a weak torsional restrain [135].

The hydrogen bond interaction between the donor acceptor atoms of the protein and GAG (HS06) were calculated from the trajectory using the CPPTRAJ tool of AMBER using a donor-acceptor distance cutoff of 3.5 Å and angle cutoff of 135° [139]. Free energy calculations on Nrp1 – HS06 complexes were computed using post-processing MM-PB(GB)SA method [140] from the MD trajectories. MM-GBSA employed single residue energy decomposition (SRED) to estimate the energy contributions of each receptor residue in the bound state. Energy calculations were performed using the default parameter settings by employing the python version of MM-PB(GB)SA module from Amber Tool (refer to http://ambermd.org/tutorials/advanced/tutorial3/). Typically, these calculations were performed using the entire simulation trajectory by taking strictures at equal intervals of time of total 12,500 frames.

2.3.3 Evolutionary Conservation

This process was adapted from a tutorial posted by Thomas Weimbs' lab at University of California-Santa Barbara [141]. FASTA formats of the Nrp1 protein in various species were collected from Uniprot (www.uniprot.org). These sequences were then pasted into Microsoft Word where species annotations were added to the sequence names. These sequences were then aligned and assessed for conservation by BoxShade (https://embnet.vital-it.ch/software/BOX_form.html) using the following settings: Output format: RTF_old, Font size: 10, Consensus Line: consensus line with symbols, Fraction of sequences: 0.5, and Input sequence format: other. The resulting file was then used to generate the images for the figure in Microsoft Word.

2.3.4 Expression and Purification of Neuropilin-1

The Nrp1 plasmid containing a1a2b1b2 domains (residues 22-586) and a C-terminal His tag was obtained from E. Yvonne Jones' Lab [12]. Nrp1 mutant plasmids were developed through Gibson Assembly using NEB HiFi Assembly Master Mix (NEB) and fragments generated from synthesize geneblocks (IDT) or from Q5 PCR amplification of the template wildtype plasmid. Primers for the Q5 PCR were designed using the NEBuilder Assembly Tool (NEB) to generate fragments containing the desired mutation. Mutant plasmids were confirmed by sequencing (Genewiz and Eton Bioscience).

Recombinant protein was produced by transfecting ExpiCHO cells (6×10^6 cells/mL) with 0.8 µg/mL plasmid DNA using ExpiFectamine and OptiPRO SFM following the ExpiCHO Expression (ThermoFisher) protocol with Max Titer feeding schedule. Cells were cultured post-transfection at 37 °C in ExpiCHO Expression Medium. On day 1 after transfection, ExpiFectamine CHO Enhancer and ExpiCHO Feed were added to the culture. On day 5 after transfection, ExpiCHO Feed was added to the culture. On day 12 post-transfection, conditioned media was collected, treated with cOmplete EDTA-free protease inhibitor (Roche Applied Science) and adjusted to 30 mM imidazole before filtration through a 0.2 µm filter.

Recombinant protein was initially purified on a 1 mL Ni2+-Sepharose 6 Fast Flow column (GE Healthcare) on an AKTA pure protein purification system (GE Healthcare). Recombinant protein was loaded onto the column followed by washing with 30 mM Imidazole, 0.5 M NaCl in 25 mM HEPES buffer (pH 7.5) and eluting with 0.3 M Imidazole, 0.5 M NaCl in 25 mM HEPES buffer (pH 7.5). Recombinant protein was concentrated by Amicon Centrifugal Filter Units (Millipore Sigma) or Pierce Protein Concentrator PES (ThermoFisher Scientific). Concentrated protein was further purified by size-exclusion chromatography (HiLoad 16/60 Superdex 200, preparation grade, GE Healthcare) with 0.2 M NaCl and 5% glycerol in 25 mM HEPES buffer (pH 7.5). Wildtype and mutant forms of Nrp1 were purified likewise by this method.

2.3.5 SDS-PAGE/Western Blotting Methods

Lung tissue of wildtype and Nrp1 mutant mice were collected and placed in a solution of 1X RIPA lysis buffer (Millipore) with cOmplete EDTA-free protease inhibitor (Roche). The tissues were homogenized using a pestle homogenizer, then centrifuged for 15 minutes at max speed at 4 ˚C. The supernatant was collected while avoiding the lipid layer formed at the top and protein was quantified by BCA Assay (Pierce BCA Protein Assay Kit). To measure Nrp1 expression in the tissues, duplicates of samples and protein ladder (PageRuler Plus Pre-Stained Protein Ladder, ThermoFisher) were separated by electrophoresis using a 4-12% Bis-Tris NuPAGE gel (Invitrogen) in NuPAGE MES SDS Running Buffer (Invitrogen). The gels were transferred onto a PVDF membrane (Immobilon-FL PVDF Membrane, Millipore, IPFL0010) in NuPAGE Transfer Buffer (Invitrogen, NP00061). The membranes were blocked 1 h at room temperature with Odyssey PBS Blocking Buffer (Li-Cor) and then incubated overnight at 4°C with anti-Nrp1 antibody (1:1000; R&D AF566) and anti-beta actin (1:2000; CST 4970) in 5% BSA (Sigma-Aldrich A9647) in TBST (150mM NaCl and 0.1% Tween-20 in 50mM Tris Buffer, pH 7.5). The membranes were incubated at room temperature for 1 hour with corresponding secondary antibodies (Donkey anti-Goat, Li-Cor, 926-32214; IRDye 680LT Donkey anti-Rabbit, Li-Cor, 926- 68023; both at 1:20,000) in 5% BSA in TBST. The bands were visualized using an Odyssey Infrared imaging system (Li-Cor) and quantified by band analysis in ImageJ.

2.3.6 Immunoblotting of Purified Neuropilin-1

For the purified Nrp1 mutant proteins, ladder (Chameleon Duo Pre-Stained Ladder, Li-Cor, 928-60000) and 1 µg of each purified Nrp1 mutant protein were separated by electrophoresis on a 15-well 4-12% Bis-Tris NuPAGE gel (Invitrogen, NP0336) in NuPAGE MOPS SDS Running Buffer (Invitrogen, NP0001). The gel was transferred onto a PVDF membrane (Immobilon-FL PVDF Membrane, Millipore, IPFL0010) in NuPAGE Transfer Buffer (Invitrogen, NP00061). The membrane was blocked one hour at room temperature with Odyssey PBS Blocking Buffer (Li-Cor, 927-40000) and then incubated overnight at 4 ˚C with either anti-Nrp1 (1:1000, R&D AF556) or anti-His (1:1000, Invitrogen MA1-21315-BTIN) in 5% BSA (Sigma-Aldrich A9647) in TBST (50mM Tris, pH 7.5; 150mM NaCl; 0.1% Tween-20). The blot was incubated at room temperature for one hour with appropriate secondary antibodies (IRDye 800CW Donkey anti-Goat, Li-Cor, 926-32214; IRDye 800CW Donkey anti-Mouse, Li-Cor, 926-32212; both at 1:20,000) in 5% BSA and 0.02% SDS in TBST. The blots were imaged using an Odyssey Infrared Imaging System (Li-Cor).

2.3.7 Gel Electrophoresis

For the purified Nrp1 mutant proteins, two 1 µg samples of each protein were run in parallel following kit directions for denaturation. One 1 µg sample was subjected to PNGase F treatment while the other was a control with no enzyme added. All samples and ladder (PageRuler Plus Pre-Stained Protein Ladder,

ThermoFisher) were then separated by electrophoresis on a 15-well 4-12% Bis-Tris NuPAGE gel (Invitrogen, NP0336) in NuPAGE MOPS SDS Running Buffer (Invitrogen, NP0001). Gels were stained with Imperial Protein Stain (ThermoFisher, 24615) and imaged on a Biorad Gel Doc XR system.

For the purified Nrp1 mutant proteins, protein standard (NativeMark Protein Standard, Invitrogen, LC0725) and 2 µg of each purified Nrp1 mutant protein were separated by electrophoresis on a 15-well 4-16% Bis-Tris NativePAGE gel (Invitrogen, BN1004) in NativePAGE Running Buffer (Invitrogen, BN2001). Gels were stained following the Coomassie R-250 staining protocol for NativePAGE gels and imaged on a Biorad Gel Doc XR system.

2.3.8 Analytical Heparin-Sepharose Chromatography

Recombinant proteins were loaded in Buffer A (Gibco DPBS adjusted to 150 mM total NaCl, pH 7.2) onto a 1 mL HiTrap heparin-Sepharose column (GE Healthcare). The column was washed with 10 column volumes (CVs) of Buffer A followed by a 10 CV gradient elution from Buffer A to Buffer B (DPBS adjusted to 0.6 M NaCl, pH 7.2). Salt concentration of the elution peak was determined for each protein.

2.3.9 Neuropilin-1 Binding to Immobilized Heparin-BSA

Heparin-BSA conjugates were prepared and purified by our collaborator [142]. High binding microplates were coated with heparin-BSA (50 µL of 2 ng/µL

solution) overnight while rotating at 4 °C. The plates were blocked for 1 hour at 32 °C with 1% BSA in PBST (Gibco DPBS with 0.05% Tween). Nrp1 proteins were incubated in the wells in triplicate and bound protein was detected with THE His Tag antibody [HRP] (Genscript) diluted 1:4000 in 1% BSA in PBST for heparin-BSA. The wells were developed with 100 µL of TMB turbo substrate for 6 minutes for heparin-BSA followed by quenching with 100 µL of 1 M sulfuric acid. The absorbance of the wells was measured at 450 nm and at 540 nm for background correction. Prism 8 (Graphpad) was used for data analysis and statistical analysis of curves.

2.3.10 Size-Exclusion Chromatography and Multi-Angle Light Scattering (SEC-MALS)

Nrp1 protein was concentrated and exchanged into gel filtration buffer (75 mM NaCl in 10 mM Phosphate Buffer, pH 7.4) in Pierce Protein Concentrator PES (10K MWCO, ThermoFisher Scientific). Concentrated protein (~2.5-3 mg/mL) was then incubated with 5-fold molar excess of heparin oligosaccharides (Iduron). For analysis by SEC-MALS, 100 µL of the protein-heparin mixes in gel filtration buffer was injected onto a Superdex 200 Increase 10/300 GL Column (GE Life Sciences). miniDAWN TREOS and Optilab T-rex detectors (Wyatt Technology) were used to collect light scattering and refractive index data, respectively. ASTRA v.6 software (Wyatt Technology) was used to calculate the molar masses of the complexes.

2.3.11 Differential Scanning Fluorimetry

Recombinant Nrp1 (2 μM), heparin oligosaccharides (2 uM-20 uM, Iduron), 5X SYPRO Orange Protein Gel Stain (Thermo Fisher Scientific) were added to 150 mM NaCl in 10 mM HEPES (pH 7.5) buffer. Thermal denaturation was achieved using a temperature gradient from 25 to 95 °C at a rate of (0.5 °C/30 seconds) on a CFX96 real-time PCR system (Bio-rad). Melting temperatures were determined from the first derivatives of the melting curve data assuming a Gaussian distribution (Prism 8).

2.3.12 Cell Surface Binding

CHO-K1 were grown to 70-80% confluency in DMEM/F-12 (Sigma) with 2 mM L-glutamine (Gibco), 10% (v/v) FBS (Omega Scientific), and 1% (v/v) Penicillin-Streptomycin (Gibco). Human Umbilical Vein Endothelial Cells (HUVECs) were grown to 70-80% confluency in EGM-2 endothelial cell growth medium-2 (Lonza) with 10% (v/v) FBS (Omega Scientific), and 1% (v/v) Penicillin-Streptomycin (Gibco). Both were grown in an environment of 37 °C, 5% CO_2, and 95% air. Cells were lifted with 10 mM EDTA in DPBS (Gibco). Cells were centrifuged and then washed with 0.5% BSA in DPBS (Gibco; the wash buffer for the HUVECs contained 5 mM EDTA). For some experiments, some of the cells were partitioned and treated with heparinases (HSase; 2.5 mU/mL Heparinase II and 5 mU/mL Heparinase III; IBEX) for 30 min at 37 °C in 0.5% BSA in DPBS. The cells were then incubated with his-tagged Nrp1 protein (recombinant a1a2b1b2) in

0.5% BSA in DPBS for 60 minutes at 4 °C. After washing the cells twice in 0.5% BSA in DPBS, the cells were incubated with an anti-his antibody (1:500 THE™ His Tag Antibody iFluor 488, Genscript) in 0.5% BSA in DPBS for 30 min at 4 °C. The cells were washed twice with 0.5% BSA in DPBS and then analyzed on a FACSCanto flow cytometer (BD Bioscience). Data were analyzed using FlowJo software (BD Bioscience) and Prism 8 (Graphpad). *p* values were determined using either a one-way or two-way ANOVA with Tukey's multiple comparison test. * is $p<0.033$ and ** is $p<0.002$.

2.3.13 Generation and Genotyping of Mouse Lines

Nrp1 floxed mice (B6.129(SJL)-*Nrp1*^{tm2Ddg}/J) were purchased from the Jackson Laboratory [26]. *Nrp1*$^{f/f}$ were crossed to *EIIa-Cre*+ mice on C57BL/6 background to generate a *Nrp1* knockout allele [143]. This line was then backcrossed into the C57BL/6 background over 5 generations. To generate the *Nrp1*^{D} mouse model, a crRNA sequence and HDR donor oligo were designed using the Deskgen platform to target and mutate the R513,K514 amino acids into alanine residues.

crRNA: GAG AAA ACA AGG UGU UCA UG;

HDR ssoligo donor: CTTGCTGTCATCCATGATAGTTTTCCAGTCAGAGCCATT GTTACTATAGGCGATCTTGAACgcCgcCATGAACACCTTGTTTTCTCGGTGCT TCCCACCCTGAATGATGACACCTCTTACTATCTT.

Alt-R S.p. Cas9 protein, TracrRNA, crRNA and HDR oligo were from IDT. An *in vitro* cleavage assay was used to determine that the sgRNA (TracrRNA + crRNA) would induce cleavage in a DNA fragment containing the target sequence. The protocol for the *in vitro* cleavage assay was received from the UC San Diego Transgenic Mouse Core. The following were combined: 0.6 µg of Cas9 protein, 0.25 µg of sgRNA (tracrRNA+crRNA), 0.15 µg targeting substrate (PCR product), 1 µL of 10X NEB Buffer, and 1 µL of 10X BSA buffer, and nuclease free buffer up to 10 µL. This reaction mixture was incubated for 1 hour at 37 °C. RNAse (4 µL) was added to reaction mixture, which was then incubated for 15 minutes at 37 °C. Stop solution (1 µL; 30% glycerol, 1.2% SDS, 250 mM EDTA, pH 8.0) was added to reaction mixture, which was then incubated for 15 minutes at 37 °C. The results were then analyzed by agarose gel electrophoresis. The following mixture was provided to the UC San Diego Transgenic Mouse Core for injection: Alt-R S.p. Cas9 protein: 0.6 uM; Tracr RNA: 0.6 uM; crRNA: 0.6 uM; HDR Oligo: 20 ng/µL and diluted with IDTE to 30 µL. Resulting offspring (five F0 offspring) were screened for transgene through genotyping (see genotyping methods section below) and sequencing. Two F0 offspring were determined to be wildtype, two F0 offspring were found to be heterozygous for the R513A,K514A mutation and the remaining F0 offspring was found to have one allele with the R513A,K514A mutation and one allele with an insertion. One of the heterozygous F0 offspring was bred to develop the experimental *Nrp1*^{D} line.

For sequencing, the genomic DNA surrounding the mutation site was PCR amplified using a Q5 High-Fidelity polymerase (New England Biolabs) and ligated into a PUC19 vector. The ligated plasmids were transformed into 10-beta competent *E. coli* (New England Biolabs) and spread on plates treated with X-gal (20 mg/mL; Apex) and IPTG (200 mg/mL). White colonies were selected for colony PCR using M13Forward and M13Reverse primers. Resulting amplicons were purified using the QIAquick PCR purification kit (QIAGEN). Sequencing of these amplicons confirmed the editing of the Nrp1 gene (Figure 2.12A) and validating the genotyping method involving BspHI digestion.

For genotyping of the Nrp1 alleles, the following primers are used. *Nrp1* Forward: AAG GAG TGG CAC AGC ATC TT; Nrp1 Reverse: TCA CAC CCA AAC TTC CTT CC; *Nrp1* Exon2-3B: GGG TGA ACT CAG CCA CTT GT; $Nrp1^{D}$ Forward: GCA TCC AAT CAA GCC GAC AG; $Nrp1^{D}$ Reverse: GCT TGG GAG GTA GAG ATG CA. The *Nrp1* Forward and Reverse primers are used to identify the floxed gene and the *Nrp1* Forward and *Nrp1* Exon2-3B primers are used to determine knockout alleles. The $Nrp1^{D}$ forward and reverse primers are used to generate a PCR-amplified region around the mutation site. The resulting amplicons are then digested with BspHI and analyzed by agarose gel electrophoresis. The amplicon is digested by BspHI if it contains the wildtype sequence, but it is resistant to digestion if the site has been mutated as in the $Nrp1^{D}$ allele. All animal husbandry and experiments were performed in accordance with relevant guidelines and regulations following standards and procedures

approved by the UC San Diego Institutional Animal Care and Use Committee (protocol #S99127).

2.3.14 Tumor Experiments

B16-F10 melanoma cells were grown to 80% confluency in DMEM (Gibco) with 10% (v/v) FBS, 1% (v/v) Penicillin-Streptomycin (Gibco) in an environment of 37 °C, 5% CO_2, and 95% air. Cells were lifted with 0.05% trypsin (Corning), which was inactivated by adding in DMEM with 10% FBS. Cells were pelleted and washed with DPBS (Gibco) twice. The cells were resuspended in DPBS and counted twice before being resuspended at 5 x 10^6 cells/mL in DPBS. 100 µL of cell suspension (5 x10^5 cells) were injected subcutaneously into the shaved flanks of anesthetized mice of various genotypes. The tumors were initially done bilaterally, but concerns about overall tumor burden led us to continue with only unilateral injections. No discernible difference was seen between the unilateral and bilateral models in the $Nrp1^{+/+}$ animals. Tumors were measured with calipers every two days. From these measurements, tumor volume was calculated using the formula Volume = length x $width^2$ x 0.5236 [144, 145]. Tumors were grown until they reached the terminal endpoint (>10mm in one dimension). Animals were sacrificed at terminal endpoint or when ulcers were found in accordance with our animal protocol. Size comparison was done at 15 days when the first tumors reached terminal endpoint and all animals were alive. Tumors that ulcerated before day 15 were removed from the data set. Those tumors deemed to be growing intramuscularly by palpation and later dissection were also removed from the data

set. Tumor volumes were plotted and statistical analysis was performed in Prism 8 (Graphpad). *p* values were determined using a two-way ANOVA with the Geisser-Greenhouse correction followed by an uncorrected Fisher's LSD test for each set of data. * is $p<0.033$ and ** is $p<0.002$.

2.4 Results

2.4.1 Molecular Modeling of Heparin Binding Site in Neuropilin-1

In order to explore the attributes of the heparin/heparan sulfate binding site in Nrp1, the a1a2b1b2 subdomains were analyzed. The surface of mouse Nrp1 (PDB ID: 4GZ9) was divided into thirteen regions (BS1-BS13, Fig. 2.2B) for elucidation of putative sites for heparin binding in an unbiased manner. First, a Combinatorial Virtual Library Screening (CVLS) algorithm was performed on each of these sites utilizing a library of 72 heparin/heparan sulfate disaccharides. The algorithm involves a dual-filter strategy consisting of a GOLDScore filter followed by evaluation of RMSD between the best 6 docked poses of each heparan sulfate sequence (Fig. 2.2A). Whereas the GOLDScore informs of the "*in silico affinity*", RMSD correlates with the "*in silico selectivity"* of each heparan sulfate sequence.

When the docked poses of disaccharides were overlaid onto the thirteen binding sites (Fig. 2.2B), the higher affinity/selectivity disaccharides preferentially aligned with the electropositive cleft formed by the b1 and b2 domains (Fig. 2.1A). Following this process, a library of 288 hexasaccharide sequences were generated

from the most optimally aligned disaccharides. This library of 288 hexasaccharides, containing a range of sulfated sequences carrying 8 to 12 sulfate groups, was then studied again using the dual filter CVLS algorithm. Figure 2.1B shows the results of these experiments, which led to the conclusion that BS1, BS4 and BS5 are the three primary putative sites of binding for heparan sulfate hexasaccharides. When the best-fit hexasaccharides were simultaneously projected onto the three binding sites, considerable overlap was noted between the best ranking sequences, suggesting a strong possibility of recognition of an extended heparan sulfate chain within the electropositive cleft in the b1 and b2 domains.

To identify the preferred chain length, the high affinity/high selectivity hexasaccharide sequences that bound in BS1, BS4 and BS5 were studied using molecular dynamics (MD) in a box of water at under NPT conditions for 1 microsecond. Whereas each hexasaccharide bound in their preferred sites led to stabilization of the co-complex (Fig. 2.1F), simultaneous occupation of both BS1 and BS5 led to considerable increase in its stability. The best scoring sequences of BS1, BS4 and BS5 were overlaid, which revealed four residues on either side of the hexasaccharides bound to BS4 in common with preferred oligosaccharides bound to BS1 and BS5. Eliminating these four residues led to a potential tetradecasaccharide (dp14) that was likely to be a better complementary fit to the electropositive surface of the binding cleft. Molecular dynamics of the 14-mer showed that following an initial stabilization period of few nanoseconds, the

simulations reached equilibrium as noted by RMSD profiles of both the protein and ligand (Figs. 2.2C and 2.2D). Visualization of the full MD trajectory (Supplemental Video 1) showed that the ligand remained anchored to BS1, BS4 and BS5.

Detailed free energy contribution and hydrogen-bond occupancy analysis indicated the involvement of an extensive set of residues in binding to the 14-mer including Glu271, Ser321, Tyr322, Lys323, Arg359, Lys373, Asn376, Lys377, Ala378, Lys397, Lys407, Lys509, Arg513, Lys514, Lys538, Glu541, Asn544, Asn545, Thr553, and His571 (Figs. 2.1G, 2.2E). Of the twenty residues, nine are evolutionary identical across multiple animal species, whereas the other eleven positions have conservative substitutions (Figs. 2.1I). Comparison of Nrp1 to Nrp2 in human, mouse, and rat reveals that six of these residues are identical, five have conservative substitutions and nine are non-conserved residues between the two isoforms. Of note, the positively charged lysine and arginine residues are highly conserved, as would be expected for a site involved in binding negatively charged polysaccharides such as heparin or heparan sulfate [78]. In addition, the b2 domain contains a conserved XBBXBX amino acid motif across residues 512-517 (MRKFKI), which corresponds to a Cardin-Weintraub glycosaminoglycan binding consensus sequence [38, 146].

Structural studies of the Nrp1 indicate that subdomains b1b2 are tightly packed and form a rigid scaffold, with a deep cleft or groove that runs across the interdomain junction, measuring ~40 Å in length [38]. This cleft has dimensions

that roughly corresponds to the length of a heparin dodecasaccharide (dp12) [38]. Mutation of specific arginine and lysine residues to glutamate (R359E, K373E, R513E, K514E, and K516E) along the cleft abolished the heparin-induced dimerization [38]. Examination of the interaction of recombinant dimeric Fc fusion of rat Nrp1 with heparin suggested amino acid residues involved in heparin binding were also present in the a1 domains [76], although molecular docking studies with the murine a1a2b1b2 protein did not support this hypothesis.

2.4.2 Recombinant Protein Production

Based on the modeling results, the conservation and location of the residues, and previous mapping studies, the amino acid residues R359, K373, K509, R513, K514, and K516 were selected for mutagenesis (Fig. 2.1H). cDNA plasmids containing wildtype and mutant forms of the a1a2b1b2 domain of mouse Nrp1 were created using a construct previously utilized in the crystallization of mouse Nrp1 [12]. In addition, Nrp1 a1a2b1b2 domain has been shown to have a three-to-eight-fold greater affinity for $VEGF_{165}$ over the b1b2 domain alone [36]. The mouse construct was selected in anticipation of *in vivo* studies to examine the functional significance of the heparin binding domain. Previous studies employed recombinant protein expressed in *E. coli* which lacks the glycosylation enzymes found in mammalian systems [38]. The a1a2b1b2 construct contains two N-glycosylation sites in the a2 domain which could affect binding to heparin/heparan sulfate. Robust expression was achieved using ExpiCHO cells.

The resulting recombinant proteins, wildtype and seven alanine substitution mutants, were expressed and purified by affinity chromatography. All of the recombinant proteins were expressed at comparable levels (0.8-2.4 mg/L). SDS-PAGE analysis showed that all of the proteins had the expected molecular weight and appeared to be stable based on the retention of the His_6Tag and recognition by anti-Nrp1 antibody in western blots (Fig. 2.4A). Each recombinant protein was also N-glycosylated as demonstrated by a comparable decrease in molecular weight following treatment of the purified proteins with PNGase to release the N-glycans (Fig. 2.4B). Similar conformations of the recombinant proteins also were observed based on their comparable migration on native PAGE (Fig. 2.4C).

Figure 2.1: Molecular Modeling of Nrp1 with Combinatorial Virtual Library Screen (CVLS) and Amino Acid Selection

A, Mapping the electrostatic potential surface of mouse Nrp1 (PDB: 4GZ9) using APBS tool in Pymol. Blue areas represent electropositive surfaces and red areas represent electronegative surfaces. **B**, CVLS predicted hexasaccharide sequences binding to multiple binding sites (BS1, BS4 and BS5) on mNrp1 from a smaller library of 288 sequences containing no sulfate (0), fewer sulfate (1-3), medium sulfate (4-7) and highly sulfated (8-12) sequences. Shown are overlays of the docked poses of hexasaccharide sequences that bind mNrp-1 with "high specificity" by satisfying the dual-filter strategy. The sequences bound at BS1 (green color by atom sticks), BS4 (cyan color by atom sticks) and BS5 (pink color by atom sticks) are shown. The sequences bound at BS4 and BS5 are partially overlapping with each other. **C,D,E** Interaction of heparin/heparan sulfate hexasaccharides at Binding Site 1 (**C**), Binding Site 4 (**D**) and Binding Site 5 (**E**), which are predicted to recognize Nrp1 with "high affinity and high specificity". The hydrogen bond interaction of the hexasaccharide sequences with the key residues of mNrp1 (are shown in the black dotted lines). The hexasaccharide sequences binding to BS1, BS4 and BS5 are shown in sticks (green, cyan and pink color by atom, respectively). The interacting residues are shown in ball and stick (white color by atom) representation. **F**, Total free energy value in kcal/mol, from MD simulation (200ns) of heparin hexasaccharide bound to BS1, BS4 and BS5 respectively. Increase in total free energy value when BS1 and BS5 occupied simultaneously. The color spectrum from red to blue shows the direction of increase in free energy values. **G**, Free energy contributions for the 14mer GAG sequence interacting amino acid residues in the binding region of the Nrp1 protein. The values from lower to higher are represented by rainbow color bars from blue to red, respectively. The MD simulation of the 14mer bound GAG sequence was carried out for one microsecond time scale. **H**, Electrostatic potential plot of Nrp1 with selected residues colored green and labeled. **I**, Conservation of amino acids in Nrp1 protein. Green boxes indicate selected amino acids. Consensus symbols are ***** for identical residues, **.** for conservative substitutions and blank for non-conserved residues.

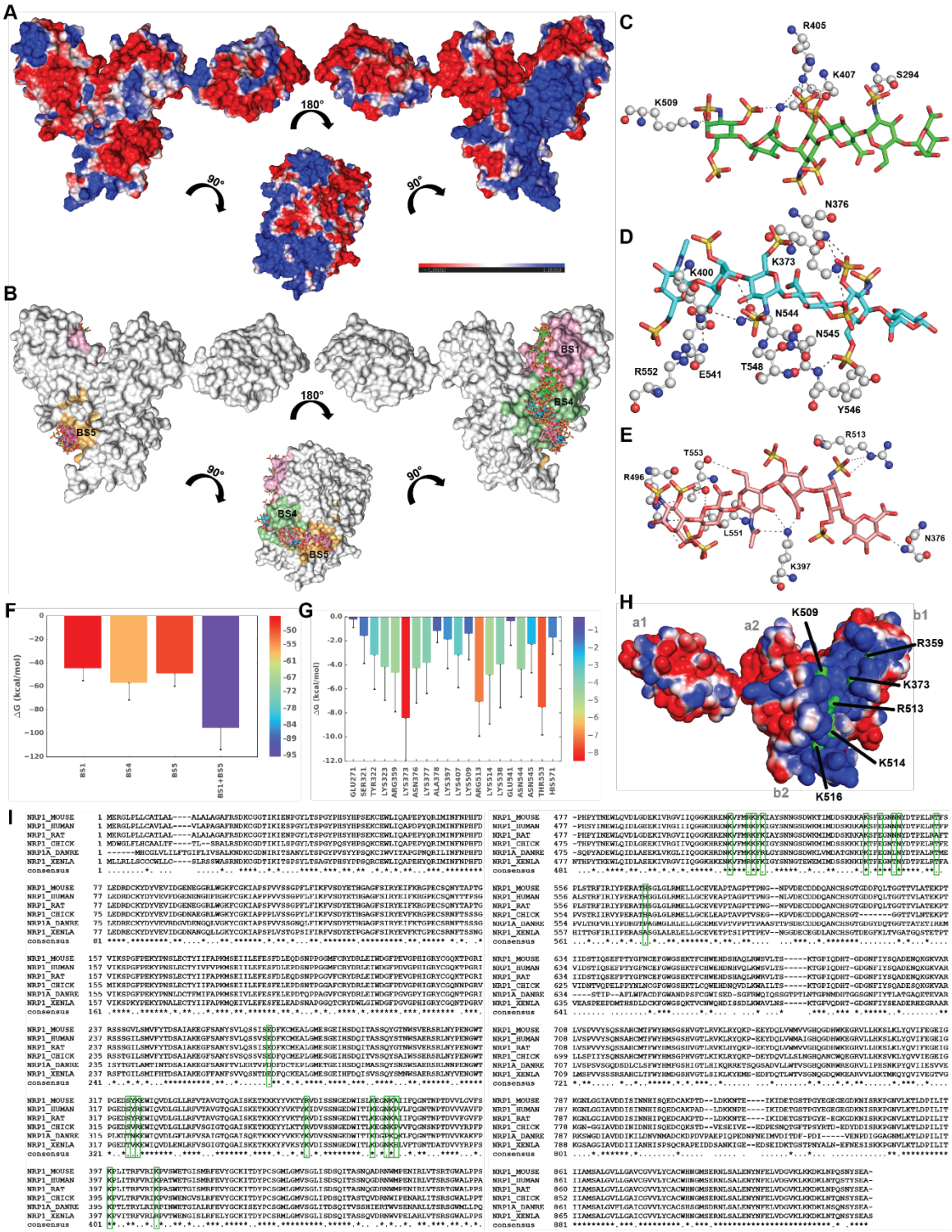
A
180°
90°
90°
B
BS1
BS4
BS5
180°
90°
90°
BS4
BS5
C
R405
K407
S294
K509
D
N376
K373
K400
N544
N545
R552
E541
T548
Y546
E
R513
T553
R496
L551
N376
K397
F
ΔG (kcal/mol)
BS1
BS4
BS5
BS1+BS5
G
ΔG (kcal/mol)
GLU271
SER321
TYR322
LYS323
ARG359
LYS373
ASP376
LYS377
ALA378
LYS397
LYS407
LYS509
ARG513
LYS514
LYS538
GLU541
ASN544
ASP545
THR551
HIS571
H
a1
a2
b1
b2
K509
R359
K373
R513
K514
K516
I

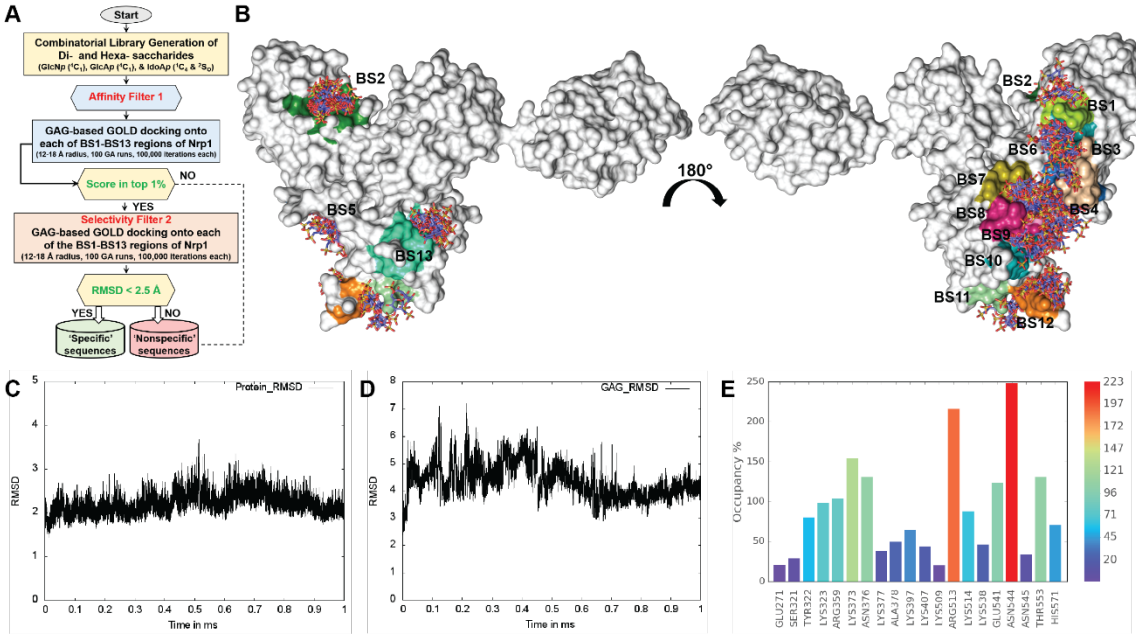

Figure 2.2: Supplement to Figure 2.1

A, The dual-filter CVLS algorithm used the library of 72 di- and 288 heparan sulfate hexasaccharides. GOLD score was the first filter (affinity filter 1), while consistency of binding (RMSD is the selectivity filter 2) was the second filter used to study GAG binding potential to Nrp1. **B**, Based on the electrostatic potential surface (EPS) of mNrp-1, the potential sites of GAG binding were identified as 13 different binding sites (BS1-BS13). A CVLS algorithm was applied using disaccharide library consisting of 72 sequences (Glycobiology, 2014, 24:1323-1333) on to each binding site and the best docked poses (blue color by atom sticks) are overlayed. The surface of each binding sites (BS1 – BS13) are labelled and colored respectively. **C**, Plot of the Root Mean Square Deviation (RMSD) of the Nrp1 protein from the starting conformation when the longer sequence heparin 14mer is bound. **D**, Plot of the Root Mean Square Deviation (RMSD) of the 14mer GAG bound to the Nrp1 from the initial binding conformation. **E**, The inter molecular hydrogen-bond occupancy for the 14mer GAG sequence interacting amino acid residues in the binding region of the Nrp1 protein. The values from lower to higher are represented by rainbow color bars from blue to red, respectively. The MD simulation of the 14mer bound GAG sequence was carried out for one microsecond time scale.

2.4.3 Binding of Recombinant Nrp1 Mutants to Heparin

In order to elucidate the contribution of these candidate amino acids to the interaction of Nrp1 with heparan sulfate, recombinant Nrp1 proteins were subjected to a battery of heparin and heparan sulfate binding assays. Heparin, a highly sulfated fractionated form of heparan sulfate, is commercially available in large quantity and is used as a surrogate for more typical heparan sulfate found on cells. To assess the interaction of the recombinant proteins with heparin, samples were bound to heparin sepharose and eluted with a salt concentration gradient from 150 mM to 600 mM NaCl. Several of the recombinant mutant proteins showed small reductions in the salt concentration needed for elution compared to the wildtype Nrp1 protein (430-500 nM NaCl versus 520 mM for wild-type Nrp1, Fig. 2.4D, Table 1). R513A, K514A, and K373A mutants eluted at much lower salt concentrations (350 mM, 430 mM and 430 mM NaCl, respectively) suggesting these amino acids contributed significantly to the interaction of Nrp1 with heparin (Fig. 2A, Fig. 2.4D, Table 1). Recombinant Nrp1 protein containing two mutations (R513A,K514A) showed an additive effect on the salt concentration, eluting at 280 mM NaCl (Δ = -240 mM NaCl for the double mutant vs. -170 and -90 mM NaCl for mutants R513A and K514A).

These results were validated in a different assay format in which binding of recombinant Nrp1 proteins was evaluated in an ELISA plate coated with heparin-BSA (Fig. 2B, Fig. 2.4E). Incubation with wildtype protein showed saturable binding with an apparent K_d value of 0.10-0.14 μM (95% CI). All of the

single amino acid mutants showed reduced affinity, but the extent of binding based on B_{max} values was comparable (Table 1). The double mutant R513A,K514A bound with much reduced affinity (1.64-4.61 μM, 95% CI) and the extent of binding was reduced as well.

2.4.4 Heparin Stabilizes Neuropilin-1 Against Thermal Denaturation

Binding of glycosaminoglycans to proteins often stabilizes them against denaturation compared to their unbound state [147, 148]. To determine the effect of heparin binding on Nrp1 stability, we utilized differential scanning fluorimetry to monitor thermal denaturation of Nrp1 in the presence and absence of heparin. Nrp1 was mixed with 5X SYPRO Orange Protein Gel Stain, a hydrophobic dye that binds to hydrophobic domains of the protein exposed by denaturation [148]. Heparin-enhanced thermal stability appears as an elevated melting temperature. Wildtype Nrp1 demonstrated a characteristic biphasic melting curve (Fig. 2.4F), which produced a melting temperature of 49.4°C based on the maximum of the first derivative of the dye binding curves (Fig. 2.4G). Increasing the molar ratio of heparin:protein from 1:1 to 10:1 resulted in further stabilization reflected in higher melting temperatures (50.6-51.6°C) (Fig. 2.4H). Analysis of the mutant proteins with a 10:1 molar ratio of heparin:protein showed that mutants K509A and K516A were similarly stabilized by heparin compared to the wildtype, whereas R359A, K373A, R513A, and K514A mutants showed less heparin-induced stabilization (Fig. 2C). The R513A,K514A double mutant was not stabilized by heparin against

thermal denaturation as reflected by virtually no increase in the melting temperature (Fig. 2C). As a control, we also examined melting of each protein construct in the absence of heparin. Some mutants exhibited slightly altered melting temperature in the absence of heparin indicating some differences in stability (K509A, R513A, R516A; Fig. 2.4I). Nevertheless, the stabilization by heparin suggests that the heparin-binding sites can still engage heparin. The lack of stabilization of the double R513/K514A mutant is consistent with diminished binding.

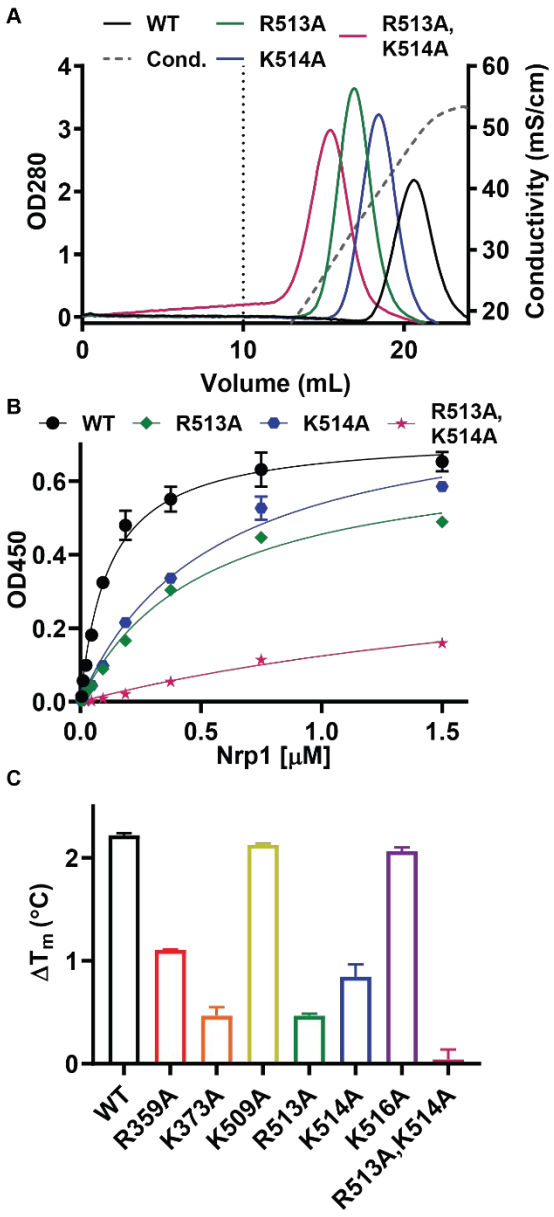

Figure 2.3: Heparin Binding of Nrp1 Mutants

A, Elution profiles of Nrp1 mutants on heparin Sepharose. Wildtype Nrp1 and Nrp1 mutants were passed over heparin Sepharose and the concentration of NaCl required for elution from the column was determined. Dashed vertical line at 10 mL is beginning of elution phase. **B**, Wildtype Nrp1 and Nrp1 mutants binding to immobilized heparin-BSA**. C**, Increases in melting temperatures of the Nrp1 proteins in the presence of heparin due to heparin-induced stabilization.

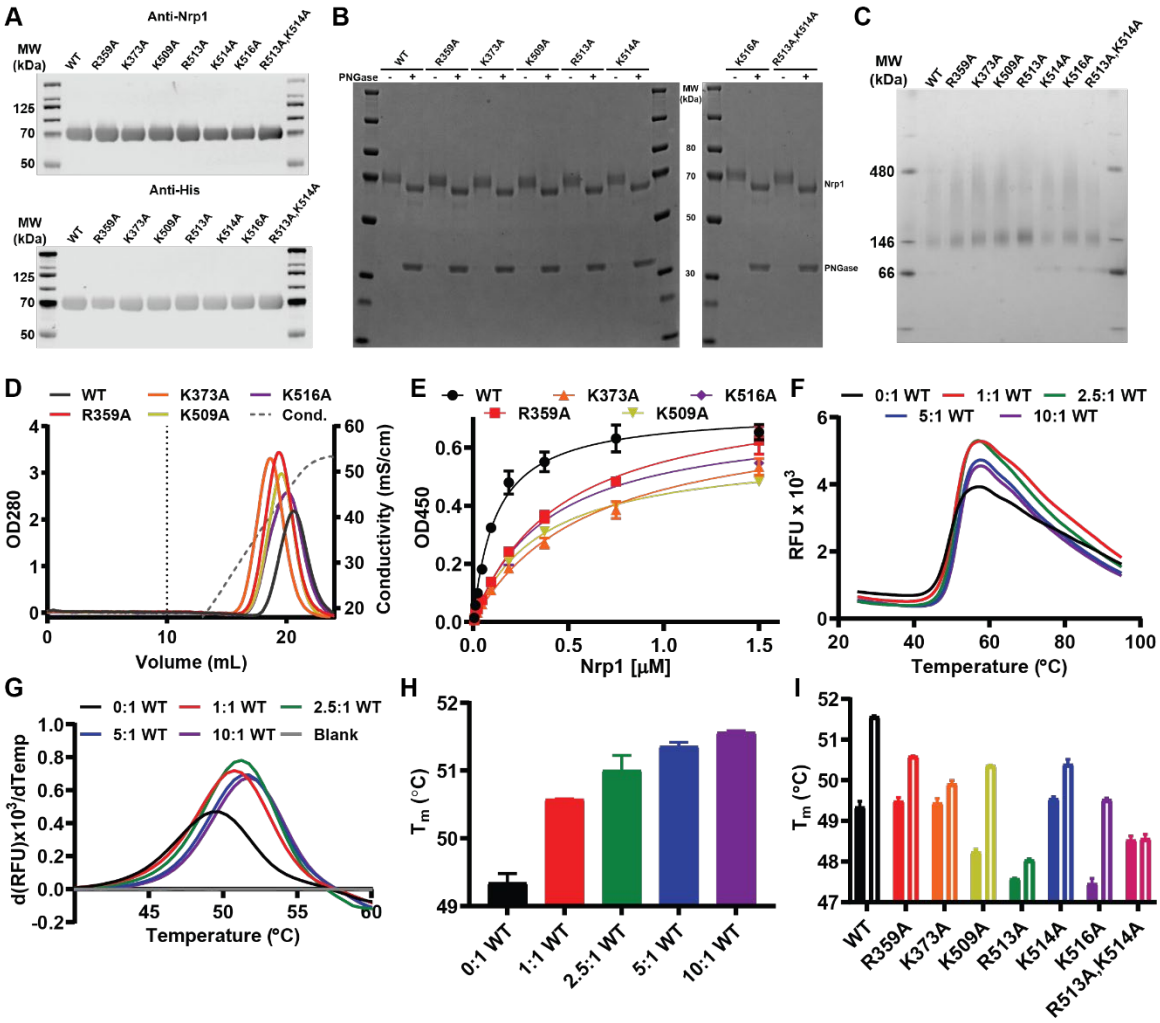

Figure 2.4: Supplement to Figure 2.3

A, Immunoblot of recombinant Nrp1 proteins using an anti-Nrp1 antibody (top) and anti-His-tag antibody (bottom)**. B**, A Coomassie-stained SDS-PAGE gel of recombinant Nrp1 proteins either untreated or treated with PNGase. **C**, A Coomassie-stained Native gel of recombinant Nrp1 proteins. **D**, Elution profiles of Nrp1 mutants on heparin Sepharose. Wildtype Nrp1 and Nrp1 mutants were passed over heparin Sepharose and the concentration of NaCl required for elution from the column was determined. Dashed vertical line at 10 mL is beginning of elution phase. **E**, Wildtype Nrp1 and Nrp1 mutants binding to immobilized heparin-BSA**. F**, Sample melting curves from the experiment in H. **G**, First derivative of sample melting curves to show determination of melting temperature as maxima. **H**, Wildtype Nrp1 (2 μM) was thermally denatured in the absence or presence of a molar excess of heparin. Ratios are given as heparin to protein. **I**, Wildtype Nrp1 and Nrp1 mutants (2 μM) were thermally denatured in the absence or presence of 10-fold molar excess of heparin.

Table 2.1: Salt Concentrations for Heparin Sepharose Elutions and K_d and B_{max} Values for BSA-Heparin ELISAs

	Heparin Sepharose			Heparin-BSA ELISA	
	Cond (mS/cm)	Salt (mM)	Δ Salt (mM)	K_d (μM, 95% CI)	B_{max} (95% CI)
Nrp1	48	520	0	0.10-0.14	0.69-0.76
R359A	43	470	-50	0.39-0.52	0.76-0.85
K373A	40	430	-90	0.50-0.73	0.67-0.80
K509A	44	480	-40	0.34-0.38	0.58-0.61
R513A	33	350	-170	0.43-0.61	0.64-0.75
K514A	39	430	-90	0.45-0.66	0.77-0.91
K516A	46	500	-20	0.34-0.45	0.68-0.75
R513A,K514A	28	280	-240	1.64-4.61	0.33-0.69

2.4.5 Heparin-Induced Dimerization of Neuropilin-1

Native Nrp1 contains a c (MAM) and transmembrane domains that have been proposed to facilitate dimerization [8, 40]. However, this domain appears to be dispensable because heparin tetradecasaccharides (dp14) induced dimerization of the human Nrp1 b1b2 domains based on size-exclusion chromatography [38]. To explore the impact of heparin-binding on oligomerization of murine a1a2b1b2 protein, we examined heparin oligosaccharides of different length. Wild-type protein was incubated with defined-sized heparin oligosaccharides (dp8-dp20) and the resulting mixtures were analyzed by size-exclusion chromatography with multi-angle light scattering (SEC-MALS). Murine Nrp1 a1a2b1b2 protein ran as a monomer with an apparent molecular mass of 74 ± 1.8 kDa by gel filtration (Table 2.2), consistent with the expected mass based on amino acid sequence as well as previously determined molecular mass for Nrp1 a1a2b1b2 [12]. The consistent molecular mass across the peak suggested a homogeneous complex. The extended binding cleft accommodated dp6 to dp18 oligosaccharides, resulting in a shift in apparent molecular masses approximately equal to the summation of the masses of the individual components for dp6-dp10 (Figs. 2.6A and 2.5A). Incubation with dp20 heparin oligosaccharides resulted in a complex with apparent molecular mass consistent with a dimer (~160 kDa; Fig. 2.5G, Table 2). These results suggest that heparin oligosaccharides shorter than dp20 can bind; the intermediate apparent molecular weights of these complexes most likely reflect the dynamic process of complex

assembly and disassembly during the gel filtration run. Smaller trailing peaks in the OD_{280} traces may be due to the presence of a double bond at the non-reducing end of the heparin oligosaccharides that arose from enzymatic processing of heparin during production of the oligosaccharides (Fig. 2.6B).

The alanine substitution of key residues in the electropositive cleft in mouse Nrp1 a1a2b1b2 decreased its ability to bind heparin (Fig. 2A), suggesting that heparin-mediated dimerization might be altered as well. Incubation of dp20 heparin oligosaccharides with the R513A and K514A mutant proteins resulted complexes of intermediate apparent molecular weights compared to wildtype protein (83 and 97 kDa *versus* 180 kDa, respectively; Table 2.3). A bound complex consisting of one heparin dp20 chain and one a1a2b1b2 monomer can account for the apparent molecular mass of the complexes formed by the single R513A and K514A mutants with dp20 heparin oligosaccharides (Fig. 2.5H, 2.5I). The R513A,K514A double mutant showed no shift in molecular weight by gel filtration supporting its lack of interaction with heparin (Fig. 2.5J). Experiments with dp18 heparin oligosaccharides yielded similar results (Fig. 2.6C-E).

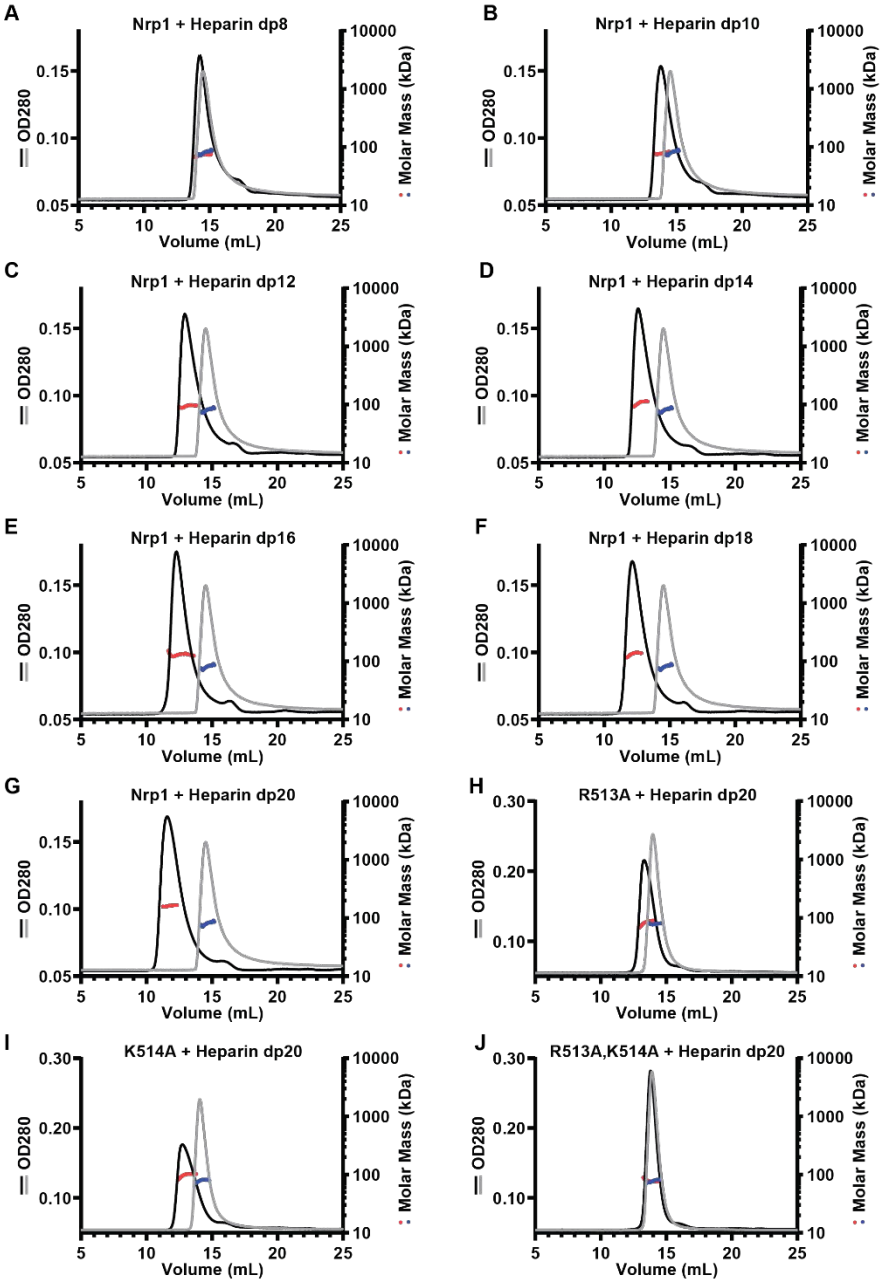

Figure 2.5: Size-Dependent Heparin-Induced Dimerization of Nrp1

SEC-MALS chromatogram of Nrp1 and **A**, heparin octasaccharide (dp8); **B,** heparin decasaccharide (dp10); **C,** heparin dodecasaccharide (dp12)**; D,** heparin tetradecasaccharide (dp14); **E,** heparin hexadecasaccharide (dp16); **F,** heparin octadecasaccharide (dp18); **G,** heparin icosasaccharide (dp20); **H,** SEC-MALS chromatogram of R513A + heparin icosasaccharide (dp20)**; I,** SEC-MALS chromatogram of K514A + heparin icosasaccharide (dp20); **J**, SEC-MALS chromatogram of R513A,K514A + heparin icosasaccharide (dp20)

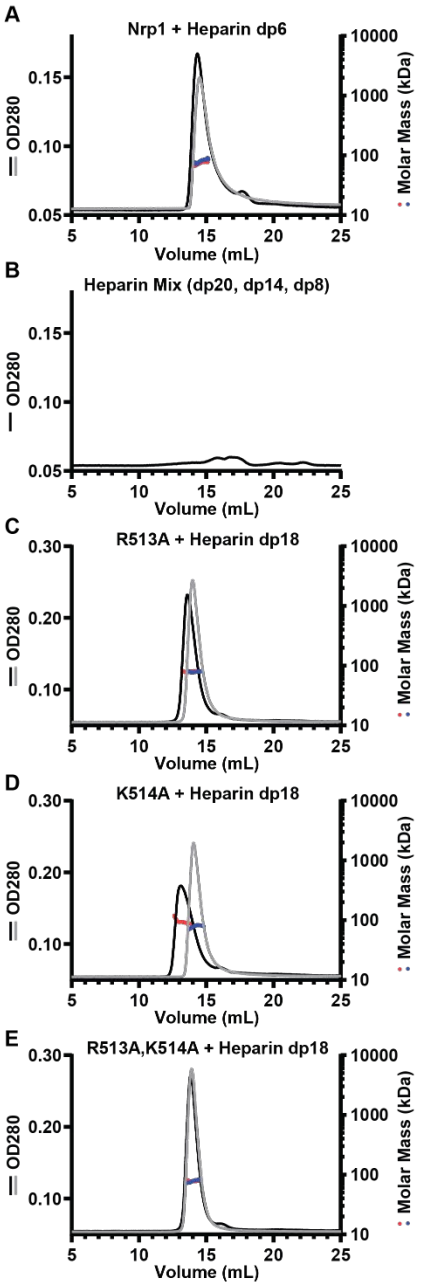

Figure 2.6: Supplement to Figure 2.5

SEC-MALS chromatograms of: **A,** Nrp1 + heparin hexasaccharide (dp6); **B,** a mix of heparin oligosaccharides (dp20, dp14, dp8); **C,** R513A + heparin octadecasaccharide (dp18); **D,** K514A + heparin octadecasaccharide (dp18); **E,** R513A,K514A + heparin octadecasaccharide (dp18)

Table 2.2: Determined Molar Masses for Heparin Oligosaccharides:Protein Complexes

Sample	Oligo Size (kDa)	MM (kDa)	Error (%)	Ratio to Monomer	Expected MM 1:1 complex (kDa)	Expected MM 1:2 complex (kDa)
Nrp1		74	2	1.0	74	
Nrp1 + dp6	1.8	73	4	1.0	76	149
Nrp1 + dp8	2.4	73	4	1.0	76	150
Nrp1 + dp10	3.0	77	3	1.0	77	150
Nrp1 + dp12	3.6	94	5	1.3	78	151
Nrp1 + dp14	4.1	106	3	1.4	78	152
Nrp1 + dp16	4.7	130	6	1.8	79	152
Nrp1 + dp18	5.2	134	3	1.8	79	153
Nrp1 + dp20	5.8	162	2	2.2	80	153

Table 2.3: Determined Molar Masses for dp18/Nrp1 and dp20/Nrp1 Complexes

	Solo		+dp18 (5.2kDa)		+dp20 (5.8kDa)		Expected Size +dp18		Expected Size +dp20	
	MM (kDa)	Error (%)	MM (kDa)	Error (%)	MM (kDa)	Error (%)	1:1 complex	2:1 complex	1:1 complex	2:1 complex
Nrp1	80	5	140	7	183	3	85	165	86	166
R513A	79	1	80	3	83	3	84	163	85	163
K514A	79	2	92	2	97	4	84	163	85	163
R513A, K514A	78	2	79	1	77	1	83	161	84	161

2.4.6 Neuropilin-1 Binds Heparin Oligosaccharides in a 1:2 Heparin/Protein Complex

The accuracy of SEC-MALS was not sufficient to accurately determine the stoichiometry of heparin binding. Thus, we analyzed the complexes by isothermal calorimetry (ITC). Titration of wild-type a1a2b1b2 protein with a heparin dp14 oligosaccharide produced a K_D value of 0.69 μM and a stoichiometry of 0.419 ± 0.004, indicating that the complex most likely consists of one heparin oligosaccharide and two a1a2b1b2 proteins (Fig. 2.7A). Analysis of complexes generated by admixture of wildtype Nrp1 with dp20 yielded similar results (K_D of 0.49 μM and a stoichiometry of 0.404 ± 0.005, Fig. 2.8A). The R513A,K514A double mutant engaged poorly with the heparin tetradecasaccharide and the shape of the binding curve did not allow accurate determination of a K_D value or stoichiometry (Fig. 2.7B). Control titration of heparin oligosaccharides (dp14 and dp20) into buffer alone showed appropriate peak magnitudes (Fig. 2.8B and 2.8C). The stoichiometry of 1:2 dp20/protein complex suggests that a single heparin oligosaccharide is adequate to dimerize the protein, even in the absence of the c domain and other ligands.

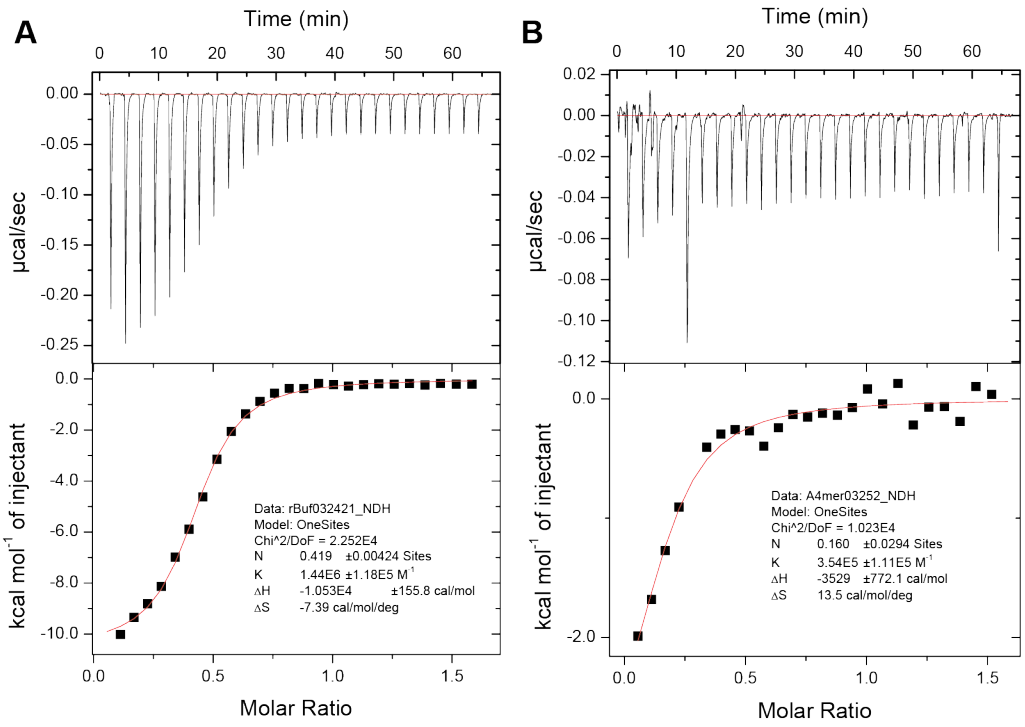

Figure 2.7: Neuropilin-1 and Heparin Oligosaccharide Form a 2:1 Nrp1:Heparin Complex

Isothermal calorimetry assessment of Nrp1/heparin complex formation was achieved by titrating Nrp1 (**A**) and R513A,K514A (**B**) with tetradecasaccharides.

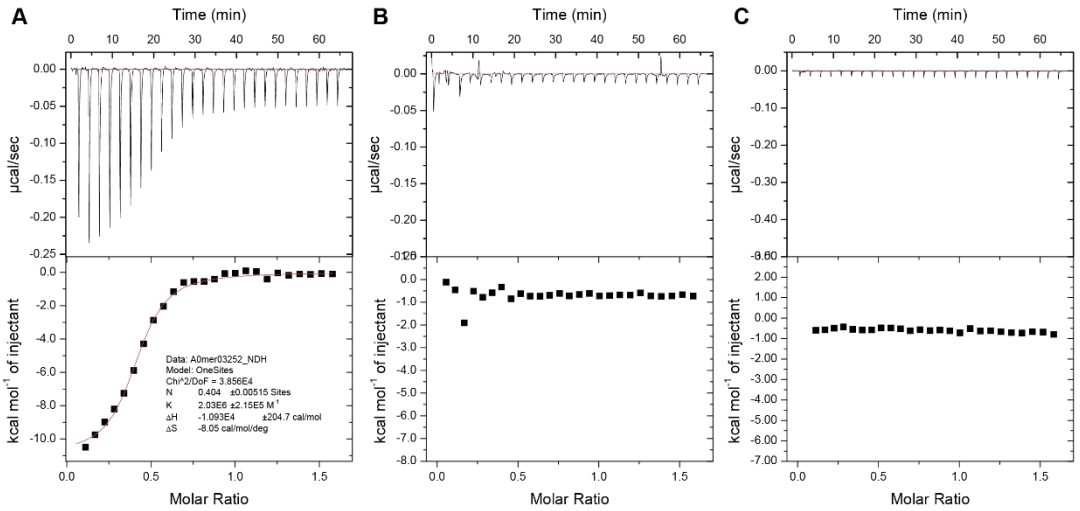

Figure 2.8: Supplement to Figure 2.7

A, Isothermal calorimetry assessment of Nrp1/heparin complex formation was achieved by titrating Nrp1 with heparin icosasaccharides (dp20). Controls were performed by titrating buffer only with heparin tetradecasaccharides (dp14) (**B**) and Nrp1 with heparin icosasaccharides (dp20) (**C**).

2.4.7 Interaction of Neuropilin-1 with Heparan Sulfate

While heparin is commonly used as a surrogate for heparan sulfate, Nrp1 on the plasma membrane of cells more likely engages heparan sulfate in the form of proteoglycans present in the glycocalyx. Prior studies showed that human recombinant human Nrp1 b1b2 domain can bind cell surface heparan sulfate based on flow cytometry assays [86]. Wild-type mouse Nrp1 a1a2b1b2 protein bound to wild-type CHO-K1 cells (Fig. 2.9A) and binding was proportional to concentration up to 3 μM, the highest concentration that was tested (Fig. 2.9A). The recombinant mutant proteins showed various levels of binding to the cells when tested at 1 μM (Fig. 2.9B). R359A and K516A mutants retained similar levels of binding as the wild-type protein, whereas K373A, K509A, R513A and K514A bound to a lesser extent (Fig. 2.9B). Engagement of recombinant R513A,K514A mutant protein with the cell surface was especially attenuated (Fig. 2.9B). Prior treatment of the cells with a combination of heparinases II and III (HSase), which removes cell surface heparan sulfate (Fig. 2.10) diminished binding of wildtype and mutants to a similar baseline level (Fig. 2.9B). Staining of untreated and heparin lyase-treated CHO-K1 cells with an anti-heparan sulfate antibody (10E4) demonstrated efficient removal of heparan sulfate from the cell surface (Fig. 2.10). Binding was also measured in human umbilical cord endothelial cells (HUVECs). Binding showed more typical signs of saturability, but heparin lyases only partially diminished binding. Nevertheless, binding of the R513A,K514A mutant was reduced to the level observed after treatment of the endothelial cells with heparin

lyases. Together, these results show that the reduced binding of the a1a2b1b2 mutants to heparin was recapitulated in studies of recombinant protein with native heparan sulfate present on mammalian cells.

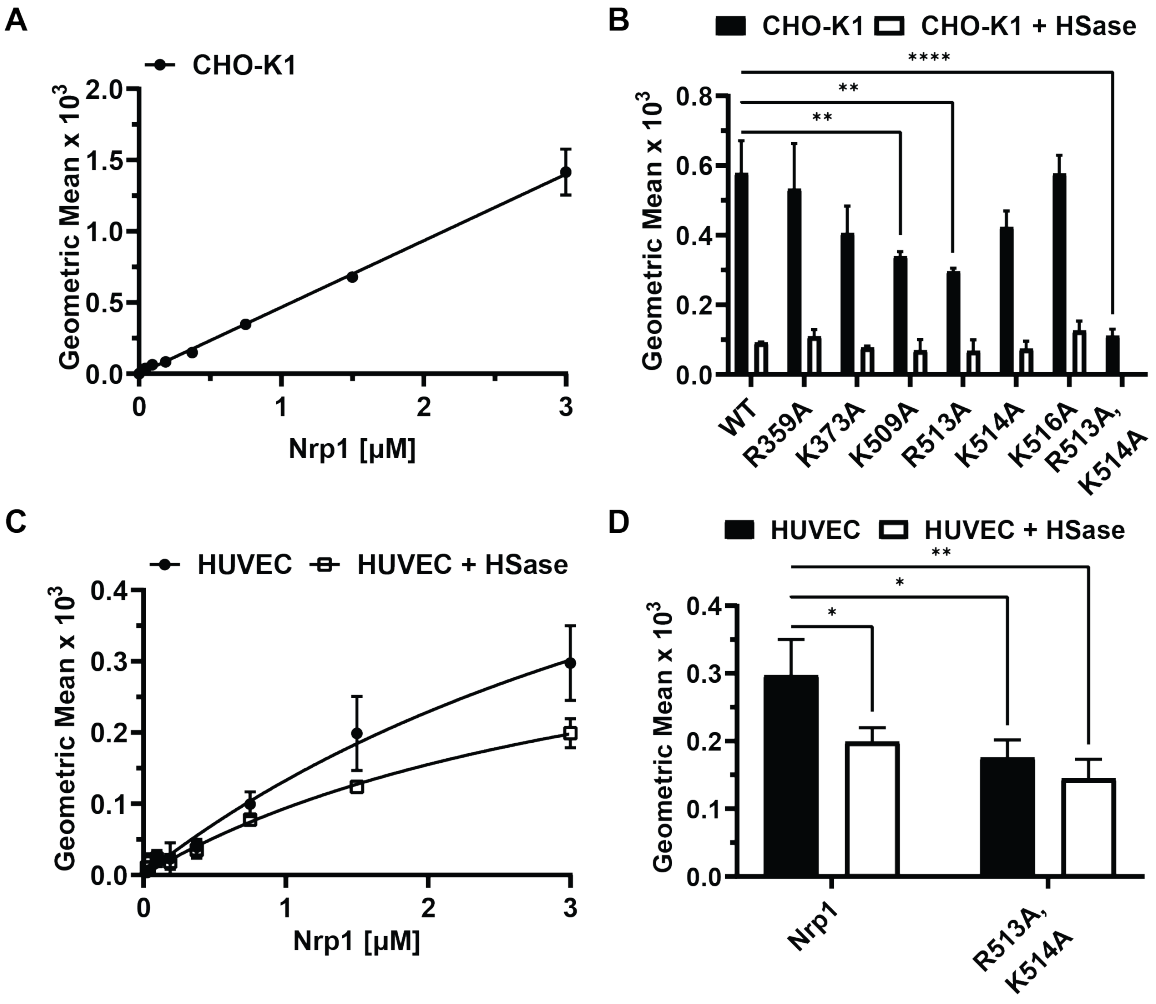

Figure 2.9: Neuropilin-1 Binding to Cell Surface Heparan Sulfate

A, CHO-K1 cells titrated with recombinant wildtype Nrp1 protein. **B**, Wildtype Nrp1 and Nrp1 mutants (1μM) binding to CHO-K1 cells with and without treatment with a combination of heparin lyases I, II and III (HSase). *p* values were determined using a one-way ANOVA with Tukey's multiple comparison test. ** is $p<0.002$ and **** is $p<0.0001$. **C**, HUVECs titrated with recombinant wildtype Nrp1 protein. **D**, Wildtype Nrp1 and Nrp1 mutants (3μM) binding to HUVECs with and without HSase treatment. *p* values were determined using a two-way ANOVA with Tukey's multiple comparison test. * is $p<0.033$ and ** is $p<0.002$.

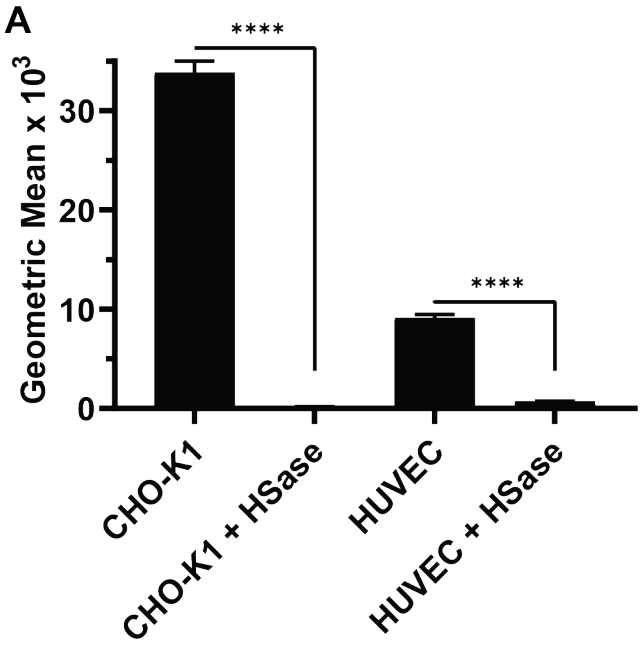

Figure 2.10: Supplement to Figure 2.9

A, 10e4 staining of CHO-K1 and HUVEC cells with and without HSase treatment. *p* values were determined using a one-way ANOVA with Tukey's multiple comparison test. **** is $p<0.0001$.

2.4.8 Generation of Heparan Sulfate Binding Deficient Nrp1 Mouse Model

Nrp1 plays important roles in developmental processes including axon guidance and angiogenesis based on the phenotype of mice bearing null alleles of *Nrp1* or mutant alleles in which binding to VEGFA or Sema3a were altered [17, 26, 71, 116, 117]. To assess how Nrp1 interaction with heparan sulfate could influence its functions *in vivo*, we created a mouse model expressing full length Nrp1 with the double mutation R513A,K514A ($Nrp1^{D}$) in order to systemically reduce its interaction with heparan sulfate. CRISPR/Cas9 gene editing was employed with an sgRNA designed to target Nrp1 near amino acid residues 513 and 514 along with a donor DNA oligonucleotide to allow for the alanine substitution of these target residues. Sequencing of the resulting heparan sulfate binding-deficient mutant confirmed the desired change in genomic sequence (Fig. 2.12A). This sequence alteration was further validated by the loss of a BspHI restriction enzyme site in the $Nrp1^{D}$ sequence, rendering PCR-generated amplicons of the site resistant to digestion (Fig. 2.12B).

To address if the $Nrp1^{D}$ allele was expressed at levels comparable to wildtype *Nrp1*, homogenates of mouse lung were separated by SDS-PAGE and immunoblotted with antibodies to Nrp1 and β-actin (Fig. 2.12C). Animals with either a single copy of the mutant allele ($Nrp1^{D/+}$) or two copies of the mutant allele ($Nrp1^{D/D}$) expressed similar levels of Nrp1 protein to that of wild-type mice (Fig. 2.12C and 2.12D). $Nrp1^{D/-}$ mice express comparable levels of protein to $Nrp1^{+/-}$, which was roughly half of the wildtype level of expression (Fig. 2.12C and

2.12D). Additionally, *Nrp1* mRNA levels were normal, as expected based on the protein expression data (Fig. 2.12E). Whereas homozygous Nrp1 knockout animals ($Nrp1^{-/-}$) are embryonic lethal [17, 117], $Nrp1^{+/-}$, $Nrp1^{D/D}$, and $Nrp1^{D/-}$ animals survived to adulthood and bred normally.

2.4.9 Pathological Angiogenesis in the Heparan Sulfate Binding Deficient Nrp1 Mouse Model

Nrp1 has been shown previously to play an important part in VEGF-stimulated pathological angiogenesis in a tumor model in which B16-F10 murine melanoma cells were implanted subcutaneously into mice [116, 149, 150]. These cells produce copious amounts of VEGF, which stimulates angiogenesis and tumor growth [150]. Injection of 5×10^5 B16-F10 cells subcutaneously on the flank of the animal yielded tumors over the next 15 days that were easily measured with calipers (Fig. 2.11A). Tumors in $Nrp1^{D/D}$ animals showed reduced growth in one set of experiments (Fig. 2.11B), but did not exhibit a diminution in growth when the experiment was repeated (Fig. 2.11C), possibly reflecting differences in the injected dose. To sensitize tumor growth and obtain more consistent results, we reduced the amount of Nrp1 protein in half by crossing the $Nrp1^{D/+}$ mice to $Nrp1^{+/-}$ mice and comparing the growth of the tumors in $Nrp1^{D/-}$ to $Nrp1^{+/-}$ and $Nrp1^{+/+}$ animals. Tumors in $Nrp1^{D/-}$ mice grew much slower and remained smaller than the other groups, which had to be sacrificed due to the tumor burden (Fig. 2.11B and 2.11C). This difference in growth is unlikely to be from the reduced expression of Nrp1 in these animals as normal tumor growth is seen in the $Nrp1^{+/-}$ mice, which

express the same amount protein and mRNA as the *Nrp1*$^{D/-}$ animals (Fig. 2.12C and 2.12D).

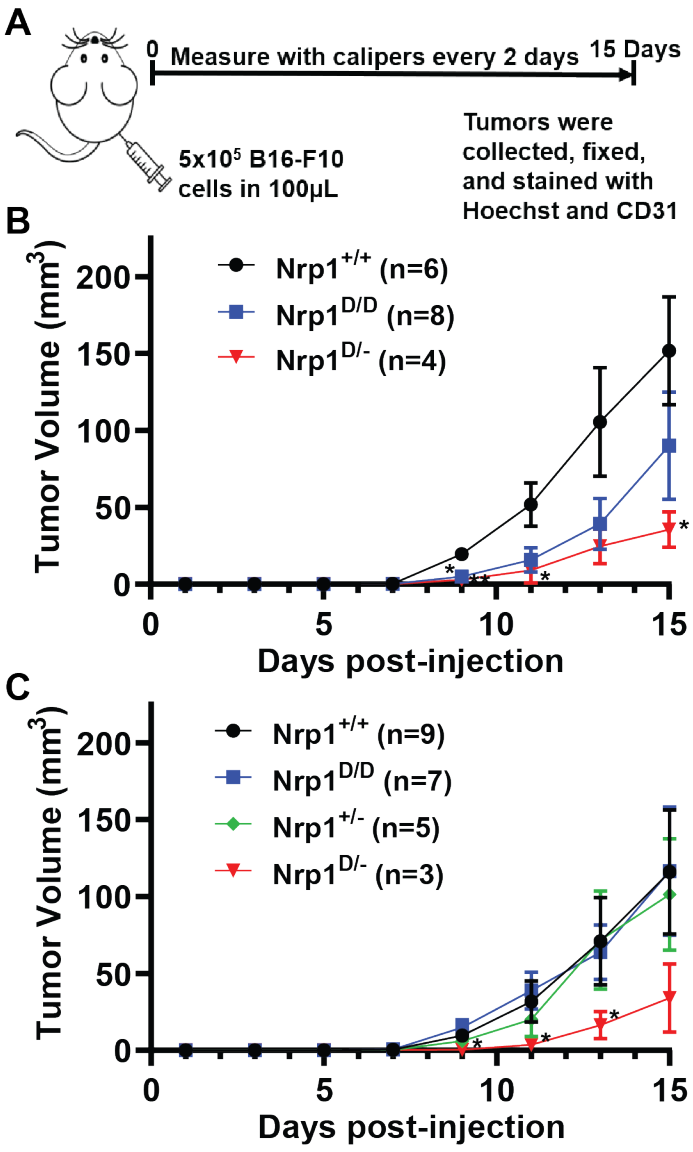

Figure 2.11: Alteration of Neuropilin-1 and Heparan Sulfate Binding Impairs Subcutaneous B16 Tumor Growth

A, Schematic of subcutaneous B16-F10 tumor model**. B,** Tumor growth curves of bilateral subcutaneous B16-F10 tumors in wildtype and mutant *Nrp1* mice. Significance between $Nrp1^{+/+}$ and $Nrp1^{D/-}$. **C**, Tumor growth curves of unilateral subcutaneous B16-F10 tumors in wildtype and mutant *Nrp1* mice**.** Significance between $Nrp1^{D/D}$ and $Nrp1^{D/-}$. There is some variability between the bilateral and unilateral models as seen by differences in the growth curves of the $Nrp1^{D/D}$ mice. *p* values were determined using a two-way ANOVA with the Geisser-Greenhouse correction followed by an uncorrected Fisher's LSD test for each set of data. * is $p<0.033$ and ** is $p<0.002$.

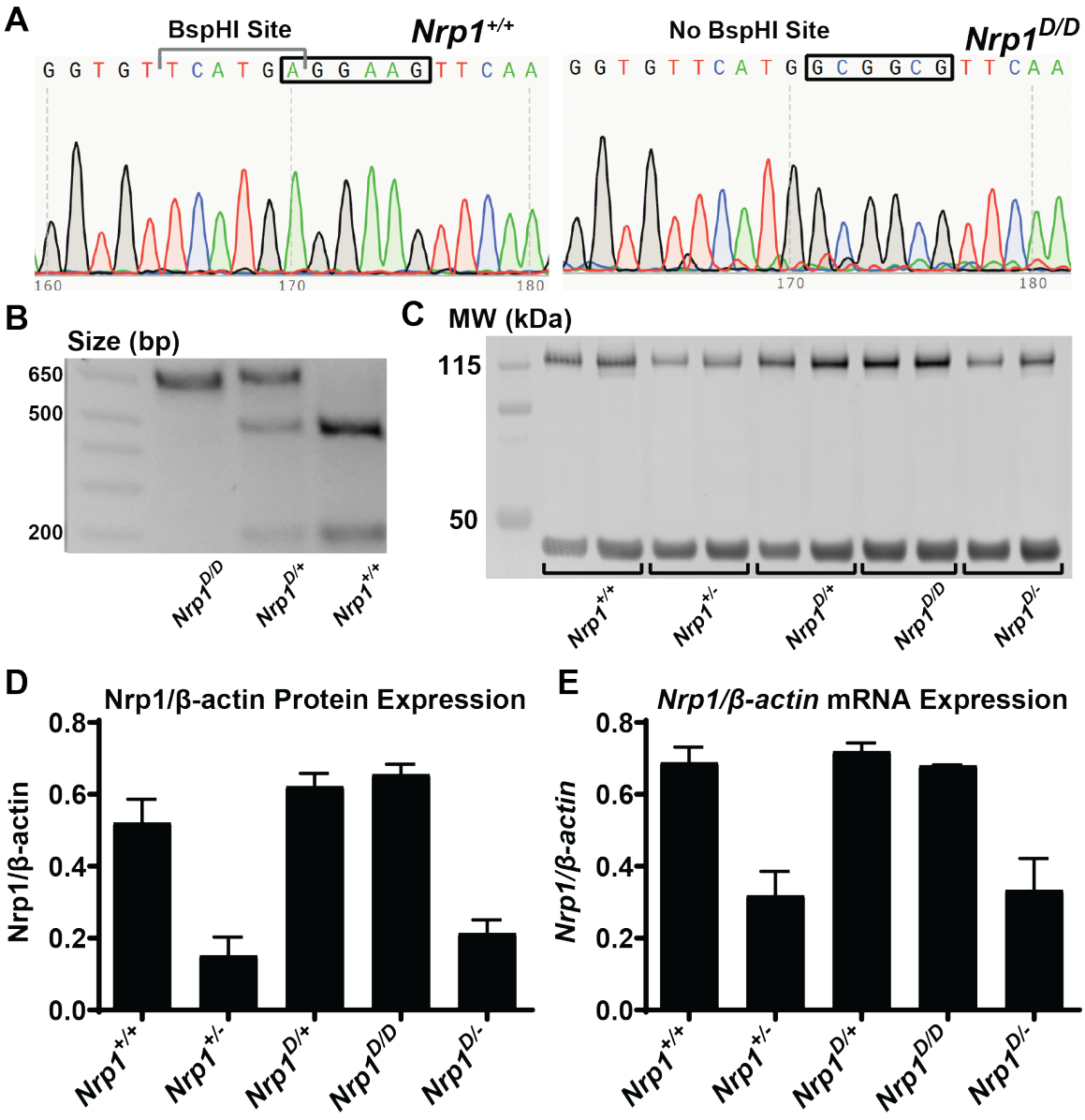

Figure 2.12: Generation and Characterization of *Nrp1*$^{D/D}$ Mouse

A, Sequencing of wildtype and *Nrp1*$^{D/D}$ mouse at mutation site. Wildtype sequence contains a BspHI restriction enzyme site that is resistant when mutation is present. **B**, Representative genotyping of *Nrp1* around mutation site. The resulting amplicon is amenable to digestion by BspHI if it contains the wildtype sequence, but it is resistant to digestion if the site has been mutated as in the *Nrp1*^{D} allele. **C**, Immunoblot of mouse lung homogenate for endogenous Nrp1 and β-actin in wildtype and mutant *Nrp1* mice**. D**, Quantification of Nrp1 protein levels in comparison to β-actin protein levels of immunoblot of mouse lung homogenate (C), n=2**. E**, *Nrp1* mRNA levels in comparison to *β-actin* mRNA levels in mouse lung, n=2

2.4.10 Summary

In summary, we mapped the heparin/heparan sulfate binding site in mouse Nrp1, and defined through molecular modeling and biochemical evaluation of alanine substitution mutants some of the amino acids crucial for Nrp1 interaction with heparin and heparan sulfate. Binding stabilizes the protein against thermal denaturation and induces dimerization in the absence of other ligands and other domains of the protein. Dimerization of Nrp1 was found to be dependent on the length of the heparin chain, with dp14 oligosaccharides able to induce a 1:2 heparin/Nrp1 complex. The mutations also affected the ability of Nrp1 to bind heparan sulfate on endothelial cells. Lastly, reduction of binding to heparan sulfate affects subcutaneous tumor growth.

2.5 Discussion

Nrp1 plays critical roles in the development of the cardiovascular and peripheral nervous system. In the nervous system, Nrp1 modulates axon guidance by acting as a coreceptor with plexin receptors and different semaphorins [12, 32]. In the vascular system, Nrp1 regulates vasculogenesis and angiogenesis by forming complexes with vascular endothelial growth factors (VEGFs) and VEGF receptors [117, 151]. These developmental processes are also modulated by heparin and heparan sulfate, which can bind both Nrp1, VEGF receptors and certain VEGF isoforms, such as $VEGF_{165}$. Previous studies have focused on heparin and heparan sulfate interactions with Nrp1 *in vitro*, using rat and human

forms of Nrp1 subdomains, in particular b1b2 and a1a2b1b2 subdomains. Here we characterized the binding of heparin and heparan sulfate to murine a1a2b1b2 domains and examined protein stability, oligomerization, and the stoichiometry of binding, and as a segue to *in vivo* studies of angiogenesis in the mouse.

It is well established that both Nrp1 and $VEGF_{165}$ can bind heparin, and in fact binding can enhance the formation of $VEGF_{165}$/Nrp1 complexes [19], specifically through the b1b2 domain [36]. Nrp1 can also bind heparin directly, and chains of 8 monosaccharides (dp8) are sufficient [36]. In contrast, a dp20-dp24 heparin chain was necessary for forming a complex with $VEGF_{165}$ and Nrp1, consistent with the idea that the heparin chain acts as a scaffold that binds both VEGF and Nrp1. This complex facilitates VEGF-mediated endothelial cell proliferation *in vitro*, suggesting that complexes that form in vivo with endothelial heparan sulfate can play a role in vasculogenesis and angiogenesis.

Heparin binding patches and clefts on proteins tend to contain many electropositive amino acids that form salt bridges with the uronic acids and sulfate groups in heparin/heparan sulfate [78]. These ionic interactions account for a substantial fraction of the free binding energy of the total interaction [78]. The structure of human b1b2 determined by x-ray crystallography and the modeling studies of murine a1a2b1b2 presented here are in general agreement regarding the location and general size of the heparin binding site located in the b1b2 domain [38]. Vander Kooi and colleagues mutated simultaneously R513, K514 and K516 simultaneously to glutamate, which resulted in a significant decrease in heparin

binding [38]. R359 and K373 were also suggested to participate in binding based on loss of binding in a mutant containing all five mutations (R359E, K373E, R513E, K514E, K516E), but the data was not shown. These residues were also identified in the CVLS simulation and cover a ~40 Å cleft spanning both b1 and b2 domains, which would correspond to a heparin oligomer of ~12 saccharides (Fig. 2.1) [38]. Other studies have suggested heparin binding sites in other domains of the protein, including a1, c (MAM), and the region between the c domain and the transmembrane domain [76]. The b2 domain contains a conserved XBBXBX amino acid motif, (512-517; MRKFKI), which corresponds to a Cardin-Weintraub glycosaminoglycan binding consensus sequence [38, 146]. We found through mutagenesis that R513 and K514, which lie in the middle of the electropositive groove, contributed highly to Nrp1 interaction with heparin and heparan sulfate. These two residues may act as “gate keepers” to allow the heparin/heparan sulfate chain further access to the protein surface. In contrast, the K516 residue, despite being part of the conserved Cardin-Weintraub motif, does not seem to contribute significantly to the interaction. K516 may be positioned past a small bend in the tertiary structure and therefore displaced from the primary binding cleft that contains R513 and K514. In addition, based on our modeling studies, the positioning of the heparin/heparan sulfate chain seems to suggest that the chain wraps around to the back of the protein to engage other amino acids (K397, K538, E541, N544, N545, T553, H571) instead of continuing down to the bottom of the b1 domain (Supplemental Video 1). Mutational manipulation of these

residues should be explored as single or combination in order to further elucidate their contribution to heparin/heparan sulfate binding.

Structural information from X-ray crystallography and size-exclusion chromatography suggests that in solution recombinant b1b2, a2b1b2 and a1a2b1b2 behave as monomers in solution [12, 38, 130]. The absence of crystal structures of Nrp1 in complex with either VEGFR1/VEGF or plexin/Sema3a makes it difficult to predict the orientation of the b1b2 domains in these higher order, functional signaling complexes. Superposition of Nrp1 dimers in the plexin/Sema3a complex positions the Nrp1 dimer as a bridge locking the components of apposing semaphorin–plexin pairs within the overall structure [12], but this does not provide any additional insight into the orientation of the heparin ligand. Inclusion of heparin induces dimerization of human b1b2 domain and the need for a stoichiometric excess of heparin to drive dimer formation *in vitro* suggested a 2:2 stoichiometry of human recombinant Nrp1 b1b2 with heparin [38]. A model was proposed in which the two heparin oligosaccharides were oriented towards each, but charge repulsion of two heparin chains makes this orientation unlikely [38]. Here, we provide direct evidence based on isothermal calorimetry, that the complex of murine a1a2b1b2 is best characterized as a 1:2 complex of heparin oligosaccharide to Nrp1. We imagine that a single heparin oligosaccharide chain acts as a scaffold, serving as the interface between the b1b2 monomers in the Nrp1 dimer. A similar arrangement has been proposed for FGF1/FGFR2 complexes, RAGE dimer, and the dimeric E2 domain of APLP1 [78, 152].

The studies reported here demonstrate the participation of heparin/heparan sulfate-protein interactions in dimerization, but we did not explore possible protein-protein interactions that might further stabilize the complex. Other studies have focused on the MAM (c) domain and the transmembrane region for Nrp1 dimerization [8, 40]. Since heparin is able to dimerize the extracellular domains (a1a2b1b2) without the MAM (c) or transmembrane domains, these interactions may be superfluous in vivo given that the cell surface is covered with a glycocalyx rich in heparan sulfate. Nevertheless, there may be protein-protein contacts between the b1b2 monomers that further stabilize the complex that are worthy of consideration. If the dimer involves weak protein-protein interactions, it might explain why longer oligosaccharides provide greater stabilization to the complex during gel filtration. Lastly, it is possible that binding of heparin/heparan sulfate to Nrp1 may induce a conformational change in the protein exposing an interface that facilitates dimerization.

Many of the earlier studies examining the glycosaminoglycan-binding properties of Nrp1 utilized heparin as a mimetic for heparan sulfate because of its commercial availability. However, heparin is a fractionated form of heparan sulfate, derived from connective mast cells resident in the mucosa of porcine and bovine intestines [78]. Like heparan sulfate, heparin is a linear polysaccharide comprised of alternating glucosamine and uronic acid units [78, 79]. A family of sulfotransferases add sulfate groups at C2 of uronic acid and at N-, C6, and C3 of the glucosamine residues [80]. In heparan sulfate, sulfation occurs

substoichiometrically and within short segments of the chain, creating a variety of partially sulfated sequences interspersed by non-sulfated or poorly sulfated domains of the chain. In contrast, in heparin the chains are more fully sulfated and the extent of epimerization of the uronic acids is more extensive. Thus, one must be careful about extrapolating the behavior of systems analyzed by the addition of heparin compared to native heparan sulfate. Indeed, studies of Nrp1 indicate that affinity for heparan sulfate is much reduced compared to heparin [77].

The modification of the glucosamine units with a 3-*O*-sulfate group is of interest with respect to Nrp1. Sulfation at the C3 position of glucosamine residues occurs at low frequency compared to sulfation at other positions, but can induce high affinity interaction with proteins, such as antithrombin [81]. 3-*O*-sulfation also enhances the binding of Nrp1 to heparan sulfate immobilized on plastic plates and to heparan sulfate present on cultured cells [86]. Synthetic 3-*O*-sulfated heparan sulfate dodecamers inhibited Nrp1-dependent, semaphorin-3a-induced growth cone collapse of neurons derived from murine dorsal root ganglia [86]. Moreover, alteration of Hs3st2 specifically affected growth cone collapse, suggesting the positioning of the 3-*O*-sulfate group within the sulfated domains enhances the affinity of the chains for Nrp1. Attempts to determine the amino acid residues in Nrp1 that interact specifically with the 3-*O*-sulfate group, for example by comparing binding of the mutant recombinant proteins to cells expressing specific 3-*O*-sulfotransferases, did not meet with success possibly due to the complex network of electrostatic and non-electrostatic interactions that facilitate ligand

binding. The CVLS and MD studies can be used to study this problem further since it can account virtually for all possible sulfation configurations.

Neuropilin expression appears to be spatiotemporally regulated in cardiovascular tissues during embryonic development, which may influence the separation of arterial and venous cells [32]. Nrp1 has been suggested to influence the trajectory of migrating cells such as endothelial tip cells at the forefront of new vessels, which parallels its influence on the trajectories of axons during neuronal development [32]. In addition, VEGF/Nrp1 signaling has been shown to be essential for cardiovascular development and Nrp1 is required in endothelial cells to support angiogenesis [26]. Nrp1 is suggested to enhance VEGF-stimulated VEGFR signaling through its complex formation with VEGFR [32]. Therefore, a change in Nrp1 function is likely to alter neuronal and cardiovascular development. To understand the function of heparin/heparan sulfate binding to Nrp1, we created a knock-in mouse containing the R514A/K514A mutation. Normal vasculogenesis and angiogenesis did not appear to be affected based on the health, maturation and normal reproductive capacity of the $Nrp1^{D/D}$ mice. However, variable penetrance of the mutation in the context of pathological angiogenesis was noted, that became penetrant when the level of Nrp1 was reduced by heterozygous mutation ($Nrp1^{D/-}$). Similar growth curves were seen for $Nrp1^{+/+}$ mice in the bilateral and unilateral subcutaneous tumor models. The $Nrp1^{D/-}$ mice consistently showed a reduction in tumor growth in the bilateral and unilateral subcutaneous tumor models as well. However, the $Nrp1^{D/D}$ mice showed

a difference in their tumor growth curves between the bilateral and unilateral model. This might be due to differences in the injected dose or the overall tumor burden between the two models.

Further studies are underway to examine how compounding the *Nrp1*$^{D/D}$ mutation with loss of function alleles in heparan sulfate might exacerbate the phenotype. Additional targeted genetic studies are also needed to prove that the reduced tumor growth resulted from altered angiogenesis in the tumor environment.

2.6 Acknowledgements

Chapter 2, in full, is currently being prepared as a manuscript for submission for publication of the material. CD Painter, NV Sankaranarayanan, B Nagarajan, TM Clausen, AMV West, J Park, PL Bartels, RN Porell, DR Sandoval, GJ Vasquez, PLSM Gordts, CW Vander Kooi, KD Corbett, UR Desai, JD Esko. Alteration of Neuropilin-1 and Heparan Sulfate Interaction Impairs Angiogenesis-Dependent Tumor Growth. *In preparation*. The dissertation author is the primary investigator and author of this material.

Special thanks to all of the Jeffrey Esko and Philip Gordts lab members for their help and guidance along the way. Thank you to our collaborating labs (the Desai lab at Virginia Commonwealth University, the Corbett Lab at UC San Diego, and the Godula Lab at UC San Diego) for their intellectual and scientific

contributions. Thank you also to Craig Vander Kooi at the University of Kentucky for advice on the project.

Thank you to the UC San Diego Microscopy Core, especially Marcy Erb and Jennifer Santini for their assistance with various microscopy methods and immunofluorescence staining. Thank you to the La Jolla Institute of Immunology Microscopy and Histology Core, in particular Katarzyna Dobaczewska for histology. Thank you to the Sanford Burnham Prebys Medical Discovery Institute Protein Analysis Facility, especially Andrey Bobkov, for performing and analyzing isothermal calorimetry experiments. Thank you to the UC San Diego Transgenic Mouse Core, especially Jun Zhao and Ella Kothari for performing our CRISPR RNA injections for transgenic mouse generation. Thank you to the Steven Dowdy lab for the B16-F10 melanoma cells for the tumor experiments. Thank you to the E. Yvonne Jones lab for the *mNrp1* plasmids. Thank you to these funding sources: National Institutes of Health (NIH) grants P01 HL131474 and AR073031 to J.D.E.; NINDS P30 NS047101 to UC San Diego Microscopy; and NIH grants: P42 ES010377, P30 CA023100, and P30 DK063491 to UC San Diego Transgenic Mouse Core.

Chapter 3: Concluding Remarks

3.1 Project Summary

In this thesis, we mapped the heparin/heparan sulfate binding site in mouse Nrp1 (a1a2b1b2), determined a 1:2 stoichiometry for the heparin/Nrp1 complex, and demonstrated the biological significance of this interaction in a subcutaneous tumor model. Amino acids critical for Nrp1 interaction with heparin and heparan sulfate were defined through molecular modeling and biochemical evaluation of alanine substitution mutants. Heparin-induced dimerization of Nrp1 was found to be dependent on the length of the heparin chain, with longer chains (dp14-dp20) able to induce a 1:2 heparin/protein complex as seen by isothermal calorimetry. Binding stabilizes the protein based on an increase in melting temperature of the heparin/protein complex versus the unliganded protein during thermal denaturation. Lastly, alteration of the heparin-binding capacity of Nrp1 affects subcutaneous tumor growth, presumably through its effect on pathological angiogenesis.

3.2 Modeling Studies

Heparin binding sites on proteins tend to contain many electropositive amino acids such as arginine and lysine residues [78]. The negative charges of the sulfate and carboxylate motifs on heparan sulfate form salt bridges with the positive charges of these amino acids. Studies aimed at the identification of residues responsible for heparin/protein interactions skew towards arginine and lysine residues since these ionic interactions account for a substantial fraction of

the free binding energy of the total interaction [78]. However, other nonionic interactions (hydrogen bonding, pi-pi stacking, Van der Waals, etc.) may also contribute significantly to heparin/protein interactions [78]. Our CVLS and MD studies identified non-charged residues (Ser, Tyr, Ala, Asn, Thr, His, etc.) that likely participate in nonionic interactions between Nrp1 and heparin/heparan sulfate. Mutational analysis of these residues could help reveal the nonionic contributions to the binding free energy and to the specificity of binding for heparin/heparan sulfate over other types of glycosaminoglycans, such as chondroitin/dermatan sulfate and hyaluronan. Lastly, Nrp1 has been shown previously to preferentially interact with heparan sulfate chains containing 3-*O*-sulfate group [86]. This relatively rare modification occurs primarily in highly sulfated domains of heparan sulfate because of the preference of the 3-*O*-sulfotransferases for sulfated domains of the chain [91, 92]. How the charged amino acids and the other residues contribute to the preferred selection of 3-*O*-sulfated segments remains unknown. Isothermal calorimetry suggests a stoichiometry of 1:2 heparin/Nrp1. Understanding how a single heparin oligosaccharide participates in dimer formation, for example through an induced conformational chain or by serving as the interface between the Nrp1 monomers, remains to be determined. Future modeling studies should incorporate a Nrp1 dimer in order to further refine which residues make contacts with the oligosaccharides in this model.

3.3 Heparin Binding

The heparin binding site in human Nrp1 has previously been mapped as an electropositive cleft approximately 40 Å in length in the b1 and b2 domains [38]. Heparin binding was decreased when multiple arginine and lysine residues within this groove were mutated to glutamic acid (R359E, K373E, R513E, K514E, and K516E) [38]. Other studies found heparin binding sites in other domains of the protein including a1, c, and the region between the c domain and the transmembrane domain [76]. To reevaluate the contribution of the a1 and a2 domains, we modeled the a1a2b1b2 construct and found that a1 and a2 subdomains do not contribute significantly to the cleft formed by the b1 and b2 domains (Fig. 2.1). The amino acids determined to be important for the Nrp1 and heparin interaction are evolutionarily conserved arginine and lysine residues in the b1b2 domain in the human, mouse and rat orthologs. Amino acids 512-517 in mouse Nrp1 (MRKFKI) constitutes a Cardin-Weintraub motif representing a glycosaminoglycan binding consensus sequence [38, 146]. R513 and K514, which lie in the middle of the electropositive groove, were found contribute the most to Nrp1 interaction with heparin and heparan sulfate. These two residues may act as “gate keepers” to allow the heparin/heparan sulfate chain further access to the protein surface or they may help dictate the positioning of the oligosaccharide chain in the Nrp1 dimer. In contrast to this, the K516 residue, despite being part of the conserved Cardin-Weintraub motif, does not seem to contribute significantly to the interaction. This may be due to its positioning past a small bend in the tertiary

structure after the R513 and K514 residues. In addition, based on our modeling studies, the positioning of the heparin/heparan sulfate chain seems to suggest that the chain wraps around to the back of the protein to engage other amino acids (K397, K538, E541, N544, N545, T553, H571) instead of continuing down to the bottom of the b1 domain. Additional mutations should be explored as single or combination in order to further elucidate their contribution to binding. In practice, this may be difficult if the relative contribution of non-electrostatic interactions makes small contributions to the overall binding. All mutants should be examined for conformation changes, altered expression and VEGF binding to ensure that the mutations do not affect the overall structure of the protein.

3.4 Structural Requirements for Heparin Binding and Heparin-Induced Dimerization

As measured in pymol, the binding cleft in mouse in a1a2b1b2 is approximately 50 Å long which would support binding an oligosaccharide of ~15 monosaccharides. The minimal length requirements of a heparin oligosaccharide to engage Nrp1 in a 1:1 ratio is about 8-10 sugars, whereas a longer oligosaccharide (dp18-20) is necessary to promote a 1:2 heparin/protein complex as seen by SEC-MALS. ITC experiments are consistent with this finding. Previous studies suggest that heparin tetradecasaccharide (dp14) is sufficient to drive complete dimerization of human Nrp1 b1b2. Whether this difference is due to species variation or the difference in behavior of the b1b2 complex versus the

a1a2b1b2 complex is unclear. Our results are corroborated by a study using sized heparin oligosaccharides to compete with binding of human b1b2 domains to heparin [36]. Octasaccharides (dp8) were capable of slightly reducing heparin binding while longer icosasaccharides (dp20) were needed to completely inhibit binding. These findings suggest a minimal length of 8 saccharides for engagement, with affinity increasing as the oligosaccharides increase in length. In a separate study using a pre-dimerized Nrp1-Fc protein, a dp14 heparin oligosaccharide was the minimal size for initial binding to the dimer demonstrating that a longer chain is needed to engage dimeric Nrp1. It is possible that the longer chain is necessary to dimerize the a1a2b1b2 since our modeling studies identified a residue just outside the main binding cleft in b1b2. In addition, the Nrp1 dimer may have a higher affinity for the longer chains promoting more robust and longer lasting complexes.

A priori, a 1:2 complex of heparin/Nrp1 suggests a sandwich-like complex, with the heparin oligosaccharide sandwiched between the two a1a2b1b2 monomers, and a longer fragment necessary for stabilization. This complex may be similar to either the heparin/FGF1 dimer or the heparin/APLP-1 dimer complexes [78]. These models vary by whether the dimer is based solely on heparan sulfate/protein interaction as in the FGF1 dimer or on weak protein/protein interactions that are stabilized by heparan sulfate binding as in the APLP-1 dimer [78].

Our studies demonstrate the need for heparin/protein interactions for dimer formation, but we did not explore protein/protein interactions that might stabilize the complex. Other studies have focused on the MAM (c) domain or the transmembrane region for Nrp1 dimerization [8, 40]. However, recent studies have indicated that the MAM domain by itself and soluble Nrp proteins containing the MAM domains are monomeric in solution by gel filtration, isothermal calorimetry and multiangle light scattering [39, 130, 153]. Since heparin is able to dimerize the extracellular domains (a1a2b1b2) without the presence of the MAM or transmembrane domains, interactions driven by the MAM and transmembrane domains would appear to be dispensable. Lastly, binding of Nrp1 to heparin could also induce a conformational change in the protein allowing an alternative dimer interface to develop. In order to elucidate the positioning and configuration of the interaction between heparin and Nrp1, structural analyses based on X-ray crystallography, cryogenic electron microscopy and small-angle X-ray scattering of the heparin/Nrp1 complexes should be completed.

The longer length requirement may also reflect the distribution and availability of high affinity binding sites for Nrp1 within the heparin oligosaccharides. Since these sized heparin oligosaccharides are derived from heparin, they represent a mix of sulfated species. Thus, it is possible that Nrp1 only engages a subset of oligosaccharides that contain the optimal specific sulfation patterns. In addition, previous research in our lab has shown that Nrp1 shows selective binding for segments that contain 3-*O*-sulfated glucosamine

residues [86]. This modification occurs on the glucosamine units of heparin/heparan sulfate within highly sulfated regions. It is of interest due to its rarity and its position as the one of the last modifications in the biosynthetic pathway [78, 80]. Heparin is a mixture of oligosaccharides varying length from 25-75 monosaccharides and only a third of the chains contain 3-*O*-sulfate groups that allow anticoagulant heparin to bind with high affinity to antithrombin [81]. This raises the possibility that only a subfraction of the chains can bind to Nrp1, an issue that would be further accentuated in heparan sulfate, which contains many fewer 3-*O*-sulfate groups and is segmented into regions of high sulfation and uronic acid epimerization separated by non-sulfated or poorly sulfated regions. Compounding this issue is the fact that only a subset of 3-*O*-sulfotransferases can generate the preferred binding sequence for Nrp1 [86, 91]. Thus, *in vivo* only a small fraction of cellular heparan sulfate might have the appropriate arrangement of sulfated monosaccharides to facilitate higher affinity binding to Nrp1. This possibility can be tested by using Nrp1 as an affinity matrix for fractionation of the chains. Such experiments could also reveal that longer chains are more likely to bind due to the higher probability that they contain the preferred 3-*O*-sulfated binding sequence.

Lastly, longer oligosaccharides may reflect that heparan sulfate could bring the remaining components of the complex into proximity of each other through a templating mechanism [36, 78]. The variably sulfated domains of heparan sulfate may be able to fit the distinctive structural requirements for VEGF, VEGFR2 and Nrp1. Other aspects of the effect of heparan sulfate binding on Nrp1, such as if

binding induces a conformational change in Nrp1 that affects interactions within the complex, remain open to further investigation.

3.5 Investigating Effects of Heparin Binding Deficient Neuropilin-1

The impact of the loss of heparin-binding in Nrp1 can be readily assessed using the R513A,K514A mutant. Altering binding of heparan sulfate or heparin on the formation of the higher order complexes of Nrp1, VEGFR, and VEGF should be explored, for example by coimmunoprecipitation or by SPR utilizing immobilized heparin to assess dynamic complex formation of the soluble components [77]. In addition, gel filtration could be used to assess how altering binding of heparin/heparan sulfate affects formation of complexes using $VEGF_{165}$ and VEGR2 extracellular domains. Transfection of cells with the double mutant would extend these studies to a more physiological context in which all of the components are embedded in the plasma membrane. In this way, the impact of altered heparin/heparan sulfate binding on $VEGF_{165}$ binding, VEGFR signaling, and receptor oligomerization could be studied in a more natural context [67, 69, 77].

In cells, heparan sulfate does not occur as a free polysaccharide, but instead is found covalently linked to heparan sulfate proteoglycans. Thus, the functional complexes that form between $VEGF_{165}$, VEGFR and Nrp1 would contain an heparan sulfate proteoglycan, not a small oligosaccharide chain. Endothelial cells, like other cell types, express only a subset of the 17 or so heparan sulfate proteoglycans encoded in the vertebrate genomes. Whether the complex is

selective for specific heparan sulfate proteoglycans or promiscuous with respect to the proteoglycan core protein remains an open question.

Lastly, as Nrp1 is known to act as a receptor and co-receptor for other ligands/receptor complexes, the R513A,K514A mutant would allow one to study how heparan sulfate binding affects these systems. An open area of investigation is the question of whether heparin/heparan sulfate binding affects the formation of sema/Nrp1/plexin complexes. As heparan sulfate proteoglycans and Nrp1 have both been identified as co-receptors for the spike protein of SARS-CoV-2, the R513A,K514A mutant could help address if the interaction of Nrp1 and heparan sulfate on the cell surface affects spike protein binding [128, 129, 142]. Combining mutations in heparan sulfate biosynthesis or mutations that affect specific heparan sulfate proteoglycans with the R513A,K514A mutant would provide additional insight into role of endogenous heparan sulfate in Nrp1 mediated processes [154].

3.6 Influence of Heparan Sulfate on Neuropilin-1 Function *in vivo*

As discussed in the introduction, the role of Nrp1 in signaling can be explored by altering its binding to other components of the signaling complexes. The knock-in $Nrp1^{D}$ mouse model allowed us to examine the interaction of heparan sulfate and Nrp1 *in vivo*. The subcutaneous tumor model using B16-F10 melanoma cells demonstrated differences in tumor growth amongst genotypes. The $Nrp1^{D/D}$ showed a small reduction in tumor size and slower growth over time in a bilateral subcutaneous tumor experiment, but was more comparable to tumor

size and growth of wildtype tumors in a unilateral subcutaneous tumor experiment, possibly due to differences in the injected dose or overall tumor burden between the two experiments. In a more sensitized model where the amount of Nrp1 was reduced, tumors in *Nrp1*$^{D/-}$ mice were much smaller and grew considerably slower than tumors in *Nrp1*$^{+/-}$, *Nrp1*$^{+/+}$, and *Nrp1*$^{D/D}$ mice. Since the *Nrp1*$^{D/-}$ mice were shown to express the same levels of mRNA for Nrp1 and protein as *Nrp1*$^{+/-}$, this difference in tumor size and growth is not likely due to the reduced expression of *Nrp1* in *Nrp1*$^{D/-}$ mice.

Analysis of the blood vessel density of these tumors could address if the reduced tumor growth was caused by a lack of vascularization. In addition, isolated endothelial cells from these animals could be examined for $VEGF_{165}$ binding and activation of downstream signaling. The ability of these isolated endothelial cells to proliferate and migrate could be assessed using tubulogenesis and migration assays [64]. As Nrp1 was previously shown to affect VEGFR2 expression [71], it would be interesting to investigate if Nrp1 binding to heparan sulfate affects its ability to regulate VEGFR2.

The *Nrp1*^{D} mouse model is the first to address the biological significance of the interaction between Nrp1 and heparan sulfate *in vivo*. In addition to our analysis of pathological angiogenesis, further characterization of this mouse model could provide insight in to the role of heparan sulfate/Nrp1 interaction in other forms of angiogenesis. As our mouse model survives to adulthood, both embryonic and postnatal angiogenesis can be assessed through hindbrain and retinal

angiogenesis assays, respectively. Although hindbrain angiogenesis occurs in a VEGF-independent manner [71, 116], Nrp1 and heparan sulfate may interact with other cell surface receptors to guide this process. Postnatal angiogenesis in the retina has been demonstrated to be VEGF-dependent [71, 116] so the effect of the Nrp1 and heparan sulfate interaction on VEGF signaling in retinal angiogenesis can be examined.

The combination of anti-VEGF and anti-Nrp1 antibodies leads to a synergistic reduction in xenograft tumor models [155] suggesting that the role of Nrp1 in pathological angiogenesis might not be limited to the VEGF/HSPG/Nrp1/VEGFR2 signaling complex. Other pathological angiogenesis models such as xenograft tumor or oxygen-induced retinopathy [23, 127] may provide additional insights into the role of the heparan sulfate-Nrp1 interaction *in vivo* in both VEGF-dependent and VEGF-independent pathways.

Nrp1 is involved in other biological processes apart from angiogenesis including facilitating growth cone collapse in axon guidance by acting as a co-receptor for other ligand/receptor pairs such as semaphorins and plexins [8, 9, 11, 12, 20]. Previous work explored the role of the 3-*O*-sulfation of heparan sulfate in Nrp1-dependent axon guidance suggesting that the interaction between Nrp1 and heparan sulfate may influence growth cone collapse [86]. The $Nrp1^{D}$ mouse model may also provide further insights into the role of the heparan sulfate-Nrp1 interaction within this Sema/Plexin complex and Nrp1-mediated growth cone collapse *in vivo* as well.

3.7 Summary

In summary, the examination of normal vascular development and pathological vascularization, such as tumor angiogenesis and retinopathy may reveal differences that can be exploited for therapy. Analysis of the structure and function of the signaling complexes that mediate these biological effects sheds light on potential targets for therapeutic intervention. Here, we demonstrated how mapping of a ligand binding site in Nrp1 led to the identification of critical amino acids (R513A,K514A) that mediate the interaction. We also determined a stoichiometry of a 1:2 heparin/Nrp1 complex that suggests a potential role for heparan sulfate proteoglycans to promote dimerization of Nrp1 on the cell surface. Lastly, the *Nrp1*^{D} mouse model demonstrates that the ability of Nrp1 to bind heparan sulfate affects subcutaneous tumor growth. Therapies are under development to target Nrp1 and VEGF [54, 69]. Thus, one might exploit the availability of heparin oligosaccharides or heparin mimetics as potential agents to interfere with this interaction [114, 156-158] in order to block pathological angiogenesis that occurs in tumors and retinopathies.

REFERENCES

1. Buschmann, I. and W. Schaper, *Arteriogenesis Versus Angiogenesis: Two Mechanisms of Vessel Growth.* News Physiol Sci, 1999. **14**: p. 121-125.
2. Patan, S., *How Is the Branching of Animal Blood Vessels Implemented?*, in *Madame Curie Bioscience Database*. 2000-2013, Landes Bioscience: Austin,TX.
3. Risau, W., *Mechanisms of angiogenesis.* Nature, 1997. **386**(6626): p. 671-4.
4. Holash, J., P.C. Maisonpierre, D. Compton, P. Boland, C.R. Alexander, D. Zagzag, G.D. Yancopoulos, and S.J. Wiegand, *Vessel cooption, regression, and growth in tumors mediated by angiopoietins and VEGF.* Science, 1999. **284**(5422): p. 1994-8.
5. Lugano, R., M. Ramachandran, and A. Dimberg, *Tumor angiogenesis: causes, consequences, challenges and opportunities.* Cell Mol Life Sci, 2020. **77**(9): p. 1745-1770.
6. Wang, X., A.M. Bove, G. Simone, and B. Ma, *Molecular Bases of VEGFR-2-Mediated Physiological Function and Pathological Role.* Front Cell Dev Biol, 2020. **8**: p. 599281.
7. Sarabipour, S. and F. Mac Gabhann, *VEGF-A121a binding to Neuropilins - A concept revisited.* Cell Adh Migr, 2018. **12**(3): p. 204-214. www.tandfonline.com.
8. Nakamura, F., M. Tanaka, T. Takahashi, R.G. Kalb, and S.M. Strittmatter, *Neuropilin-1 extracellular domains mediate semaphorin D/III-induced growth cone collapse.* Neuron, 1998. **21**(5): p. 1093-100.
9. Takahashi, T., A. Fournier, F. Nakamura, L.H. Wang, Y. Murakami, R.G. Kalb, H. Fujisawa, and S.M. Strittmatter, *Plexin-neuropilin-1 complexes form functional semaphorin-3A receptors.* Cell, 1999. **99**(1): p. 59-69.
10. Kolodkin, A.L., D.J. Matthes, and C.S. Goodman, *The semaphorin genes encode a family of transmembrane and secreted growth cone guidance molecules.* Cell, 1993. **75**(7): p. 1389-99.
11. Koncina, E., L. Roth, B. Gonthier, and D. Bagnard, *Role of semaphorins during axon growth and guidance.* Adv Exp Med Biol, 2007. **621**: p. 50-64.
12. Janssen, B.J., T. Malinauskas, G.A. Weir, M.Z. Cader, C. Siebold, and E.Y. Jones, *Neuropilins lock secreted semaphorins onto plexins in a ternary signaling complex.* Nat Struct Mol Biol, 2012. **19**(12): p. 1293-9.

13. Kitsukawa, T., A. Shimono, A. Kawakami, H. Kondoh, and H. Fujisawa, *Overexpression of a membrane protein, neuropilin, in chimeric mice causes anomalies in the cardiovascular system, nervous system and limbs.* Development, 1995. **121**(12): p. 4309-18.

14. Takagi, S., T. Tsuji, T. Amagai, T. Takamatsu, and H. Fujisawa, *Specific cell surface labels in the visual centers of Xenopus laevis tadpole identified using monoclonal antibodies.* Dev Biol, 1987. **122**(1): p. 90-100.

15. Takagi, S., Y. Kasuya, M. Shimizu, T. Matsuura, M. Tsuboi, A. Kawakami, and H. Fujisawa, *Expression of a cell adhesion molecule, neuropilin, in the developing chick nervous system.* Dev Biol, 1995. **170**(1): p. 207-22.

16. Kawakami, A., T. Kitsukawa, S. Takagi, and H. Fujisawa, *Developmentally regulated expression of a cell surface protein, neuropilin, in the mouse nervous system.* J Neurobiol, 1996. **29**(1): p. 1-17.

17. Kitsukawa, T., M. Shimizu, M. Sanbo, T. Hirata, M. Taniguchi, Y. Bekku, T. Yagi, and H. Fujisawa, *Neuropilin-semaphorin III/D-mediated chemorepulsive signals play a crucial role in peripheral nerve projection in mice.* Neuron, 1997. **19**(5): p. 995-1005.

18. Chen, H., A. Chedotal, Z. He, C.S. Goodman, and M. Tessier-Lavigne, *Neuropilin-2, a novel member of the neuropilin family, is a high affinity receptor for the semaphorins Sema E and Sema IV but not Sema III.* Neuron, 1997. **19**(3): p. 547-59.

19. Soker, S., S. Takashima, H.Q. Miao, G. Neufeld, and M. Klagsbrun, *Neuropilin-1 is expressed by endothelial and tumor cells as an isoform-specific receptor for vascular endothelial growth factor.* Cell, 1998. **92**(6): p. 735-45.

20. Kolodkin, A.L., D.V. Levengood, E.G. Rowe, Y.T. Tai, R.J. Giger, and D.D. Ginty, *Neuropilin is a semaphorin III receptor.* Cell, 1997. **90**(4): p. 753-62.

21. Fujisawa, H., *Discovery of semaphorin receptors, neuropilin and plexin, and their functions in neural development.* J Neurobiol, 2004. **59**(1): p. 24-33.

22. Gagnon, M.L., D.R. Bielenberg, Z. Gechtman, H.Q. Miao, S. Takashima, S. Soker, and M. Klagsbrun, *Identification of a natural soluble neuropilin-1 that binds vascular endothelial growth factor: In vivo expression and antitumor activity.* Proc Natl Acad Sci U S A, 2000. **97**(6): p. 2573-8.

23. Raimondi, C., J.T. Brash, A. Fantin, and C. Ruhrberg, *NRP1 function and targeting in neurovascular development and eye disease.* Prog Retin Eye Res, 2016. **52**: p. 64-83.

24. Brown, C.B., L. Feiner, M.M. Lu, J. Li, X. Ma, A.L. Webber, L. Jia, J.A. Raper, and J.A. Epstein, *PlexinA2 and semaphorin signaling during cardiac neural crest development.* Development, 2001. **128**(16): p. 3071-80.

25. Feiner, L., A.L. Webber, C.B. Brown, M.M. Lu, L. Jia, P. Feinstein, P. Mombaerts, J.A. Epstein, and J.A. Raper, *Targeted disruption of semaphorin 3C leads to persistent truncus arteriosus and aortic arch interruption.* Development, 2001. **128**(16): p. 3061-70.

26. Gu, C., E.R. Rodriguez, D.V. Reimert, T. Shu, B. Fritzsch, L.J. Richards, A.L. Kolodkin, and D.D. Ginty, *Neuropilin-1 conveys semaphorin and VEGF signaling during neural and cardiovascular development.* Dev Cell, 2003. **5**(1): p. 45-57.

27. Roy, S., A.K. Bag, R.K. Singh, J.E. Talmadge, S.K. Batra, and K. Datta, *Multifaceted Role of Neuropilins in the Immune System: Potential Targets for Immunotherapy.* Front Immunol, 2017. **8**: p. 1228.

28. Tordjman, R., Y. Lepelletier, V. Lemarchandel, M. Cambot, P. Gaulard, O. Hermine, and P.H. Romeo, *A neuronal receptor, neuropilin-1, is essential for the initiation of the primary immune response.* Nat Immunol, 2002. **3**(5): p. 477-82.

29. Klagsbrun, M., S. Takashima, and R. Mamluk, *The role of neuropilin in vascular and tumor biology.* Adv Exp Med Biol, 2002. **515**: p. 33-48.

30. Bielenberg, D.R., C.A. Pettaway, S. Takashima, and M. Klagsbrun, *Neuropilins in neoplasms: expression, regulation, and function.* Exp Cell Res, 2006. **312**(5): p. 584-93.

31. Miao, H.Q., P. Lee, H. Lin, S. Soker, and M. Klagsbrun, *Neuropilin-1 expression by tumor cells promotes tumor angiogenesis and progression.* FASEB J, 2000. **14**(15): p. 2532-9.

32. Pellet-Many, C., P. Frankel, H. Jia, and I. Zachary, *Neuropilins: structure, function and role in disease.* Biochem J, 2008. **411**(2): p. 211-26.

33. Takagi, S., T. Hirata, K. Agata, M. Mochii, G. Eguchi, and H. Fujisawa, *The A5 antigen, a candidate for the neuronal recognition molecule, has homologies to complement components and coagulation factors.* Neuron, 1991. **7**(2): p. 295-307.

34. Lee, C.C., A. Kreusch, D. McMullan, K. Ng, and G. Spraggon, *Crystal structure of the human neuropilin-1 b1 domain.* Structure, 2003. **11**(1): p. 99-108.

35. Gu, C., B.J. Limberg, G.B. Whitaker, B. Perman, D.J. Leahy, J.S. Rosenbaum, D.D. Ginty, and A.L. Kolodkin, *Characterization of neuropilin-1 structural features that confer binding to semaphorin 3A and vascular endothelial growth factor 165.* J Biol Chem, 2002. **277**(20): p. 18069-76.

36. Mamluk, R., Z. Gechtman, M.E. Kutcher, N. Gasiunas, J. Gallagher, and M. Klagsbrun, *Neuropilin-1 binds vascular endothelial growth factor 165, placenta growth factor-2, and heparin via its b1b2 domain.* J Biol Chem, 2002. **277**(27): p. 24818-25.

37. Giger, R.J., E.R. Urquhart, S.K. Gillespie, D.V. Levengood, D.D. Ginty, and A.L. Kolodkin, *Neuropilin-2 is a receptor for semaphorin IV: insight into the structural basis of receptor function and specificity.* Neuron, 1998. **21**(5): p. 1079-92.

38. Vander Kooi, C.W., M.A. Jusino, B. Perman, D.B. Neau, H.D. Bellamy, and D.J. Leahy, *Structural basis for ligand and heparin binding to neuropilin B domains.* Proc Natl Acad Sci U S A, 2007. **104**(15): p. 6152-7.

39. Yelland, T. and S. Djordjevic, *Crystal Structure of the Neuropilin-1 MAM Domain: Completing the Neuropilin-1 Ectodomain Picture.* Structure, 2016. **24**(11): p. 2008-2015.

40. Roth, L., C. Nasarre, S. Dirrig-Grosch, D. Aunis, G. Cremel, P. Hubert, and D. Bagnard, *Transmembrane domain interactions control biological functions of neuropilin-1.* Mol Biol Cell, 2008. **19**(2): p. 646-54.

41. Fukahi, K., M. Fukasawa, G. Neufeld, J. Itakura, and M. Korc, *Aberrant expression of neuropilin-1 and -2 in human pancreatic cancer cells.* Clin Cancer Res, 2004. **10**(2): p. 581-90.

42. Shintani, Y., S. Takashima, Y. Asano, H. Kato, Y. Liao, S. Yamazaki, O. Tsukamoto, O. Seguchi, H. Yamamoto, T. Fukushima, K. Sugahara, M. Kitakaze, and M. Hori, *Glycosaminoglycan modification of neuropilin-1 modulates VEGFR2 signaling.* EMBO J, 2006. **25**(13): p. 3045-55.

43. Frankel, P., C. Pellet-Many, P. Lehtolainen, G.M. D'Abaco, M.L. Tickner, L. Cheng, and I.C. Zachary, *Chondroitin sulphate-modified neuropilin 1 is expressed in human tumour cells and modulates 3D invasion in the U87MG human glioblastoma cell line through a p130Cas-mediated pathway.* EMBO Rep, 2008. **9**(10): p. 983-9.

44. Olsson, A.K., A. Dimberg, J. Kreuger, and L. Claesson-Welsh, *VEGF receptor signalling - in control of vascular function.* Nat Rev Mol Cell Biol, 2006. **7**(5): p. 359-71.

45. Tischer, E., R. Mitchell, T. Hartman, M. Silva, D. Gospodarowicz, J.C. Fiddes, and J.A. Abraham, *The human gene for vascular endothelial growth factor. Multiple protein forms are encoded through alternative exon splicing.* J Biol Chem, 1991. **266**(18): p. 11947-54.

46. Peach, C.J., V.W. Mignone, M.A. Arruda, D.C. Alcobia, S.J. Hill, L.E. Kilpatrick, and J. Woolard, *Molecular Pharmacology of VEGF-A Isoforms: Binding and Signalling at VEGFR2.* Int J Mol Sci, 2018. **19**(4).

47. Ruhrberg, C., *Growing and shaping the vascular tree: multiple roles for VEGF.* Bioessays, 2003. **25**(11): p. 1052-60.

48. Vempati, P., A.S. Popel, and F. Mac Gabhann, *Extracellular regulation of VEGF: isoforms, proteolysis, and vascular patterning.* Cytokine Growth Factor Rev, 2014. **25**(1): p. 1-19.

49. Parker, M.W., P. Xu, X. Li, and C.W. Vander Kooi, *Structural basis for selective vascular endothelial growth factor-A (VEGF-A) binding to neuropilin-1.* J Biol Chem, 2012. **287**(14): p. 11082-9.

50. Waltenberger, J., L. Claesson-Welsh, A. Siegbahn, M. Shibuya, and C.H. Heldin, *Different signal transduction properties of KDR and Flt1, two receptors for vascular endothelial growth factor.* J Biol Chem, 1994. **269**(43): p. 26988-95.

51. Ruch, C., G. Skiniotis, M.O. Steinmetz, T. Walz, and K. Ballmer-Hofer, *Structure of a VEGF-VEGF receptor complex determined by electron microscopy.* Nat Struct Mol Biol, 2007. **14**(3): p. 249-50.

52. Pan, Q., Y. Chathery, Y. Wu, N. Rathore, R.K. Tong, F. Peale, A. Bagri, M. Tessier-Lavigne, A.W. Koch, and R.J. Watts, *Neuropilin-1 binds to VEGF121 and regulates endothelial cell migration and sprouting.* J Biol Chem, 2007. **282**(33): p. 24049-56.

53. Leppanen, V.M., A.E. Prota, M. Jeltsch, A. Anisimov, N. Kalkkinen, T. Strandin, H. Lankinen, A. Goldman, K. Ballmer-Hofer, and K. Alitalo, *Structural determinants of growth factor binding and specificity by VEGF receptor 2.* Proc Natl Acad Sci U S A, 2010. **107**(6): p. 2425-30.

54. Djordjevic, S. and P.C. Driscoll, *Targeting VEGF signalling via the neuropilin co-receptor.* Drug Discov Today, 2013. **18**(9-10): p. 447-55.

55. King, C. and K. Hristova, *Direct measurements of VEGF-VEGFR2 binding affinities reveal the coupling between ligand binding and receptor dimerization.* J Biol Chem, 2019. **294**(23): p. 9064-9075.

56. von Wronski, M.A., M.F. Tweedle, and A.D. Nunn, *Binding of the C-terminal amino acids of VEGF121 directly with neuropilin-1 should be considered.* FASEB J, 2007. **21**(7): p. 1292; author reply 1293.

57. Shibuya, M., S. Yamaguchi, A. Yamane, T. Ikeda, A. Tojo, H. Matsushime, and M. Sato, *Nucleotide sequence and expression of a novel human receptor-type tyrosine kinase gene (flt) closely related to the fms family.* Oncogene, 1990. **5**(4): p. 519-24.

58. Terman, B.I., M.E. Carrion, E. Kovacs, B.A. Rasmussen, R.L. Eddy, and T.B. Shows, *Identification of a new endothelial cell growth factor receptor tyrosine kinase.* Oncogene, 1991. **6**(9): p. 1677-83.

59. Matthews, W., C.T. Jordan, M. Gavin, N.A. Jenkins, N.G. Copeland, and I.R. Lemischka, *A receptor tyrosine kinase cDNA isolated from a population of enriched primitive hematopoietic cells and exhibiting close genetic linkage to c-kit.* Proc Natl Acad Sci U S A, 1991. **88**(20): p. 9026-30.

60. Fuh, G., K.C. Garcia, and A.M. de Vos, *The interaction of neuropilin-1 with vascular endothelial growth factor and its receptor flt-1.* J Biol Chem, 2000. **275**(35): p. 26690-5.

61. Wiesmann, C., G. Fuh, H.W. Christinger, C. Eigenbrot, J.A. Wells, and A.M. de Vos, *Crystal structure at 1.7 A resolution of VEGF in complex with domain 2 of the Flt-1 receptor.* Cell, 1997. **91**(5): p. 695-704.

62. Muller, Y.A., B. Li, H.W. Christinger, J.A. Wells, B.C. Cunningham, and A.M. de Vos, *Vascular endothelial growth factor: crystal structure and functional mapping of the kinase domain receptor binding site.* Proc Natl Acad Sci U S A, 1997. **94**(14): p. 7192-7.

63. Fuh, G., B. Li, C. Crowley, B. Cunningham, and J.A. Wells, *Requirements for binding and signaling of the kinase domain receptor for vascular endothelial growth factor.* J Biol Chem, 1998. **273**(18): p. 11197-204.

64. Herzog, B., C. Pellet-Many, G. Britton, B. Hartzoulakis, and I.C. Zachary, *VEGF binding to NRP1 is essential for VEGF stimulation of endothelial cell migration, complex formation between NRP1 and VEGFR2, and signaling via FAK Tyr407 phosphorylation.* Mol Biol Cell, 2011. **22**(15): p. 2766-76.

65. Soker, S., H.Q. Miao, M. Nomi, S. Takashima, and M. Klagsbrun, *VEGF165 mediates formation of complexes containing VEGFR-2 and neuropilin-1 that enhance VEGF165-receptor binding.* J Cell Biochem, 2002. **85**(2): p. 357-68.

66. Whitaker, G.B., B.J. Limberg, and J.S. Rosenbaum, *Vascular endothelial growth factor receptor-2 and neuropilin-1 form a receptor complex that is responsible for the differential signaling potency of VEGF(165) and VEGF(121).* J Biol Chem, 2001. **276**(27): p. 25520-31.

67. King, C., D. Wirth, S. Workman, and K. Hristova, *Interactions between NRP1 and VEGFR2 molecules in the plasma membrane.* Biochim Biophys Acta Biomembr, 2018. **1860**(10): p. 2118-2125.

68. Shraga-Heled, N., O. Kessler, C. Prahst, J. Kroll, H. Augustin, and G. Neufeld, *Neuropilin-1 and neuropilin-2 enhance VEGF121 stimulated signal transduction by the VEGFR-2 receptor.* FASEB J, 2007. **21**(3): p. 915-26.

69. Auriau, J., C. Roujeau, Z. Belaid Choucair, A. Oishi, C. Derviaux, T. Roux, E. Trinquet, O. Hermine, R. Jockers, and J. Dam, *Gain of affinity for VEGF165 binding within the VEGFR2/NRP1 cellular complex detected by an HTRF-based binding assay.* Biochem Pharmacol, 2018. **158**: p. 45-59.

70. Mac Gabhann, F. and A.S. Popel, *Differential binding of VEGF isoforms to VEGF receptor 2 in the presence of neuropilin-1: a computational model.* Am J Physiol Heart Circ Physiol, 2005. **288**(6): p. H2851-60.

71. Gelfand, M.V., N. Hagan, A. Tata, W.J. Oh, B. Lacoste, K.T. Kang, J. Kopycinska, J. Bischoff, J.H. Wang, and C. Gu, *Neuropilin-1 functions as a VEGFR2 co-receptor to guide developmental angiogenesis independent of ligand binding.* Elife, 2014. **3**: p. e03720.

72. Soker, S., H. Fidder, G. Neufeld, and M. Klagsbrun, *Characterization of novel vascular endothelial growth factor (VEGF) receptors on tumor cells that bind VEGF165 via its exon 7-encoded domain.* J Biol Chem, 1996. **271**(10): p. 5761-7.

73. Starzec, A., P. Ladam, R. Vassy, S. Badache, N. Bouchemal, A. Navaza, C.H. du Penhoat, and G.Y. Perret, *Structure-function analysis of the antiangiogenic ATWLPPR peptide inhibiting VEGF(165) binding to neuropilin-1 and molecular dynamics simulations of the ATWLPPR/neuropilin-1 complex.* Peptides, 2007. **28**(12): p. 2397-402.

74. Teesalu, T., K.N. Sugahara, V.R. Kotamraju, and E. Ruoslahti, *C-end rule peptides mediate neuropilin-1-dependent cell, vascular, and tissue penetration.* Proc Natl Acad Sci U S A, 2009. **106**(38): p. 16157-62.

75. Parker, M.W., A.D. Linkugel, and C.W. Vander Kooi, *Effect of C-terminal sequence on competitive semaphorin binding to neuropilin-1.* J Mol Biol, 2013. **425**(22): p. 4405-14.

76. Uniewicz, K.A., A. Ori, Y.A. Ahmed, E.A. Yates, and D.G. Fernig, *Characterisation of the interaction of neuropilin-1 with heparin and a heparan sulfate mimetic library of heparin-derived sugars.* PeerJ, 2014. **2**: p. e461.

77. Teran, M. and M.A. Nugent, *Synergistic Binding of Vascular Endothelial Growth Factor-A and Its Receptors to Heparin Selectively Modulates Complex Affinity.* J Biol Chem, 2015. **290**(26): p. 16451-62.

78. Xu, D. and J.D. Esko, *Demystifying heparan sulfate-protein interactions.* Annu Rev Biochem, 2014. **83**: p. 129-57.

79. Esko, J.D. and S.B. Selleck, *Order out of chaos: assembly of ligand binding sites in heparan sulfate.* Annu Rev Biochem, 2002. **71**: p. 435-71.

80. Thacker, B.E., D. Xu, R. Lawrence, and J.D. Esko, *Heparan sulfate 3-O-sulfation: a rare modification in search of a function.* Matrix Biol, 2014. **35**: p. 60-72.

81. Pejler, G., G. Backstrom, U. Lindahl, M. Paulsson, M. Dziadek, S. Fujiwara, and R. Timpl, *Structure and affinity for antithrombin of heparan sulfate chains derived from basement membrane proteoglycans.* J Biol Chem, 1987. **262**(11): p. 5036-43.

82. de Agostini, A.I., J.C. Dong, C. de Vantery Arrighi, M.A. Ramus, I. Dentand-Quadri, S. Thalmann, P. Ventura, V. Ibecheole, F. Monge, A.M. Fischer, S. HajMohammadi, N.W. Shworak, L. Zhang, Z. Zhang, and R.J. Linhardt, *Human follicular fluid heparan sulfate contains abundant 3-O-sulfated chains with anticoagulant activity.* J Biol Chem, 2008. **283**(42): p. 28115-24.

83. Marcum, J.A., D.H. Atha, L.M. Fritze, P. Nawroth, D. Stern, and R.D. Rosenberg, *Cloned bovine aortic endothelial cells synthesize anticoagulantly active heparan sulfate proteoglycan.* J Biol Chem, 1986. **261**(16): p. 7507-17.

84. Zhang, L., D.L. Beeler, R. Lawrence, M. Lech, J. Liu, J.C. Davis, Z. Shriver, R. Sasisekharan, and R.D. Rosenberg, *6-O-sulfotransferase-1 represents a critical enzyme in the anticoagulant heparan sulfate biosynthetic pathway.* J Biol Chem, 2001. **276**(45): p. 42311-21.

85. Zhang, L., R. Lawrence, J.J. Schwartz, X. Bai, G. Wei, J.D. Esko, and R.D. Rosenberg, *The effect of precursor structures on the action of glucosaminyl 3-O-sulfotransferase-1 and the biosynthesis of anticoagulant heparan sulfate.* J Biol Chem, 2001. **276**(31): p. 28806-13.

86. Thacker, B.E., E. Seamen, R. Lawrence, M.W. Parker, Y. Xu, J. Liu, C.W. Vander Kooi, and J.D. Esko, *Expanding the 3-O-Sulfate Proteome--Enhanced Binding of Neuropilin-1 to 3-O-Sulfated Heparan Sulfate Modulates Its Activity.* ACS Chem Biol, 2016. **11**(4): p. 971-80.

87. Bishop, J.R., M. Schuksz, and J.D. Esko, *Heparan sulphate proteoglycans fine-tune mammalian physiology.* Nature, 2007. **446**(7139): p. 1030-7.

88. He, Z. and M. Tessier-Lavigne, *Neuropilin is a receptor for the axonal chemorepellent Semaphorin III.* Cell, 1997. **90**(4): p. 739-51.

89. Yabe, T., T. Hata, J. He, and N. Maeda, *Developmental and regional expression of heparan sulfate sulfotransferase genes in the mouse brain.* Glycobiology, 2005. **15**(10): p. 982-93.

90. Cadwallader, A.B. and H.J. Yost, *Combinatorial expression patterns of heparan sulfate sulfotransferases in zebrafish: II. The 6-O-sulfotransferase family.* Dev Dyn, 2006. **235**(12): p. 3432-7.

91. Lawrence, R., T. Yabe, S. Hajmohammadi, J. Rhodes, M. McNeely, J. Liu, E.D. Lamperti, P.A. Toselli, M. Lech, P.G. Spear, R.D. Rosenberg, and N.W. Shworak, *The principal neuronal gD-type 3-O-sulfotransferases and their products in central and peripheral nervous system tissues.* Matrix Biol, 2007. **26**(6): p. 442-55.

92. Mochizuki, H., K. Yoshida, Y. Shibata, and K. Kimata, *Tetrasulfated disaccharide unit in heparan sulfate: enzymatic formation and tissue distribution.* J Biol Chem, 2008. **283**(45): p. 31237-45.

93. Ferrara, N. and W.J. Henzel, *Pituitary follicular cells secrete a novel heparin-binding growth factor specific for vascular endothelial cells.* Biochem Biophys Res Commun, 1989. **161**(2): p. 851-8.

94. Soker, S., D. Goldstaub, C.M. Svahn, I. Vlodavsky, B.Z. Levi, and G. Neufeld, *Variations in the size and sulfation of heparin modulate the effect of heparin on the binding of VEGF165 to its receptors.* Biochem Biophys Res Commun, 1994. **203**(2): p. 1339-47.

95. Zhao, W., S.A. McCallum, Z. Xiao, F. Zhang, and R.J. Linhardt, *Binding affinities of vascular endothelial growth factor (VEGF) for heparin-derived oligosaccharides.* Biosci Rep, 2012. **32**(1): p. 71-81.

96. Fairbrother, W.J., M.A. Champe, H.W. Christinger, B.A. Keyt, and M.A. Starovasnik, *Solution structure of the heparin-binding domain of vascular endothelial growth factor.* Structure, 1998. **6**(5): p. 637-48.

97. Ono, K., H. Hattori, S. Takeshita, A. Kurita, and M. Ishihara, *Structural features in heparin that interact with VEGF165 and modulate its biological activity.* Glycobiology, 1999. **9**(7): p. 705-11.

98. Wijelath, E., M. Namekata, J. Murray, M. Furuyashiki, S. Zhang, D. Coan, M. Wakao, R.B. Harris, Y. Suda, L. Wang, and M. Sobel, *Multiple mechanisms for exogenous heparin modulation of vascular endothelial growth factor activity.* J Cell Biochem, 2010. **111**(2): p. 461-8.

99. Robinson, C.J., B. Mulloy, J.T. Gallagher, and S.E. Stringer, *VEGF165-binding sites within heparan sulfate encompass two highly sulfated domains and can be liberated by K5 lyase.* J Biol Chem, 2006. **281**(3): p. 1731-40.

100. Cole, C.L., S.U. Hansen, M. Barath, G. Rushton, J.M. Gardiner, E. Avizienyte, and G.C. Jayson, *Synthetic heparan sulfate oligosaccharides inhibit endothelial cell functions essential for angiogenesis.* PLoS One, 2010. **5**(7): p. e11644.

101. Keyt, B.A., L.T. Berleau, H.V. Nguyen, H. Chen, H. Heinsohn, R. Vandlen, and N. Ferrara, *The carboxyl-terminal domain (111-165) of vascular endothelial growth factor is critical for its mitogenic potency.* J Biol Chem, 1996. **271**(13): p. 7788-95.

102. Krilleke, D., A. DeErkenez, W. Schubert, I. Giri, G.S. Robinson, Y.S. Ng, and D.T. Shima, *Molecular mapping and functional characterization of the VEGF164 heparin-binding domain.* J Biol Chem, 2007. **282**(38): p. 28045-56.

103. Koehler, L., G. Ruiz-Gomez, K. Balamurugan, S. Rother, J. Freyse, S. Moller, M. Schnabelrauch, S. Kohling, S. Djordjevic, D. Scharnweber, J. Rademann, M.T. Pisabarro, and V. Hintze, *Dual Action of Sulfated Hyaluronan on Angiogenic Processes in Relation to Vascular Endothelial Growth Factor-A.* Sci Rep, 2019. **9**(1): p. 18143.

104. Tessler, S., P. Rockwell, D. Hicklin, T. Cohen, B.Z. Levi, L. Witte, I.R. Lemischka, and G. Neufeld, *Heparin modulates the interaction of VEGF165 with soluble and cell associated flk-1 receptors.* J Biol Chem, 1994. **269**(17): p. 12456-61.

105. Cohen, T., H. Gitay-Goren, R. Sharon, M. Shibuya, R. Halaban, B.Z. Levi, and G. Neufeld, *VEGF121, a vascular endothelial growth factor (VEGF) isoform lacking heparin binding ability, requires cell-surface heparan sulfates for efficient binding to the VEGF receptors of human melanoma cells.* J Biol Chem, 1995. **270**(19): p. 11322-6.

106. Gitay-Goren, H., S. Soker, I. Vlodavsky, and G. Neufeld, *The binding of vascular endothelial growth factor to its receptors is dependent on cell surface-associated heparin-like molecules.* J Biol Chem, 1992. **267**(9): p. 6093-8.

107. Terman, B., L. Khandke, M. Dougher-Vermazan, D. Maglione, N.J. Lassam, D. Gospodarowicz, M.G. Persico, P. Bohlen, and M. Eisinger, *VEGF receptor subtypes KDR and FLT1 show different sensitivities to heparin and placenta growth factor.* Growth Factors, 1994. **11**(3): p. 187-95.

108. Ashikari-Hada, S., H. Habuchi, Y. Kariya, and K. Kimata, *Heparin regulates vascular endothelial growth factor165-dependent mitogenic activity, tube formation, and its receptor phosphorylation of human endothelial cells. Comparison of the effects of heparin and modified heparins.* J Biol Chem, 2005. **280**(36): p. 31508-15.

109. Gengrinovitch, S., B. Berman, G. David, L. Witte, G. Neufeld, and D. Ron, *Glypican-1 is a VEGF165 binding proteoglycan that acts as an extracellular chaperone for VEGF165.* J Biol Chem, 1999. **274**(16): p. 10816-22.

110. Dougher, A.M., H. Wasserstrom, L. Torley, L. Shridaran, P. Westdock, R.E. Hileman, J.R. Fromm, R. Anderberg, S. Lyman, R.J. Linhardt, J. Kaplan, and B.I. Terman, *Identification of a heparin binding peptide on the extracellular domain of the KDR VEGF receptor.* Growth Factors, 1997. **14**(4): p. 257-68.

111. Fuster, M.M., L. Wang, J. Castagnola, L. Sikora, K. Reddi, P.H. Lee, K.A. Radek, M. Schuksz, J.R. Bishop, R.L. Gallo, P. Sriramarao, and J.D. Esko, *Genetic alteration of endothelial heparan sulfate selectively inhibits tumor angiogenesis.* J Cell Biol, 2007. **177**(3): p. 539-49.

112. Xu, D., M.M. Fuster, R. Lawrence, and J.D. Esko, *Heparan sulfate regulates VEGF165- and VEGF121-mediated vascular hyperpermeability.* J Biol Chem, 2011. **286**(1): p. 737-45.

113. Chiodelli, P., S. Mitola, C. Ravelli, P. Oreste, M. Rusnati, and M. Presta, *Heparan sulfate proteoglycans mediate the angiogenic activity of the vascular endothelial growth factor receptor-2 agonist gremlin.* Arterioscler Thromb Vasc Biol, 2011. **31**(12): p. e116-27.

114. Zhang, X., V. Pagadala, H.M. Jester, A.M. Lim, T.Q. Pham, A.M.P. Goulas, J. Liu, and R.J. Linhardt, *Chemoenzymatic synthesis of heparan sulfate and heparin oligosaccharides and NMR analysis: paving the way to a diverse library for glycobiologists.* Chem Sci, 2017. **8**(12): p. 7932-7940.

115. Kisanuki, Y.Y., R.E. Hammer, J. Miyazaki, S.C. Williams, J.A. Richardson, and M. Yanagisawa, *Tie2-Cre transgenic mice: a new model for endothelial cell-lineage analysis in vivo.* Dev Biol, 2001. **230**(2): p. 230-42.

116. Fantin, A., B. Herzog, M. Mahmoud, M. Yamaji, A. Plein, L. Denti, C. Ruhrberg, and I. Zachary, *Neuropilin 1 (NRP1) hypomorphism combined with defective VEGF-A binding reveals novel roles for NRP1 in developmental and pathological angiogenesis.* Development, 2014. **141**(3): p. 556-62.

117. Kawasaki, T., T. Kitsukawa, Y. Bekku, Y. Matsuda, M. Sanbo, T. Yagi, and H. Fujisawa, *A requirement for neuropilin-1 in embryonic vessel formation.* Development, 1999. **126**(21): p. 4895-902.

118. Takashima, S., M. Kitakaze, M. Asakura, H. Asanuma, S. Sanada, F. Tashiro, H. Niwa, J. Miyazaki Ji, S. Hirota, Y. Kitamura, T. Kitsukawa, H. Fujisawa, M. Klagsbrun, and M. Hori, *Targeting of both mouse neuropilin-1 and neuropilin-2 genes severely impairs developmental yolk sac and embryonic angiogenesis.* Proc Natl Acad Sci U S A, 2002. **99**(6): p. 3657-62.

119. Carmeliet, P., V. Ferreira, G. Breier, S. Pollefeyt, L. Kieckens, M. Gertsenstein, M. Fahrig, A. Vandenhoeck, K. Harpal, C. Eberhardt, C. Declercq, J. Pawling, L. Moons, D. Collen, W. Risau, and A. Nagy,

Abnormal blood vessel development and lethality in embryos lacking a single VEGF allele. Nature, 1996. **380**(6573): p. 435-9.

120. Ferrara, N., K. Carver-Moore, H. Chen, M. Dowd, L. Lu, K.S. O'Shea, L. Powell-Braxton, K.J. Hillan, and M.W. Moore, *Heterozygous embryonic lethality induced by targeted inactivation of the VEGF gene.* Nature, 1996. **380**(6573): p. 439-42.

121. Rosen, R.D. and B. Bordoni, *Embryology, Aortic Arch*, in *StatPearls*. 2021: Treasure Island (FL).

122. Plein, A., A. Calmont, A. Fantin, L. Denti, N.A. Anderson, P.J. Scambler, and C. Ruhrberg, *Neural crest-derived SEMA3C activates endothelial NRP1 for cardiac outflow tract septation.* J Clin Invest, 2015. **125**(7): p. 2661-76.

123. Gerhardt, H., C. Ruhrberg, A. Abramsson, H. Fujisawa, D. Shima, and C. Betsholtz, *Neuropilin-1 is required for endothelial tip cell guidance in the developing central nervous system.* Dev Dyn, 2004. **231**(3): p. 503-9.

124. Ruhrberg, C. and V.L. Bautch, *Neurovascular development and links to disease.* Cell Mol Life Sci, 2013. **70**(10): p. 1675-84.

125. Fantin, A., A. Lampropoulou, G. Gestri, C. Raimondi, V. Senatore, I. Zachary, and C. Ruhrberg, *NRP1 Regulates CDC42 Activation to Promote Filopodia Formation in Endothelial Tip Cells.* Cell Rep, 2015. **11**(10): p. 1577-90.

126. Gerhardt, H., *VEGF and endothelial guidance in angiogenic sprouting.* Organogenesis, 2008. **4**(4): p. 241-6.

127. Raimondi, C., A. Fantin, A. Lampropoulou, L. Denti, A. Chikh, and C. Ruhrberg, *Imatinib inhibits VEGF-independent angiogenesis by targeting neuropilin 1-dependent ABL1 activation in endothelial cells.* J Exp Med, 2014. **211**(6): p. 1167-83.

128. Daly, J.L., B. Simonetti, K. Klein, K.E. Chen, M.K. Williamson, C. Anton-Plagaro, D.K. Shoemark, L. Simon-Gracia, M. Bauer, R. Hollandi, U.F. Greber, P. Horvath, R.B. Sessions, A. Helenius, J.A. Hiscox, T. Teesalu, D.A. Matthews, A.D. Davidson, B.M. Collins, P.J. Cullen, and Y. Yamauchi, *Neuropilin-1 is a host factor for SARS-CoV-2 infection.* Science, 2020. **370**(6518): p. 861-865.

129. Cantuti-Castelvetri, L., R. Ojha, L.D. Pedro, M. Djannatian, J. Franz, S. Kuivanen, F. van der Meer, K. Kallio, T. Kaya, M. Anastasina, T. Smura, L. Levanov, L. Szirovicza, A. Tobi, H. Kallio-Kokko, P. Osterlund, M. Joensuu, F.A. Meunier, S.J. Butcher, M.S. Winkler, B. Mollenhauer, A. Helenius, O. Gokce, T. Teesalu, J. Hepojoki, O. Vapalahti, C. Stadelmann, G. Balistreri, and M. Simons, *Neuropilin-1 facilitates SARS-CoV-2 cell entry and infectivity.* Science, 2020. **370**(6518): p. 856-860.

130. Appleton, B.A., P. Wu, J. Maloney, J. Yin, W.C. Liang, S. Stawicki, K. Mortara, K.K. Bowman, J.M. Elliott, W. Desmarais, J.F. Bazan, A. Bagri, M. Tessier-Lavigne, A.W. Koch, Y. Wu, R.J. Watts, and C. Wiesmann, *Structural studies of neuropilin/antibody complexes provide insights into semaphorin and VEGF binding.* EMBO J, 2007. **26**(23): p. 4902-12.

131. Sankaranarayanan, N.V. and U.R. Desai, *Toward a robust computational screening strategy for identifying glycosaminoglycan sequences that display high specificity for target proteins.* Glycobiology, 2014. **24**(12): p. 1323-33.

132. Sankarayanarayanan, N.V., T.R. Strebel, R.S. Boothello, K. Sheerin, A. Raghuraman, F. Sallas, P.D. Mosier, N.D. Watermeyer, S. Oscarson, and U.R. Desai, *A Hexasaccharide Containing Rare 2-O-Sulfate-Glucuronic Acid Residues Selectively Activates Heparin Cofactor II.* Angew Chem Int Ed Engl, 2017. **56**(9): p. 2312-2317.

133. Sankaranarayanan, N.V., Y. Bi, B. Kuberan, and U.R. Desai, *Combinatorial virtual library screening analysis of antithrombin binding oligosaccharide motif generation by heparan sulfate 3-O-Sulfotransferase 1.* Comput Struct Biotechnol J, 2020. **18**: p. 933-941.

134. Jones, G., P. Willett, R.C. Glen, A.R. Leach, and R. Taylor, *Development and validation of a genetic algorithm for flexible docking.* J Mol Biol, 1997. **267**(3): p. 727-48.

135. Sankaranarayanan, N.V., B. Nagarajan, and U.R. Desai, *So you think computational approaches to understanding glycosaminoglycan-protein interactions are too dry and too rigid? Think again!* Curr Opin Struct Biol, 2018. **50**: p. 91-100.

136. Case, D.A., I.Y. Ben-Shalom, S.R. Brozell, D.S. Cerutti, I. Cheatham, T. E. , V.W.D. Cruzeiro, T.A. Darden, R.E. Duke, D. Ghoreishi, M.K. Gilson, H. Gohlke, A.W. Goetz, D. Greene, R. Harris, N. Homeyer, Y. Huang, S. Izadi, A. Kovalenko, T. Kurtzman, T.S. Lee, S. LeGrand, P. Li, C. Lin, J. Liu, T. Luchko, R. Luo, D.J. Mermelstein, K.M. Merz, Y. Miao, G. Monard, C. Nguyen, H. Nguyen, I. Omelyan, A. Onufriev, F. Pan, R. Qi, D.R. Roe, A. Roitberg, C. Sagui, S. Schott-Verdugo, J. Shen, C.L. Simmerling, J. Smith, R. Salomon-Ferrer, J. Swails, R.C. Walker, J. Wang, H. Wei, R.M. Wolf, X. Wu, L. Xiao, D.M. York, and P.A. Kollman, *AMBER 2018*. 2018, University of California, San Francisco.

137. Kirschner, K.N., A.B. Yongye, S.M. Tschampel, J. Gonzalez-Outeirino, C.R. Daniels, B.L. Foley, and R.J. Woods, *GLYCAM06: a generalizable biomolecular force field. Carbohydrates.* J Comput Chem, 2008. **29**(4): p. 622-55.

138. Tian, C., K. Kasavajhala, K.A.A. Belfon, L. Raguette, H. Huang, A.N. Migues, J. Bickel, Y. Wang, J. Pincay, Q. Wu, and C. Simmerling, *ff19SB: Amino-Acid-Specific Protein Backbone Parameters Trained against Quantum Mechanics Energy Surfaces in Solution.* J Chem Theory Comput, 2020. **16**(1): p. 528-552.

139. Roe, D.R. and T.E. Cheatham, 3rd, *PTRAJ and CPPTRAJ: Software for Processing and Analysis of Molecular Dynamics Trajectory Data.* J Chem Theory Comput, 2013. **9**(7): p. 3084-95.

140. Miller, B.R., 3rd, T.D. McGee, Jr., J.M. Swails, N. Homeyer, H. Gohlke, and A.E. Roitberg, *MMPBSA.py: An Efficient Program for End-State Free Energy Calculations.* J Chem Theory Comput, 2012. **8**(9): p. 3314-21.

141. Weimbs, T. *Tutorial: How to generate a publication-quality multiplesequence alignment*. 2012; Available from: https://labs.mcdb.ucsb.edu/weimbs/thomas/sites/labs.mcdb.ucsb.edu.weimbs.thomas/files/docs/multiplesequencealignmenttutorial.pdf.

142. Clausen, T.M., D.R. Sandoval, C.B. Spliid, J. Pihl, H.R. Perrett, C.D. Painter, A. Narayanan, S.A. Majowicz, E.M. Kwong, R.N. McVicar, B.E. Thacker, C.A. Glass, Z. Yang, J.L. Torres, G.J. Golden, P.L. Bartels, R.N. Porell, A.F. Garretson, L. Laubach, J. Feldman, X. Yin, Y. Pu, B.M. Hauser, T.M. Caradonna, B.P. Kellman, C. Martino, P. Gordts, S.K. Chanda, A.G. Schmidt, K. Godula, S.L. Leibel, J. Jose, K.D. Corbett, A.B. Ward, A.F. Carlin, and J.D. Esko, *SARS-CoV-2 Infection Depends on Cellular Heparan Sulfate and ACE2.* Cell, 2020. **183**(4): p. 1043-1057 e15.

143. Lakso, M., J.G. Pichel, J.R. Gorman, B. Sauer, Y. Okamoto, E. Lee, F.W. Alt, and H. Westphal, *Efficient in vivo manipulation of mouse genomic sequences at the zygote stage.* Proc Natl Acad Sci U S A, 1996. **93**(12): p. 5860-5.

144. Janik, P., P. Briand, and N.R. Hartmann, *The effect of estrone-progesterone treatment on cell proliferation kinetics of hormone-dependent GR mouse mammary tumors.* Cancer Res, 1975. **35**(12): p. 3698-704.

145. Neukirch, L., T.K. Nielsen, H. Laursen, J. Daradoumis, C. Thirion, and P.J. Holst, *Adenovirus based virus-like-vaccines targeting endogenous retroviruses can eliminate growing colorectal cancers in mice.* Oncotarget, 2019. **10**(14): p. 1458-1472.

146. Cardin, A.D. and H.J. Weintraub, *Molecular modeling of protein-glycosaminoglycan interactions.* Arteriosclerosis, 1989. **9**(1): p. 21-32.

147. Sandoval, D.R., A. Gomez Toledo, C.D. Painter, E.M. Tota, M.O. Sheikh, A.M.V. West, M.M. Frank, L. Wells, D. Xu, R. Bicknell, K.D. Corbett, and J.D. Esko, *Proteomics-based screening of the endothelial heparan sulfate interactome reveals that C-type lectin 14a (CLEC14A) is a heparin-binding protein.* J Biol Chem, 2020. **295**(9): p. 2804-2821.

148. Uniewicz, K.A., A. Ori, R. Xu, Y. Ahmed, M.C. Wilkinson, D.G. Fernig, and E.A. Yates, *Differential scanning fluorimetry measurement of protein stability changes upon binding to glycosaminoglycans: a screening test for binding specificity.* Anal Chem, 2010. **82**(9): p. 3796-802.

149. Franco, S., I. Segura, H.H. Riese, and M.A. Blasco, *Decreased B16F10 melanoma growth and impaired vascularization in telomerase-deficient mice with critically short telomeres.* Cancer Res, 2002. **62**(2): p. 552-9.

150. Prewett, M., J. Huber, Y. Li, A. Santiago, W. O'Connor, K. King, J. Overholser, A. Hooper, B. Pytowski, L. Witte, P. Bohlen, and D.J. Hicklin, *Antivascular endothelial growth factor receptor (fetal liver kinase 1) monoclonal antibody inhibits tumor angiogenesis and growth of several mouse and human tumors.* Cancer Res, 1999. **59**(20): p. 5209-18.

151. Yamada, Y., N. Takakura, H. Yasue, H. Ogawa, H. Fujisawa, and T. Suda, *Exogenous clustered neuropilin 1 enhances vasculogenesis and angiogenesis.* Blood, 2001. **97**(6): p. 1671-8.

152. Pellegrini, L., D.F. Burke, F. von Delft, B. Mulloy, and T.L. Blundell, *Crystal structure of fibroblast growth factor receptor ectodomain bound to ligand and heparin.* Nature, 2000. **407**(6807): p. 1029-34.

153. Windwarder, M., T. Yelland, S. Djordjevic, and F. Altmann, *Detailed characterization of the O-linked glycosylation of the neuropilin-1 c/MAM-domain.* Glycoconj J, 2016. **33**(3): p. 387-97.

154. Esko, J.D., T.E. Stewart, and W.H. Taylor, *Animal cell mutants defective in glycosaminoglycan biosynthesis.* Proc Natl Acad Sci U S A, 1985. **82**(10): p. 3197-201.

155. Pan, Q., Y. Chanthery, W.C. Liang, S. Stawicki, J. Mak, N. Rathore, R.K. Tong, J. Kowalski, S.F. Yee, G. Pacheco, S. Ross, Z. Cheng, J. Le Couter, G. Plowman, F. Peale, A.W. Koch, Y. Wu, A. Bagri, M. Tessier-Lavigne, and R.J. Watts, *Blocking neuropilin-1 function has an additive effect with anti-VEGF to inhibit tumor growth.* Cancer Cell, 2007. **11**(1): p. 53-67.

156. Xu, Y., K. Chandarajoti, X. Zhang, V. Pagadala, W. Dou, D.M. Hoppensteadt, E.M. Sparkenbaugh, B. Cooley, S. Daily, N.S. Key, D. Severynse-Stevens, J. Fareed, R.J. Linhardt, R. Pawlinski, and J. Liu, *Synthetic oligosaccharides can replace animal-sourced low-molecular weight heparins.* Sci Transl Med, 2017. **9**(406).

157. Mohamed, S. and D.R. Coombe, *Heparin Mimetics: Their Therapeutic Potential.* Pharmaceuticals (Basel), 2017. **10**(4).

158. Schuksz, M., M.M. Fuster, J.R. Brown, B.E. Crawford, D.P. Ditto, R. Lawrence, C.A. Glass, L. Wang, Y. Tor, and J.D. Esko, *Surfen, a small molecule antagonist of heparan sulfate.* Proc Natl Acad Sci U S A, 2008. **105**(35): p. 13075-80.

APPENDIX

I was a co-author on the following two papers and my contributions are given below.

1. Sandoval DR, Gomez Toledo A, **Painter CD**, Tota EM, Sheikh MO, West AMV, Frank MM, Wells L, Xu D, Bicknell R, Corbett KD, Esko JD. Proteomics-based screening of the endothelial heparan sulfate interactome reveals that C-type lectin 14a (CLEC14A) is a heparin-binding protein. J Biol Chem. 2020 Feb 28;295(9):2804-2821.

For this research article, I developed and optimized the heparin ELISA protocol and assessed the heparin binding abilities of the clec14a proteins with this assay.

2. Clausen TM, Sandoval DR, Spliid CB, Pihl J, Perrett HR, **Painter CD**, Narayanan A, Majowicz SA, Kwong EM, McVicar RN, Thacker BE, Glass CA, Yang Z, Torres JL, Golden GJ, Bartels PL, Porell RN, Garretson AF, Laubach L, Feldman J, Yin X, Pu Y, Hauser BM, Caradonna TM, Kellman BP, Martino C, Gordts PLSM, Chanda SK, Schmidt AG, Godula K, Leibel SL, Jose J, Corbett KD, Ward AB, Carlin AF, Esko JD. SARS-CoV-2 Infection Depends on Cellular Heparan Sulfate and ACE2. Cell. 2020 Nov 12;183(4):1043-1057.e15.

For this research article, I optimized the immunoblotting protocol for the ACE2 receptor and assessed various cell lines for the expression of the ACE2 receptor. I also assisted with the analysis of the spike protein binding to cellular heparan sulfate by flow cytometry.